Materials & Design 258 (2025) 114633

Contents lists available at ScienceDirect

Materials & Design

journal homepage: www.elsevier.com/locate/matdes

Recent advances in high-entropy alloys for electrocatalysis: From rational design to functional performance

Víctor M. Jiménez-Arévalo [a,*], P. Martin [b], María Fernanda Sepúlveda [a], Manuel I. Azocar [a], Xiaorong Zhou [c,**], Felipe M. Galleguillos Madrid [d], C.G. Ramirez [a], José H. Zagal [a], Maritza Páez [a,*]

[a] Departamento de Química de los Materiales, Facultad de Química y Biología, Universidad de Santiago de Chile, Av. L. B. O'Higgins 3363, Casilla 40, Correo 33, Santiago, Chile
[b] Universidad Técnica Federico Santa María, Departamento de Ingeniería Metalúrgica y de Materiales, Av. España, 1680 Valparaíso, Chile
[c] Department of Materials, University of Manchester, Oxford Road, M13 9PL Manchester, United Kingdom
[d] Centro de Desarrollo Energético Antofagasta, Universidad de Antofagasta, Antofagasta 1240000, Chile

ARTICLE INFO

Keywords:
High-entropy alloys
Electrocatalysis
Renewable Energy
Advanced Materials
Hydrogen Economy

ABSTRACT

High-entropy alloys (HEAs) represent a transformative class of materials for electrocatalysis, challenging conventional alloy design by incorporating five or more principal elements into single- or multiphase solid solutions. This compositional complexity enables exceptional tunability of electronic structures, adsorption energies, and catalytic behavior. HEAs offer a promising route to overcome the limitations of noble-metal-based catalysts, such as high cost, limited availability, and poor long-term stability. This review critically evaluates recent advances in the design, synthesis, and electrochemical performance of HEAs across key electrocatalytic reactions, including the hydrogen evolution reaction (HER), oxygen evolution (OER), oxygen reduction (ORR), methanol and ethanol oxidation (MOR and EOR), carbon dioxide reduction (CO_2RR), and nitrogen reduction (NRR). Emphasis is placed on the synergistic effects, hybridization of orbitales in HEAs, configurational entropy contributions, and defect-rich surfaces that collectively enhance catalytic activity and durability. We highlight emerging synthetic strategies, such as thermal shock, solvothermal methods, and dealloying, that enable controlled fabrication of HEA nanostructures with optimized properties. In parallel, we examine computational and data-driven approaches, including semi-empirical models, CALPHAD, first-principles simulations, and AI-based frameworks, that facilitate rational design and accelerated discovery. Finally, we outline current challenges and future directions toward scalable production, stability under realistic conditions, and integration into sustainable energy systems.

1. Introduction

Since the Industrial Revolution, the intensive consumption of fossil fuels has resulted in a dramatic increase in greenhouse gas emissions particularly carbon dioxide which is directly associated with global warming [1]. Over the past five decades, the urgent need to address both environmental degradation and rising energy demands has driven the global transition toward cleaner and renewable energy sources [2,3]. Among emerging technologies, the electrocatalytic production of hydrogen via water electrolysis stands out as a zero-emission alternative provided that the electricity used in the process originates from renewable sources [4].

Electrocatalysis plays a crucial role in the advancement of sustainable carbon energy technologies, facilitating key processes such as water electrolysis, fuel cells, and carbon dioxide electrochemical reduction. Despite its potential, the field remains heavily dependent on scarce and expensive noble metals electrode materials, such as platinum (Pt), iridium (Ir), and rhenium (Re),which, although highly active, suffer from high costs, limited scalability, and in some cases poor long-term stability. These challenges underscore the urgent need for alternative, earth-abundant catalysts with comparable or superior performance [5–7].

At the core of electrocatalysis lies heterogeneous catalysis at the

* Corresponding author at: Departamento de Química de los Materiales, Facultad de Química y Biología, Universidad de Santiago de Chile, Av. L. B. O'Higgins 3363, Casilla 40, Correo 33, Santiago, Chile.
** Corresponding author at: Department of Materials, University of Manchester, Oxford Road, M13 9PL Manchester, United Kingdom.
E-mail addresses: Victor.jimenez@usach.cl (V.M. Jiménez-Arévalo), xiaorong.zhou@manchester.ac.uk (X. Zhou), Maritza.paez@usach.cl (M. Páez).

https://doi.org/10.1016/j.matdes.2025.114633
Received 23 July 2025; Received in revised form 18 August 2025; Accepted 24 August 2025
Available online 29 August 2025
0264-1275/© 2025 The Author(s). Published by Elsevier Ltd. This is an open access article under the CC BY license (http://creativecommons.org/licenses/by/4.0/).

Nomenclature

Acronym	Meaning
HEAs	High-Entropy Alloys
HER	Hydrogen Evolution Reaction
OER	Oxygen Evolution Reaction
ORR	Oxygen Reduction Reaction
MOR	Methanol Oxidation Reaction
EOR	Ethanol Oxidation Reaction
NRR	Nitrogen Reduction Reaction
FCC	Face-Centered Cubic
BCC	Body-Centered Cubic
CALPHAD	CALculation of PHAse Diagrams
DFT	Density Functional Theory
SQS	Special Quasirandom Structure
CPA	Coherent Potential Approximation
AI	Artificial Intelligence
HEAPS	High-Entropy Alloy Predicting Software
VEC	Valence Electron Concentration
SFE	Stacking Fault Energy
PM	Powder Metallurgy
SPS	Spark Plasma Sintering
HP	Hot Pressing
HPS	High-Pressure Sintering
DMFC	Direct Methanol Fuel Cell
DEFC	Direct Ethanol Fuel Cell
CV	Cyclic Voltammetry
GO	Graphene Oxide
CNF	Carbon Nanofibers
rGO	Reduced Graphene Oxide
STS	Shock Thermal Synthesis
PBS	Phosphate Buffered Saline
ECSA	Electrochemical Surface Area

electrode–electrolyte interface. In this process, the electrode functions both as an electron source/sink and as a catalytic surface. Reactant molecules adsorb or bind onto specific active sites, forming transient bonds with intermediates that lower the activation energy of the several steps that can be involved since more than one electron participates, and each electron transfer step represent different energy barriers. Modifying the electrode surface, either by introducing active species that interact with target molecules or by altering its composition and microstructure, can enhance reaction kinetics by facilitating intermediate stabilization and charge transfer.

An response to these limitations, various alternative materials from different families have been explored [2,8–10], among which high-entropy alloys (HEAs) have emerged as a particularly promising class. First independently proposed by Yeh and Cantor in 2004 [11,12], HEAs depart from traditional alloy design by combining five or more elements in near-to-equiatomic ratios. This particular compositional feature elevates the configurational entropy of mixing, this last coming from the number of possible ways that the different atoms can be arranged on the lattice sites of a solid solution. Hence, if the alloy contain more elements and they are closer to the equiatomic proportion, the configurational entropy of mixing increases and the solid solutions becomes more stable This compositional complexity additionally results in a series of remarkable and differential features, known in the field as core effects, that includes the enhanced stability, the sluggish diffusion, the cocktail – synergistics – effect, and a severe lattice distortion [13]. Although early studies suggested a predominance of single-phase structures, subsequent research has revealed that multiphase HEAs are way more common; nevertheless, many advantageous features of the originally conceived single-phase HEAs remain valid to multiphase HEAs systems. It is important to highlight that with the years, other terms have been employed to refer to these metallic materials, such as multicomponent alloys, multi-principal elemental alloys, or complex compositional alloys; in any case, all of them refers to these alloys constituted by various alloys in similar proportions.

Several fundamental properties render HEAs particularly appealing as next generation electrocatalysts:

1. Thermodynamic stabilization via configurational entropy: the high configurational entropy intrinsic to HEAs favors the formation of stable single-phase solid solutions. This structural stability enhances resistance to degradation during electrochemical operation, thereby ensuring long-term durability [14].
2. Electronic tunability: the flexible compositional design of HEAs allows for precise control over their electronic structure. This enables the adjustment of adsorption energies for key intermediates, such as *H in the HER and *O in the OER and ORR, leading to improved catalytic activity and energy conversion efficiency [15,16].
3. Defect-rich and heterogeneous surfaces: The multielement nature of HEAs promotes the formation of structurally- and chemically-heterogeneous surfaces, that includes a severely-distorted lattice – caused by the difference in atomic radii and bonding energy of the constituents of the phase –, a distribution of stacking fault energies throughout the lattice, a distribution of Burger's vectors, etc., as well as typical metal lattices defects – such as vacancies, dislocations, twins, grain boundaries, etc. Various of these features increase the density of catalytically active sites, thereby enhancing reaction kinetics and selectivity [17].
4. Synergistic elemental interactions: the interplay between different metallic species within HEAs gives rise to synergistic effects, known as the cocktail effect, that optimize reaction pathways. For instance, Mo and Ni can enhance hydrogen adsorption kinetics, while Co and Fe contribute to improved electrocatalytic performance [18].
5. Exceptional corrosion resistance: HEAs exhibit superior resistance to corrosion even under severe electrochemical conditions, a property particularly beneficial for reactions such as OER and CO_2RR that occur in aggressive electrolytes [19].
6. Reduced reliance on noble metals: unlike conventional catalysts that depend heavily on platinum-group metals, HEAs can be formulated using earth-abundant and low-cost elements without compromising electrocatalytic performance. This compositional flexibility enables the development of cost-effective materials suitable for large-scale deployment [20].

Collectively, these characteristics establish HEAs as a versatile and promising platform for electrocatalysis, with the potential to address the major limitations of conventional catalysts, including cost, scarcity, and poor long-term stability. A growing body of research has demonstrated that HEAs can deliver competitive, or even superior performance in key electrochemical reactions, such as HER, OER, and CO_2RR, while maintaining structural integrity over extended operation [21–26]. Furthermore, the virtually limitless compositional space of HEAs enables the rational design of catalysts with application-specific properties, marking a shift from empirical alloying toward data-guided discovery. Nevertheless, this complexity presents substantial challenges: predicting catalytic behavior requires sophisticated computational models and high-throughput experimentation, while the synthesis of compositionally uniform and scalable HEA structures remains an open issue.

The versatility of HEAs lies in their ability to address the limitations of traditional catalysts. By tailoring the composition and synthesis methods, HEAs can optimize catalytic activity, durability, and

selectivity for a wide range of reactions such Green Hydrogen Production: This process encompasses two distinct electrochemical reactions: HER occurring at the cathode and the OER taking place at the anode [27,28]. For fuel cells and zinc/air batteries, OER typically encompasses two charge transport mechanisms, characterized by a substantial activation energy. As a result, the reaction exhibits slow kinetics and reduced faradaic efficiency Consequently, this leads to sluggish reaction kinetics and diminished faradaic efficiency [5,29]. Similar attributes hold for the nitrogen reduction reaction (NRR) as well [30,31]. MOR similarly exhibits gradual reaction kinetics, thereby impeding its practical application as a fuel source in DMFC on a commercial scale [32,33]. This highlights the current emphasis in materials science on exploring materials that are not only cost-effective but also more efficient, aiming to enhance their applicability across a diverse range of systems.

These challenges underscore the growing demand for advanced catalyst platforms that combine high activity, selectivity, and resilience under severe conditions, all which HEAs are well positioned to deliver. Their ability to incorporate both noble and non-noble elements, coupled with rich surface chemistry and tunable structures defect, makes them ideal candidates for overcoming the kinetic and stability bottlenecks that limit conventional catalyst performance.

In this review, we present a comprehensive assessment of recent progress in the development of HEAs for electrocatalytic applications. We examine the relationships between composition, structure, hybridization and function, covering synthetic approaches, theoretical frameworks, and performance in key electrochemical reactions. Special attention is given to the integration of computational and machine-learning methods in the rational design of HEAs, as well as the challenges and opportunities for their large-scale implementation in sustainable energy technologies.

2. High-entropy alloys design

The microstructure of HEAs is sustained on their elevated configurational entropy as a result of their complex composition. In a solid solution, the ideal configurational entropy of mixing (ΔS^{id}_{mix}) is obtained as described in Equation (1). This term can be understood as all the possible arrangement of the atoms distributed throughout the lattice considering that all the lattice sites can be occupied by any of the substitutional atoms that constitute the alloy in a random manner. In general terms, ΔS^{id}_{mid} increases if the proportion between constituent elements is closer to 1:1, and also, in an equiatomic alloy, if the number of elements increases. These both were the main compositional characteristics of one of the first and most famous HEA, the Cantor alloy [12].

$$\Delta S^{id}_{mix} = -R\sum_{i=1}^{N} x_i \ln x_i \quad (1)$$

Where R is the gas constant, N the number of elements of the alloy, and x_i the molar fraction of the element.

The importance that the ΔS^{id}_{mix} term has on the microstructure rely on the fact that this term, alongside the temperature (T) and the enthalpy of mixing (ΔH_{mix}), are the ones that define the Gibbs free energy of mixing (ΔG_{mix}) as is described in Equation (2).

$$\Delta G_{mix} = \Delta H_{mix} - T\Delta S_{mix} \quad (2)$$

The phase that will be formed (just considering thermodynamical aspects, and not kinetics) will be that that presents the most negative Gibbs free energy of formation (ΔG_f) (that in the case of a solid solution is equal to ΔG_{mix}). The competition between phases in a 5-component system is schematized in Fig. 1: in this, the solid solution is the most stable phase in the whole range of composition, in comparison to the intermetallic compounds indicated in the scheme, whose ΔG_f are less negative.

In order to calculate ΔH_{mix}, the scientific community has employed

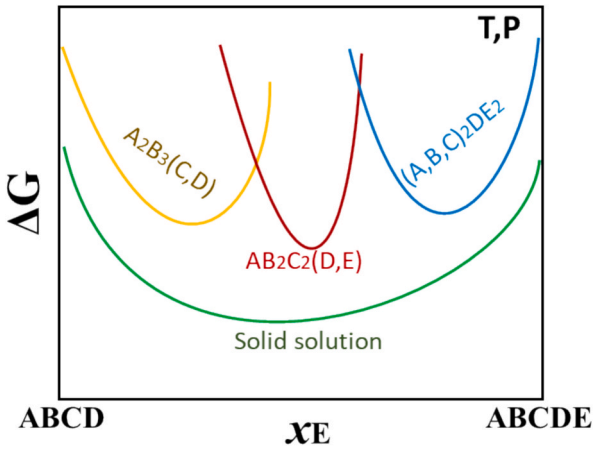

Fig. 1. Representative scheme of Gibbs free energy curves of different phases in competition in the hypothetic ABCDE high-entropy system.

Eq. (3), which exclusively considers the binary enthalpies of mixing (ΔH^{mix}_{AB}), but not those of superior order. This approach may be adequate for diluted solutions, but in the case of HEAs, where all the components are in similar proportions, the third- and higher-order interactions are quite important for the calculation of the energy of the phases in competition. Additionally, the entropic term not only considers the distribution of the occupancy in the lattice, the configurational contribution , but also vibrational, magnetic, and electronic contributions. Even more, the ΔS^{id}_{mix} term is a simplified version of the first; a real solid solution is not necessarily randomly distributed, since the characteristics (atomic radius, bonding energy, electronegativity, among others) of each element may influence the occupancy of the neighboring atomic sites (Eq. (3).

$$\Delta H_{mix} = \sum_{i=1,\, i\neq J}^{N} 4\Delta H^{mix}_{AB} x_i x_j \quad (3)$$

From the previous discussion, the design of HEAs from a microstructural point of view is far from simple and multiple factors influence the phase stability. However, since the trial-and-error approach is expensive in terms of economical cost (because of the raw materials, consumables, and characterization), time, and human effort, various design strategies have been utilized to predict the microstructure of HEAs from their composition. The two most important ones include semi-empirical parameters approach and the CALculation of PHAse Diagrams (CALPHAD) methodology; others such as theoretical first principle calculations or the effervescent artificial intelligence methods have been applied as well to predict and design the microstructure and phase equilibria of HEAs [34].

It is essential to consider the surface properties that directly govern the electrocatalytic behaviour of HEAs. These include: (i) the adsorption energy of reactive species (H*, OH*, OOH*), which determines the catalyst's affinity for reaction intermediates; (ii) the surface electronic density of states, which influences reactivity by modifying the occupancy level of d orbitals; (iii) surface segregation; (iv) potential-induced structural reconstruction, which is related to catalyst activation during redox cycles; (v) stability against selective leaching; (vi) the distribution of surface active sites, which can be studied via DFT or Monte Carlo simulations on the surface; (vii) the configuration and symmetry of the exposed surfaces; (viii) hydrophobic/hydrophilic surface properties, which affect the transport of reactants/products (H_2, O_2) and the stability of gas bubbles; (ix) resistance to oxidation or surface leaching; and (x) interaction with electrolytes and anion effects, where anion adsorption ($SO_4 2^-$, Cl^-, OH^-) on the surface may block active sites or modify the adsorption energy of key species. These characteristics define the activity, selectivity, and durability of HEAs and should be incorporated as central criteria in the rational design of commercial

electrocatalysts.

2.1. Semi-empirical parameters approach

In traditional alloys, the Hume-Rothery rules establish the necessary conditions for the solubility of two metals in a binary system: a difference in atomic size less than 15 %, a low difference in electronegativity, a low difference in valence electrons, and the same lattice structure in their pure state. These rules set hints about which are the elemental parameters and properties that must be considered in order to find relationships between composition and microstructure. Hence, the first approach to design HEAs was proposed in 2008 by Zhang and Zhou [35], utilizing the ΔH_{mix} and the average difference of atomic radius (δr) to cluster HEAs according to their microstructure in a visual manner. Hence, the authors established regions of ΔH_{mix}-δr in which the HEAs mostly presented disordered solid solutions, ordered solid solutions, intermetallic compounds, or an amorphous structure. From that point and onwards, several parameters have been proposed, including the number of itinerant electrons (e/a) [36], the valence electron concentration (VEC) [37], the electronegativity standard deviation ($\Delta\chi$) [36] the Ω-parameter (that summarizes into a single parameter both the entropic and enthalpic contributions) [38], etc.

The main advantage of this framework is that the design of HEAs becomes relatively accessible and at low cost, considering that no complex or time-consuming computing is necessary, as well as no paid software or databases are needed. In this sense, some free tools have been developed in order to facilitate the use of this approach, such as the High-Entropy Alloy Predicting Software (HEAPS) [39], that summarizes most of the available criteria and predicting parameters in a graphical user interface. Hence, the methodology offers a large scalability, that is not guaranteed by some of the other methods.

Nonetheless, as has been reported by some authors, the accuracy of the semi-empirical methodology is quite limited, and the approach is recommended only for rapid and early screening tasks rather than for accurate and specific design challenges, that can be appropriately addressed through the methods described in the following subsections. Additionally, since it is mostly based on the use of only two parameters to predict the microstructure, it can lead to a huge oversimplification of the problem, not being enough to have a deep physical interpretability.

Santiago-Andrades et al. [40] applied a wide range of semiempirical stability criteria, such as atomic size mismatch (δ), mixing enthalpy (ΔH_{mix}), valence electron concentration (VEC), Ω, and other parameters based on metallic bonding potentials, to two Al-rich Co-based HEAs produced by mechanical alloying. Although several criteria placed the alloys within the predicted single-phase region, metastable single-phase fcc structures were only observed in the as-milled state, while annealing led to multiphase microstructures. This highlights both the partial predictive power and the limitations of current semiempirical descriptors, especially for metastable systems beyond thermodynamic equilibrium. In this way, this method is not recommended for alloys synthetized by other techniques out of casting-based technologies, since most of the data utilized to define the criteria was based on alloys produced by these methods.

2.2. CALPHAD

The CALculation of PHAse Diagrams (CALPHAD) method is based on the computation of the Gibbs free energy of formation of all the possible phases in a defined system, considering interaction parameters of up to 3rd order (that is, that considers all the possible combinations in clusters of two and three elements) and their extrapolation into 4rd- or higher-order-parameters. This approach is extensively used in materials science and engineering via softwares such as ThermoCalc or PANDAT, coupled with commercial self-consistent thermodynamic databases for conventional alloys made of experimental and first principles calculated data. Hence, the equilibrium state is calculated by minimizing the Gibbs free energy of the system, resulting in mostly accurate phase diagrams, isothermal sections, transformation pathways, among others.

This method exhibits a considerably higher accuracy rate in the prediction of multicomponent alloys than the semi-empirical parameter methodology. This excellent prediction rate of the method is sustained not only in the excellent quality of the binary and ternary databases – which is crucial for the success in the prediction – but also on the findings of Tsai et al. [41] who reported that the intermetallic phases found in HEAs are inevitably inherited from their parent binary and ternary systems. Additionally, the method is computationally efficient – and less computationally costly than *ab initio* methods and can be coupled with high-throughput routines to expand the compositional space of the design context. It possesses two main drawbacks though: i) specialized databases for HEAs, such as TCHEA for ThermoCalc [42] – the most employed one for these purposes –, are not free; hence, its use is not as easy-to-access as the semi-empirical parameters methodology, and ii) accurate thermodynamic descriptions of the binary and ternary systems are fundamental for reliable predictions in HEAs, which are not available for absolutely all the elements employed to develop HEAs. In this way, the reliability of the results will be subjected to the systems that are included in the version of the used database. Thus, for novel HEAs where such data is scarce, the extrapolations can lead to significant uncertainties. Additionally, CALPHAD methodologies are only utilized to predict bulk microstructural features – phases formed and the distribution of these elements between them. Nonetheless, this methodology is not capable to predict how the atoms are distributed in the lattice, for example, forming short-range ordering (SRO), as it is typically observed in certain families of HEAs. Despite this may not be relevant for mechanical applications, it is quite important in order to understand the mechanisms and the phenomena occurring in the surface of the samples during electrocatalytic reactions.

Still, the literature offers multiple cases in which the CALPHAD methodology is successful in predicting the microstructure of HEAs [43–45]. For instance, Kozlík et al. [46] investigated the phase formation in three refractory HEAs (AlTiNbMoV, AlTiNbTaZr, and AlTiNbMoCr) and demonstrated that CALPHAD predictions qualitatively matched the experimentally observed microstructures in two out of *three* cases. While the method correctly predicted the formation of a single-phase BCC structure in AlTiNbMoV, and the presence of an intermetallic phase in AlTiNbTaZr, it overestimated the stability of the Laves phase in AlTiNbMoCr at high temperatures, highlighting both its potential and current limitations in multicomponent systems.

2.3. Ab initio methods

Ab initio, or first-principles methods prescind of experimental or semi-empirical data as the previous approaches. These computational approaches, primarily based on density functional theory (DFT), enable the evaluation of fundamental material properties directly from the electronic structure. In the context of HEAs, where compositional complexity and configurational disorder are intrinsic features, first-principles provide a rigorous framework to investigate phase stability, mechanical behavior, and electronic characteristics.

One of the main challenges in modeling HEAs arises from their inherent chemical disorder and vast compositional space. To address this, several techniques have been developed to incorporate disorder into DFT-based calculations. The Special Quasirandom Structure (SQS) method allows the construction of supercells that simulate the local atomic neighborhood of a random solid solution [47]. Similarly, the Coherent Potential Approximation (CPA) offers an effective medium approach to model disordered alloys within the framework of multiple scattering theory [48] and is particularly useful for exploring electronic and thermodynamic properties across broad composition ranges.

Despite their predictive power, first-principles methods face several limitations when applied to HEAs. The main one, is the high computational cost associated with modeling large supercells necessary to

represent disordered systems accurately. This is especially relevant, if is compared with the rest of the approaches. SQS structures, for example, become increasingly expensive as the number of elements and degree of disorder grow. Additionally, standard DFT approximations may struggle to capture the delicate energy differences between competing phases, especially in systems with strong magnetic or electronic correlations [49]. In this case, this methodology may not be worth in order to design HEAs with more elements than the usual, over 7 elements, for example – since the computational cost would be quite high, and may not be totally adequate addressing the design of HEAs containing magnetic elements. Just as the other methods, it may not be helpful to predict the presence of unexpected phases; for example, refractory high-entropy alloys fabricated via powder metallurgy use to exhibit oxides or carbides dispersed in the matrix [50]. These phases will not be considered in DFT approaches, and most importantly, the oxide- or carbide-forming element will still be considered in the computed solid solution, despite not totally constituting it.

First-principles methods have been successfully employed in the case of HEAs. For instance, the thermodynamic stability of the CoCrFeMnNi FCC solid solution has been validated through DFT calculations [51]. Cluster expansion methods have been employed to address the phase segregation in refractory high-entropy alloys such as the NbTiVZr, HfNbTaTiZr, and AlHfNbTaTiZr [52]. Several other cases have been reported not only describing microstructure, but also with a focus on mechanical properties [53], nuclear applications [54], electrocatalysis [55].

2.4. Artificial intelligence (AI) methods

Recently, the exponential rise of artificial intelligence (AI) and machine learning (ML) has permeated a wide range of fields, including, notably, the design and microstructural prediction of alloys from both compositional and processing perspectives. In this context, the use of AI in the prediction of new high-entropy alloys (HEAs) has become especially attractive, due to its relative novelty and enormous potential [34,56].

The most commonly used AI methods rely on datasets that include a set of input parameters and at least one output parameter. The goal is to uncover complex, non-explicit relationships between these variables, unlike traditional semi-empirical methods, which typically use simple, explicit correlations between two parameters to predict microstructural outcomes. With AI-driven approaches, users can compute results for new combinations of input variables by leveraging the patterns and relationships embedded in the original dataset.

This AI approach offers several advantages against the previously mentioned HEAs synthesis methods. In comparison with the semi-empirical methodology, the AI methods offer the possibility of find relationships in a multi-dimensional space, considering for example, all the semi-empirical parameters at the same time to obtain a classification or prediction model; the semi-empirical parameter approach is mostly based on the use of only two parameters simultaneously, since is based on a simple and visual clustering method.

Unlike CALPHAD, the AI methods do not depend on a paid database and can process an enormous amount of data in less time. In this manner, once the dataset is already prepared (this will be detailed in the next paragraph), the AI methods are computationally cheap. This is also an important advantage when compared with the first principles methodology. Additionally, unlike CALPHAD prediction, the AI not only can be used to design alloys and their microstructure from their composition, but it can also be used to predict stacking fault energy values [57], electrocatalysis [58], hardness [59]. Clausen et al. [60] developed a computational workflow combining DFT, graph convolutional neural networks (GCNNs), and Bayesian optimization to predict and optimize the catalytic activity of HEAs for the oxygen reduction reaction. By sampling adsorption energies across the Ag–Ir–Pd–Pt–Ru composition space and training a GCNN model, they could rapidly predict site-specific adsorption properties. This enabled an efficient estimation of net catalytic activity, accounting for co-adsorption effects, and guided the search for optimal alloy compositions. Their framework illustrates how machine learning can overcome the challenges of modeling vast HEA composition spaces not only for microstructural prediction but also for catalyst discovery.

The main limitation of the method relies on the training dataset. In the case of HEAs prediction, the dataset should include a wide range of compositions with a representative number of entries for each subsystem. Nevertheless, there are certain HEAs that are considerably most studied than others (such as the FeCoNiMnCr – Cantor – alloy, or the HfNbTaTiZr – Senkov – alloy) and thus, the datasets can be unbalanced, and insufficient datapoints may there be for alloys that escape from the typical compositions. In this manner, if an element is not sufficiently contained in the data, the methodology will not provide accurate microstructural predictions. For example, rhenium is a promising element for electrocatalytic applications, but for various reasons it has not been widely explored as a constituent element in HEAs. Hence, AI-based predictions for a Re-containing HEA will not be reliable enough yet.

Additionally, there is a lot of features that may not be considered as an input parameter – for example, related to the fabrication route – that may have an influence in the outcoming microstructure. However, this may be the only method that can include that into their algorithm, if enough quality data is provided. In this way, the database not only must be diverse and numerous, but also must be curated. Additionally, AI-models usually lack physical interpretation and since in some cases are not explicit, they work as black boxes.

Multiple articles have addressed the design of HEAs employing IA-based approaches [61], including neural networks [62–64], support vector machines [64,65], k-nearest neighbors [64,65], random forest [66], gradient boosting trees [67] and support vector regression [68]. However, the most important advantage is that AI methods offer the possibility of integrating all the previous methods into one. This, by using both experimental data, their calculated semi-empirical parameters, thermodynamic predictions obtained by CALPHAD, and theoretical data in the dataset, training the model with a diverse set of sources that can enhance the accuracy of the model. This is, for sure, the most promising feature of AI methods. Hence, various articles combining *ab initio* and machine learning [69,70] or CALPHAD and machine learning [71,72] have been published addressing HEA design.

2.5. Summary of the section

From a design perspective, each of the methodologies described in the present section offers different strengths and limitations. These are summarized in Table 1. Semi-empirical approaches are rapid, low-cost, and easily accessible, making them useful for initial screening, but they often oversimplify phase stability and have limited predictive accuracy. Since this method is mainly based in data obtained from samples produced via casting methods, it may not be useful for samples produced by other methods, such as powder metallurgy as-cast or homogeneized conditions predicted microstructure are not CALPHAD, on the other hand, provides higher reliability for multicomponent systems when robust thermodynamic databases are available, yet its predictive power decreases for novel compositions with scarce binary/ternary data; nonetheless, they are currently employed as the method of reference for HEA design. However, its main disadvantage relies on the fact that most HEA-specific databases are not freely accessible. *Ab initio* methods deliver the highest physical interpretability and accuracy at the electronic level, but are computationally expensive and limited to smaller supercell sizes, restricting their use for broad compositional exploration. AI and machine-learning frameworks can integrate experimental, thermodynamic, and first-principles data to explore vast compositional spaces efficiently, but they depend critically on the quality, balance, and representativeness of the training dataset. In practice, hybrid strategies

Table 1
Summary of design methods of HEAs.

Prediction methodology	First principles	CALPHAD approach	Artificial Intelligence	Semi-empirical approach
Accuracy	High (electronic level)	Moderate to high (thermodynamic level)	Variable (depending on training data)	Low to moderate (approximate)
Computational cost	Very high	Low to moderate	Low (after training)	Very low
Physical interpretability	High (quantum-based)	High (thermodynamic basis)	Often low (black-box models)	Medium to low (simple physical basis)
Scalability to large systems	Poor (limited to small systems and idealized models)	Good (multicomponent systems supported)	Excellent	Excellent
Data requirements	Minimal (no prior data needed)	High, requires databases (with commercial ones as the most used)	High (needs large and curated datasets)	None (based on atomic properties)
Ability to model disorder	Moderate (e.g., SQS, CPA)	Good (via mixing models and sublattices)	Indirect (via features or learned patterns)	None explicitly
Predictive scope	Ground-state properties, enthalpies, bonding, etc.	Phase equilibria, free energies, transformations	Broad: mechanical, thermal, phase stability, etc.	Phase formation tendencies only
Use cases	Validation and fundamental understanding	Process and alloy design, phase selection	Rapid screening, inverse design, hidden trend discovery	Quick screening and filtering
Limitations	High cost, small cells, slow	Needs assessed databases, extrapolation uncertainty	Data scarcity, generalizability, interpretability	Oversimplification, exceptions to rules

that combine these methods – for example, CALPHAD-guided composition selection refined by DFT, or AI models trained on both calculated and experimental data – are increasingly proving to be the most effective route for rational HEA design, and they are expected to govern the HEA – and alloys, in general – design during the following decades.

3. Synthesis methods of HEAs for electrocatalysis applications

HEAs can be synthesized by means of different fabrication routes in order to produce either powder, thin films, ribbons, or bulk parts. Additionally, the preparation of HEA nanoparticles (HEA-NPs) has been reported as well employing different techniques. All of them result in particularities in their composition (homogeneity, interstitial elements content, etc.), microstructure (grain size, dislocation density, metastable phases, twins, etc.) and therefore, in their performance; hence, it is quite relevant to have a notion of how HEAs are prepared and how the fabrication routes affects them in order to design and synthetize novel HEAs with excellent. Additionally, the microstructure of HEAs used in electrocatalysis can adopt various forms, including single-phase solid solutions, dual-phase microstructures, amorphous or nanocrystalline phases, each influencing catalytic performance through surface area, electronic structure, and defect density. Straightforwardly, the fabrication route plays a fundamental role in the formed microstructure, not only in terms of formed phases, but also in terms of interstitial elements content, grain size, surface area, defects density, and of course, cost and scalability.

In the present section, the main preparation routes for HEAs employed in electrocatalytic applications according to the current literature will be reviewed.

3.1. Casting

Casting techniques are the most used to fabricate HEAs at the laboratory scale, including arc melting by far the most utilized for the study of mechanical properties of HEAs – induction melting, beam melting, and melt spinning [73]. In the case of arc melting, it is usually conducted in vacuum or argon atmospheres to avoid oxidation of the constituent metals, especially when these are highly susceptible to oxidation, such as refractory metals. These metals also possess elevated melting points; therefore, if one of them is included in the alloy, higher temperatures will be required to melt all components [74].

The typical microstructures obtained through casting present dendritic patterns with chemical segregation and coarse grain sizes, as is depicted in Fig. 2. To minimize this issue, multiple re-melting steps are often employed, and subsequent homogenizing treatments can be applied as well. Although this extended high-temperature exposure promotes grain growth, it results in a more homogeneous microstructure. However, uncontrolled cooling rates can lead to metastable microstructures, which may evolve into closer-to-equilibrium structures after further heat or thermomechanical treatments. Nevertheless, since electrocatalytic studies are conducted at room temperature, metastable microstructures that can be beneficial for these applications offer an interesting possibility.

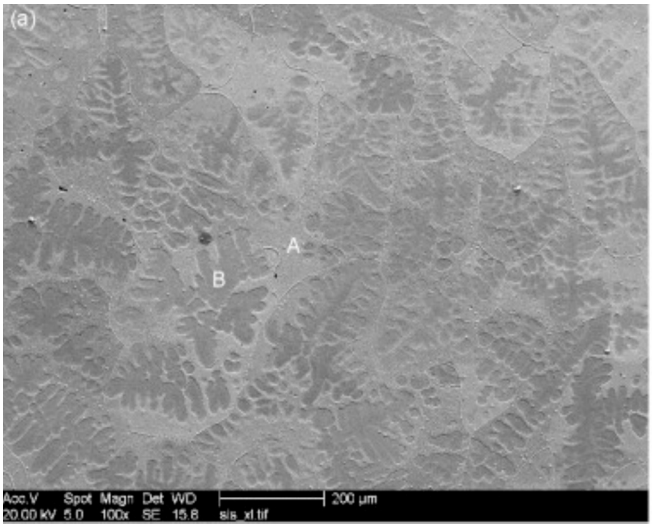

Fig. 2. SEM image of the microstructure of as-cast AlCrFeCoNi HEA [75].

Overall, these processes are much simpler than other fabrication techniques and allow the preparation of larger bulk samples, typically in the form of rods or bars. For this reason, casting techniques are preferred for structural applications due to the size scale of structural parts. The most significant drawback of this technology for electrocatalytic applications though is the low specific surface area – while pores may form as solidification defects, their contribution to enhancing the exposed electrocatalytic area is negligible.

Some bulk HEAs for electrocatalytic applications have been fabricated employing this route. For example, equiatomic FeNiMnCrCu and FeCoNiCrAl HEAs were prepared by arc melting, employing 4 re-melting steps to ensure homogeneity [76]. Meanwhile the latter presented a single-phase FCC solid solution, the first possessed a microstructure constituted by two FCC phases and a BCC phase. Zhang et al. [77] reported the fabrication of the Cr15Fe20Co35Ni20Mo10 (at. %) HEA by means of arc melting under an Ar atmosphere. Subsequently, the ingots

were subjected to homogenization in vacuum at 1200 °C for 48 h, followed by hot rolling at 1100 °C and cold rolling. After that, annealing treatments at either 800 or 1150 °C for 1 h followed by air cooling were conducted. With the final annealing at high temperature, a single-phase solid solution microstructure was obtained; after annealing at 800 °C instead, the precipitation of the μ phase – an intermetallic compound with A_7B_6 stoichiometric formulae – was observed. In this way, both the composition and the thermomechanical history play a fundamental role on the microstructure of the alloys.

As was mentioned before, casting techniques usually conduct to parts with low or null porosity. This aspect is quite desired for structural applications, since pores can act as stress raiser, conducting to poorer mechanical performance. Nonetheless, electrochemical performance is usually enhanced by the presence of pores, since these increase the geometrical component of the active electrochemical surface. In this manner, the casting route has been usually followed by a dealloying process [78,79]. This consists of the application of a etching agent (a strong acid or alkaline reagent) that will corrode preferably one constituent of the bulk alloy, generating pores and channel that will increase the exposed area of the part.

3.2. Powder metallurgy

The powder metallurgy (PM) includes techniques where powder is employed as the raw material to obtain bulk samples through compaction and sintering steps, mostly in the solid state [80]. The powder can be pre-alloyed, via mechanical alloying or atomization techniques, or alternatively, elemental powders can be blended and alloyed in situ during the sintering step. However, a certain degree of chemical heterogeneity may result in the latter case if the sintering time is insufficient [81]. Samples produced from pre-alloyed powders usually present more homogeneous microstructures; nevertheless, in the case of mechanical alloying, higher oxygen and nitrogen content can be found compared to those produced by atomization. This has been particularly considered in those HEAs constituted by oxide- and nitride-forming elements, such as Al or refractory metals, but those cases where interstitial elements remain dissolved in the interstitial voids of the lattice are still relevant, especially for electrocatalysis applications. This will be discussed in the following section.

During mechanical alloying, the powder is subjected to continuous impacts from milling balls, accelerated by a centrifugal field. Thus, fracture, plastic deformation, agglomeration, cold welding, and eventually diffusion led to the alloying. The process is usually conducted in a protective atmosphere, mainly Ar, to avoid contamination due to the high surface area of the powder. Other sources of contamination include the milling balls and container material, especially relevant if they have lower hardness than the milled powders, or the use of organic reagents (referred as process control agent, aimed to hinder cold welding) which may lead to carbon contamination.

In this way, Dai et al. [82] synthesized a MnFeCoNi HEA by means of mechanical alloying to study its electrocatalyst performance. The authors blended pure elemental powder materials (with purity over 99.5 % and a particle size inferior to 45 μm) in equiatomic proportion and loaded them into a cemented carbide vial. Then, the sealing procedure was carried out in a glove box filled with Ar, as is usually done during mechanical alloying of metallic materials (susceptible of oxidation). The mechanical alloying was conducted in a planetary ball mill, with a rotational speed of 500 rpm and a ball-to-powder ratio of 20:1. Additionally, 0.5 ml of ethanol as process control agent was utilized. As can be appreciated in Fig. 3.a and Fig. 3.b, after 60 h of milling, the powder presented a sheet-like morphology; more importantly, according to the XRD pattern, a FCC single-phase solid solution was formed. In the same way, a homogeneous distribution of the elements was observed in the analyzed particle, as is illustrated in Fig. 3.f-i.

Regarding consolidation technologies, the most common include pressure or conventional sintering, where the powder is first compacted into a green sample, then heated inside of a furnace under an inert atmosphere, a reductive atmosphere, or vacuum. The consolidation relies on diffusional mechanisms, which is why relatively high temperatures between 0.6 and 0.8 times the melting point of the alloy, typically are

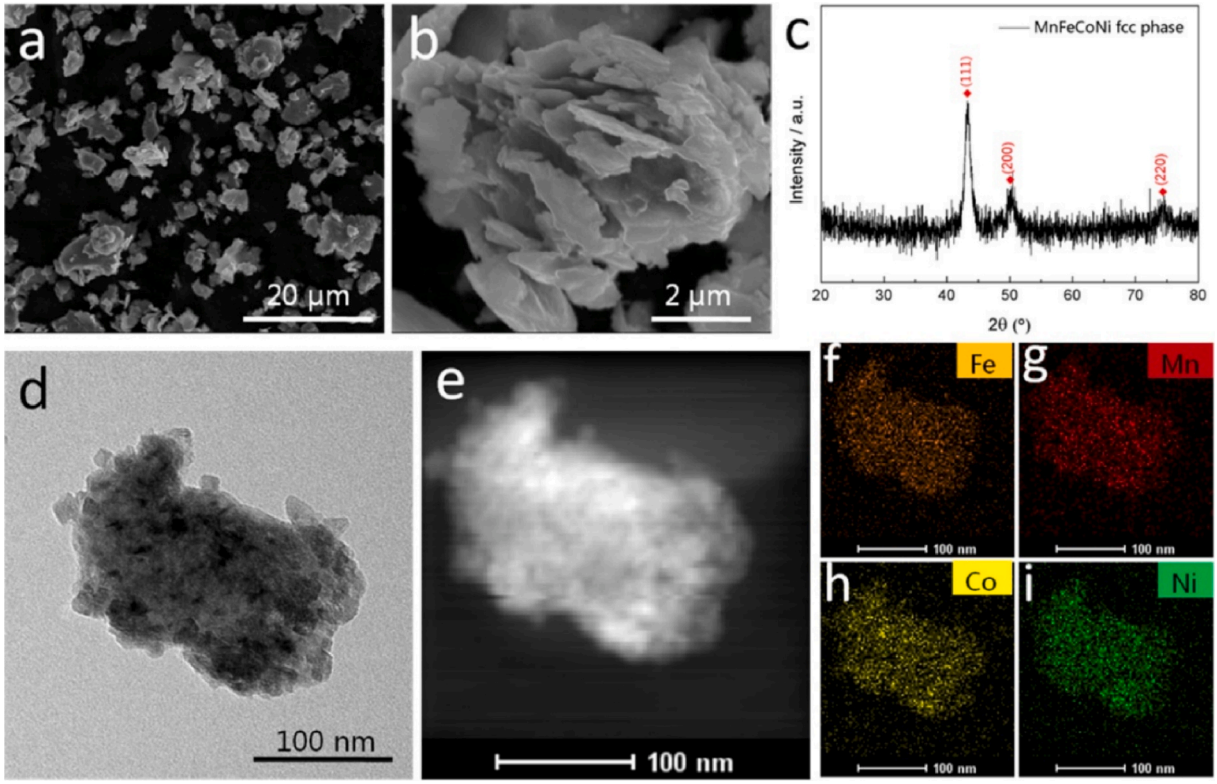

Fig. 3. a,b) SEM images, c) XRD pattern, d) TEM, e) HAADF-STEM, and f-i) EDS mapping images of 60 h-milled powders of MnFeCoNi HEA [82].

required. To facilitate the sintering process, other technologies – such as hot pressing (HP) and high-pressure sintering (HPS) – additionally involve the application of a uniaxial load. In these cases, stress typically ranges between 10 and 50 MPa for HP and over 500 MPa for HPS [81,83]. Lastly, spark plasma sintering (SPS) has been widely used in the powder metallurgy development of HEAs. In SPS, the powder is loaded into a mold and subjected to a uniaxial stress – typically between 10 and 50 MPa – while a current flows through the powder. The contact points between particles – where diffusion occurs, and thus sintering – act as high-resistance points, generating localized high temperatures due to the Joule effect.

The major advantage of powder metallurgy processes – especially for electrocatalytic applications – is the ability to fabricate porous parts, either by using shorter sintering times or lower temperatures than those required for full densification (leading to uncontrolled porosity distribution, size, and shape) or by using the space-holder technique. In the latter, the alloy powder is blended with an easily removable material that does not interact with the alloy – such as NaCl, that is soluble in water, on the contrary of the metallic alloys, for example. After consolidation, the space-holder material is removed, leaving pores whose size and shape are determined by the characteristics of the space-holder particles, allowing for controlled porosity. This approach was employed by Tang et al. [84] preparing porous CoCrFeNiMo parts employing Mg powder as a space-holder. This last presented negligible effect on the phase formation or phase composition – as expected from a space-holder and was mostly eliminated during microwave sintering at 950 °C.

Similar to bulk parts produced by casting, dealloying post-processes can also be utilized with PM-ed parts. Ma et al. [85] reported the fabrication of the equiatomic CoCrFeNiAl HEA powder by means of mechanical alloying for 60 h under 250 rpm in an Ar atmosphere. Then, the sample was consolidated using SPS at 950 °C for 10 min under 50 MPa of stress in Ar atmosphere as well. Fig. 4.a depicts the SEM image of the surface of the as-sintered part. Additionally, a sheet was cut from the as-sintered part an put into an autoclave containing 20 ml of 0.04 M HF solution at 90 °C for 5 h. Fig. 4.b illustrates how the microstructure evolved due to the action of the acid solution, presenting a highly superior exposed area for electrochemical reactions. It is important to highlight though that the action of the HF reagent also altered the composition of the surface of the sample, as was demonstrated by XPS experiments, shown in Fig. 5.

Alternatively, milling processes at extremely low temperatures have been employed to produce HEA particles in the micro- and nanoscale. This process, known as cryomilling or cryogrinding, employs cryogenic liquids (such as liquid H_2 or liquid N_2) to cool the vial, hindering cold welding, and increasing the brittleness of the powder (that was alloyed in a previous step). As a result, the fracture mechanism is promoted, and fine particles are produced. An illustrative example of this approach is provided by Madan et al. [58] who reported the preparation of an ingot of the equiatomic CuCoMnNiFe HEA, by means of vacuum arc melting (with three to four remelting steps) followed by homogenization at 1000 °C for 10 h and quenched. After that, the ingot was cut into smaller pieces and subjected to cryomilling using liquid N_2 for 7 h, in Ar atmosphere to avoid oxidation. In this manner, a homogeneous powder of the previously mentioned composition with an average particle size of 14 nm was obtained.

3.3. Liquid-medium nanoparticle synthesis

In the previous approaches, the focus was on increasing the electroactive surface by the generation of nano- and micro-pores and channels. Other synthesis techniques, alternatively, are focused on the obtention of nanoparticles (NPs) – that is, particles in the nanometric scale with an enhanced surface-to-volume ratio. There are different ways to produce nanoparticles, but all of them are based on the competition of nucleation and growth (or coalescence) rate: in order to produce NPs, the nucleation rate should be higher than others in competition. Some reviews are already available in literature covering the main routes for the obtention of HEA-NPs, and can be found elsewhere [86].

One of the most promising ones corresponds to wet chemical methods, that include colloidal synthesis, co-precipitation, and solvothermal methods, among others. These are characterized by their relative simplicity and low temperatures (especially the two firsts), as well as by adequate control of the NPs features. In the colloidal method, the nanoparticles are formed in a liquid medium and stabilized by means of surfactants. Li et al. [55] reported the fabrication of non-equiatomic Pt-Ni-Fe-Co-Cu HEA-NPs starting from acetylacetonate-based complexes of the individual metallic constituents as precursors in an oleylamine solution, using also a cationic surfactant (CTAC) for NP stabilization. The synthesis included simple processes such as sonication, magnetic stirring (at 220 °C for 2 h), centrifugation, and washing steps. Fig. 6 illustrates the microstructural features of the resulting NPs: as can be seen, a narrow particle size distribution centered around 3.4 nm was obtained, as well as a homogeneous distribution of the elements in the particles, despite they were added to the solution separately.

In the solvothermal method, the solution containing the precursors is loaded into an autoclave and subjected to relatively high temperatures (over 100 °C, causing the evaporation of the solvent). Hence, the pressure inside the sealed vessel increases and in conjunction with the high temperature, promotes the nucleation of the nanoparticles. This procedure was followed by Broge et al. [87] synthetizing HEA-NPs with 8 to 12 components. For this, the authors employed acetylacetonate −based precursors and dissolved in anhydrous ethylene glycol. Then, the solutions were transferred into steel autoclaves and sealed and heated up to 170, 200, and 230 °C for 20 h. Subsequently, the products were washed in ethanol and acetone and dried. In the case of the 8-components HEA-NPs, an average particle size of 2.55 nm was obtained. Additionally, a

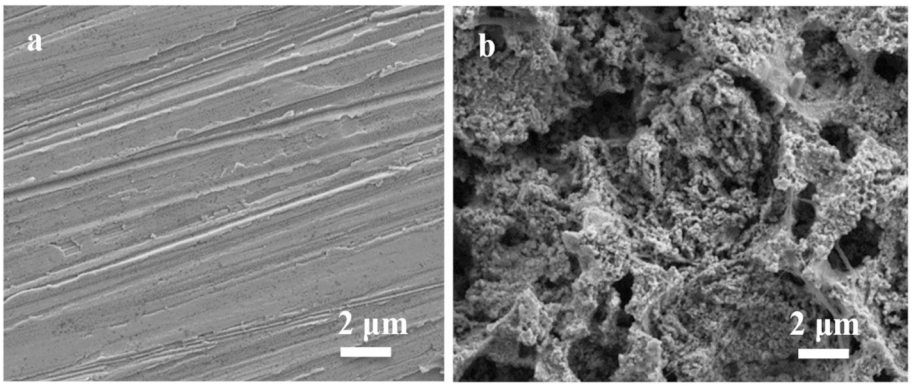

Fig. 4. SEM images of a) as-sintered and b) dealloyed HEAs parts [85].

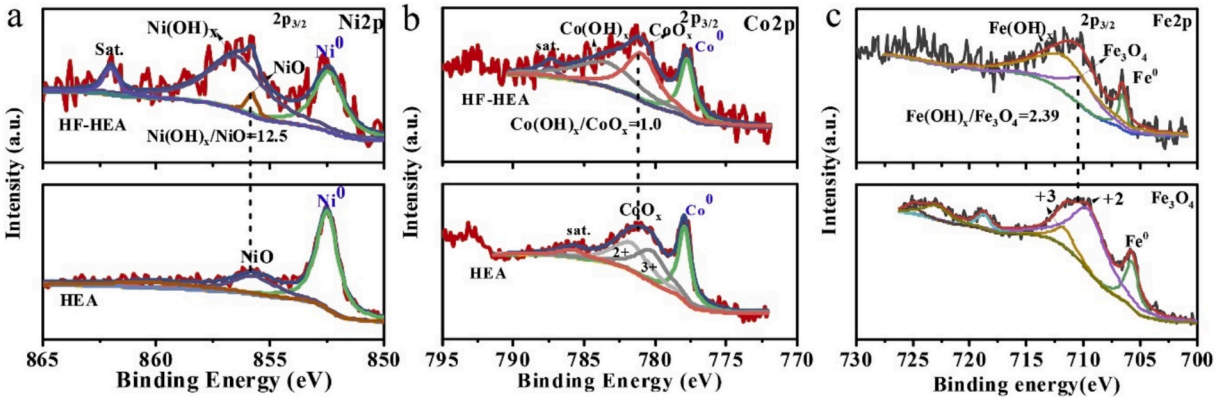

Fig. 5. High-resolution XPS analysis of as-sintered sample (indicated just as HEA in bottom images) and of sample additionally subjected to dealloying with HF solution (indicated with HF-Hea in top images) and the spectra of a) Ni2p, b) Co2p, and c) Fe2p [85].

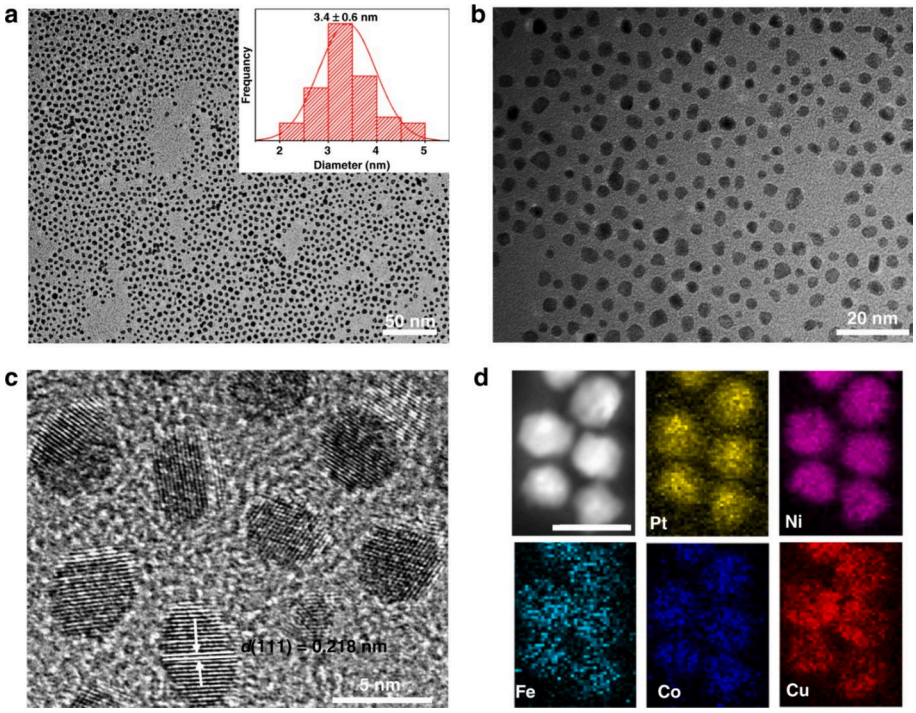

Fig. 6. A) tem image of nanoparticle and particle size distribution in the insert, b) tem image, c) hrtem image, and d) eds-stem mapping images of hea-np[55].

single FCC lattice structure was obtained. Nevertheless, in the other cases, at least more than one phase was obtained.

3.4. *Thermal shock nanoparticle synthesis*

Shock thermal synthesis (STS) techniques have also been employed to synthesize HEA-NPs. In these methods, metal precursors are decomposed or reduced at extremely high peak temperatures (up to 3000 K) for very short durations, using rapid heating and cooling rates on the order of 10^2–10^5 K/s. These rapid thermal changes are facilitated by high-conductivity substrates that additionally help limit nanoparticle growth. Besides, the high cooling rate also hinders elemental separation, maintaining a homogeneous distribution of the elements throughout the NPs. Common substrate materials include carbon-based materials such as carbon nanofibers (CNF), graphene, and graphene oxide (GO), that besides their good conductivity can act as reducing agents; in these cases, the preparation method is usually referred to as carbothermal shock synthesis.

Different technologies can be used for heating purposes: microwave heating, Joule heating, and laser heating – ranked from least to most energetic, and from greatest to least mass production capacity. The synthesis of PtPdFeCoNi HEA-NPs employing microwave heating has been reported by Qiao et al. [88]. In this case, the authors used a partially reduced graphene oxide (rGO) film as a substrate, due to its enhanced thermal conductivity but still good microwave absorbability. Additionally, they also tested CNF and carbonized wood as substrates as well. Chloride-based metal precursors were dissolved in deionixed water and then dropped into the substrate, to then be sealed in a bottle filled with Ar. After that, the bottle was transferred into a microwave of 1200 W of power and heated for 10 s, reaching a temperature of 1850 K in the case of rGO substrate. Hence, homogeneously mixed NPs of 12 nm of average (and with a d95 of 20 nm) were distributed in the film.

Zhao et al. [89] reported the synthesis of NiCoFeCrMo HEA-NPs by means of wet synthesis followed by Joule-heating-based shock thermal synthesis. Chloride-based metal precursors were added to a graphene solution and then reduced with sodium borohydride. After collecting the product, it was wrapped in a carbon cloth, that was connected to the Joule heating device in a nitrogen atmosphere. Hence, the sample was

exposed to 1300 K during 0.1 s followed by rapid cooling to room temperature. Hence, NPs with an average particle size of 17.49 nm were homogeneously distributed across the graphene substrate.

On the other hand, laser-based spark ablation (STS) was employed to synthesize HEA nanoparticles containing 5 to 20 components, as reported by Yu et al. [90]. The main results and steps for the preparation are illustrated in Fig. 7. For this, CNFs were dipped into a solution already containing the metal precursors. Then, the substrate loaded with the precursors are placed in a chamber filled with Ar and exposed to the wave fiber laser (with an energy density of 12.5 J cm^{-2}); hence, the temperature of the CNFs can reach up to 2000 K in 10 ms. As it is shown in Fig. 7.g, the temperature not only increases rapidly, but also decreases down to room temperature in less than 2 s, preventing elemental separation. Hence, the HEA-NPs with an average particle size of 11.6 nm are produced, presenting a homogeneous distribution of the elements, as can be seen in Fig. 7.g.

An alternative to the previous techniques is the fast-moving bed pyrolysis. In these techniques, the metal precursors supported by a granular substrate are rapidly displaced at the interior of a furnace to reach high heating rates. Hence, the precursors are decomposed by fast pyrolysis. However, in opposition to thermal shock techniques, the material is maintained at high temperatures for a prolonged time. This was the approach used by Gao et al. [91] to prepare quinary-to-denary HEA-NPs using chloride-based metal precursors, different granular substrates (carbon materials, alumina, and zeolite) and exposition to 923 K for 120 min in Ar (for alumina and zeolite as substrate, H_2 was employed as reduction gas). In this manner, NPs of 2 nm were produced, exhibiting a homogeneous distribution of the elements.

3.5. Heas thin films synthesis

This category groups various technologies that enable the synthesis of HEA coatings over a substrate. Since the electrocatalytic reactions occur at the surface of the electrodes, thin films is an excellent alternative to obtain outstanding electrocatalytic performance, by means on composition and defects tuning, but at a reduced price, since the employed elements will be only deposited at the surface of a substrate. Among these techniques, the most widely used are magnetron sputtering, pulsed laser deposition, and electrodeposition. Magnetron sputtering allows the co-deposition of multiple metal targets (that provide the elements that will constitute the film) to produce complex and uniform compositions by means of the collision of charged ions of Ar that eject metallic atoms from the target and then are directed to the substrate by means of the application of an electrical field [92]. In pulsed laser deposition instead, the metal target is irradiated with a high energy laser pulse that vaporize the atoms that then will be deposited on the substrate [93].Electrodeposition, in turn, is a still good but cheaper alternative because it does not require the equipments of the other thin film synthesis techniques. Besides, the low processing temperatures and the possibility of using versatile or complex geometries of the substrates gives several advantages to electrodeposition [56]. The readed are referred to the following references or further detail of the experimental setups and the microstructures resulting from these techniques [94–96].

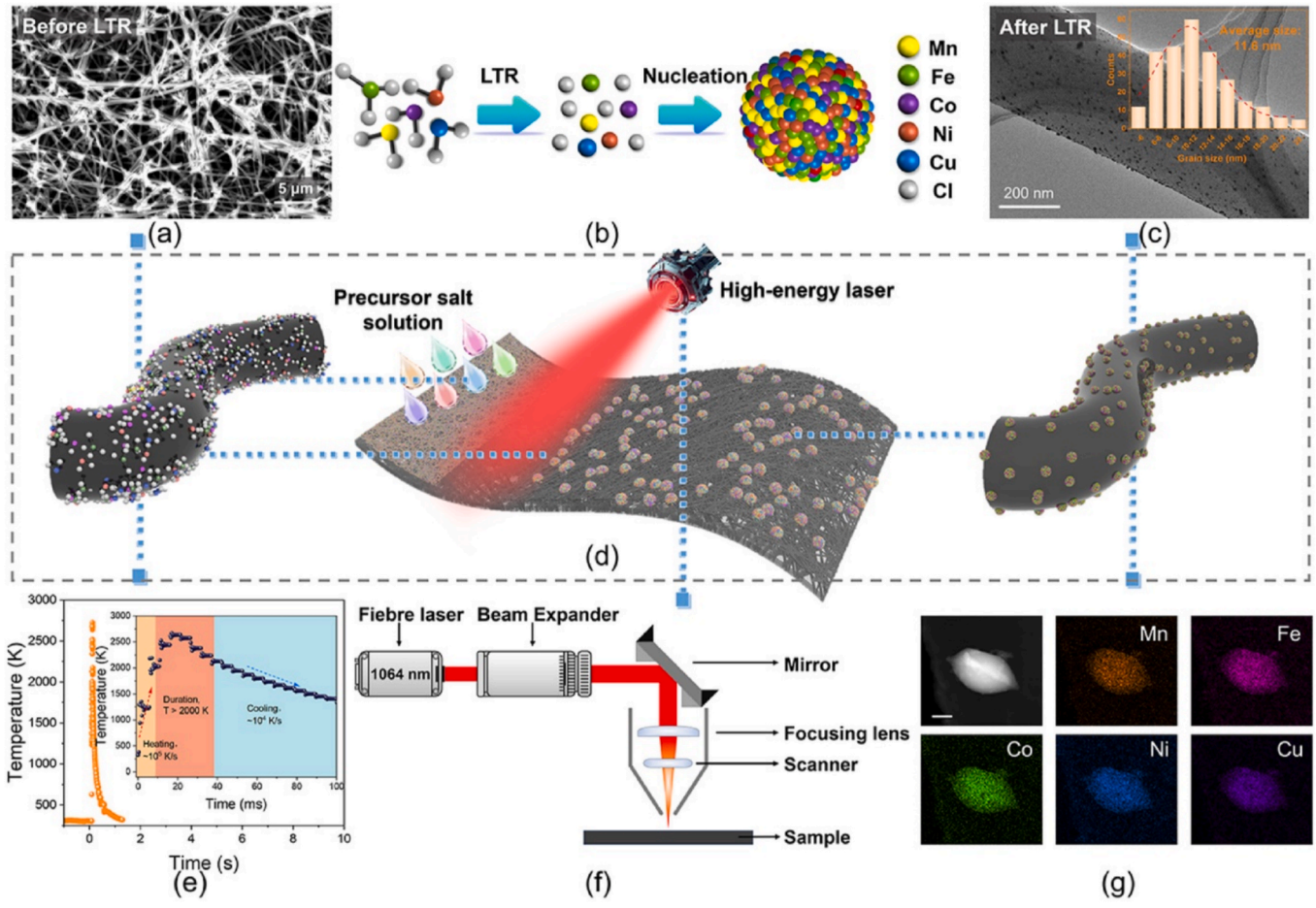

Fig. 7. A) sem image depicting salt metal precursors on cnfs before laser-based sts; b) scheme illustrating decomposition of metal precursors and nucleation of nps; c) tem image of hea-nps on cnfs after sts with the insert showing the particle size distribution; d) scheme of the synthesis process; e) temperature profile during synthesis; f) scheme of the experimental laser setup; and g) haadf-stem image and eds mapping images of constituent elements in a nanoparticle.[90]. Reproduced with permission of Elsevier.

3.6. Summary of the section

Fig. 8 classifies common HEA synthesis methods by scalability and relative cost. Powder metallurgy occupies the first quadrant (high scalability, high cost) due to its industrial applicability and precise compositional control, offset by the high cost of producing high-purity multicomponent powders and energy-intensive sintering. Thermal shock nanoparticles synthesis is placed in the second quadrant (low scalability, high cost) as extreme thermal gradients, low throughput, and specialized equipment limit scale-up and raise costs. The third quadrant (low scalability, low cost) includes liquid-medium nanoparticles synthesis, a laboratory-scale method with simpler equipment and lower cost, yet constrained by particle size and dispersion control during upscaling. The fourth quadrant (high scalability, low cost) contains the casting process, which under economies of scale and existing industrial infrastructure can achieve high production capacity with reduced unit cost. This framework facilitates direct comparison of synthesis strategies in terms of technical feasibility and economic viability.

Table 2summarizes the main HEA synthesis methods, complementing the scalability–cost diagram in Fig. 8 Given that quantitative metrics such as yield or surface area strongly depend on alloy composition, precursor purity, and processing conditions, values are expressed qualitatively to provide a representative and comparable overview across techniques. This qualitative approach highlights the trade-offs in cost, scalability, and achievable surface area that define each method's positioning within the quadrants.

Table 2
Comparative overview of HEA synthesis methods. Yield termed qualitatively (—/–/+) based on typical literature descriptions; actual values depend on precursors, setup, and composition.

Synthesis method	Yield	Relative cost	Scalability	Specific surface area
Thermal shock nanoparticle synthesis	–	High	Low	High (laboratory-scale NPs)
Liquid-medium nanoparticle synthesis	–	Low–Medium	Low	High
Powder metallurgy	+	Medium	High	Medium (porous samples)
Casting process	++	Low*	High	Low

*Low cost under economies of scale; initial capital investment remains high.

4. Electrocatalytic performance of HEAs

Recently interest in high-entropy alloys (HEAs) has grown rapidly due to their emerging role as functional materials, particularly as highly promising electrocatalysts. This growing attention is driven by both theoretical and experimental advances that highlight their unique structural and electronic properties under electrochemical conditions.

Analyses relating to energy efficiency are lacking and further validation is needed. Most studies have been carried out under laboratory conditions with idealized configurations, such as glassy carbon electrodes and low current densities. It is necessary to move towards testing in complete electrochemical devices, such as PEM, AEM, or alkaline electrolyzes, operating under industrial conditions. Synthesis methods such as dealloying, liquid-phase reduction, or electrochemical reconstruction processes must be assessed in terms of scalability, cost, and structural control. Moreover, there is still a lack of in-depth studies addressing the selective leaching of noble elements or surface reconfiguration over prolonged operating hours. It is crucial to evaluate the performance of HEAs in operational fuel cells or complete electrolyzes, considering phenomena such as sintering, detachment of the active layer, or support degradation.

Currently, the introduction of HEAs has redefined conventional catalyst design, enabling the development of multicomponent alloys

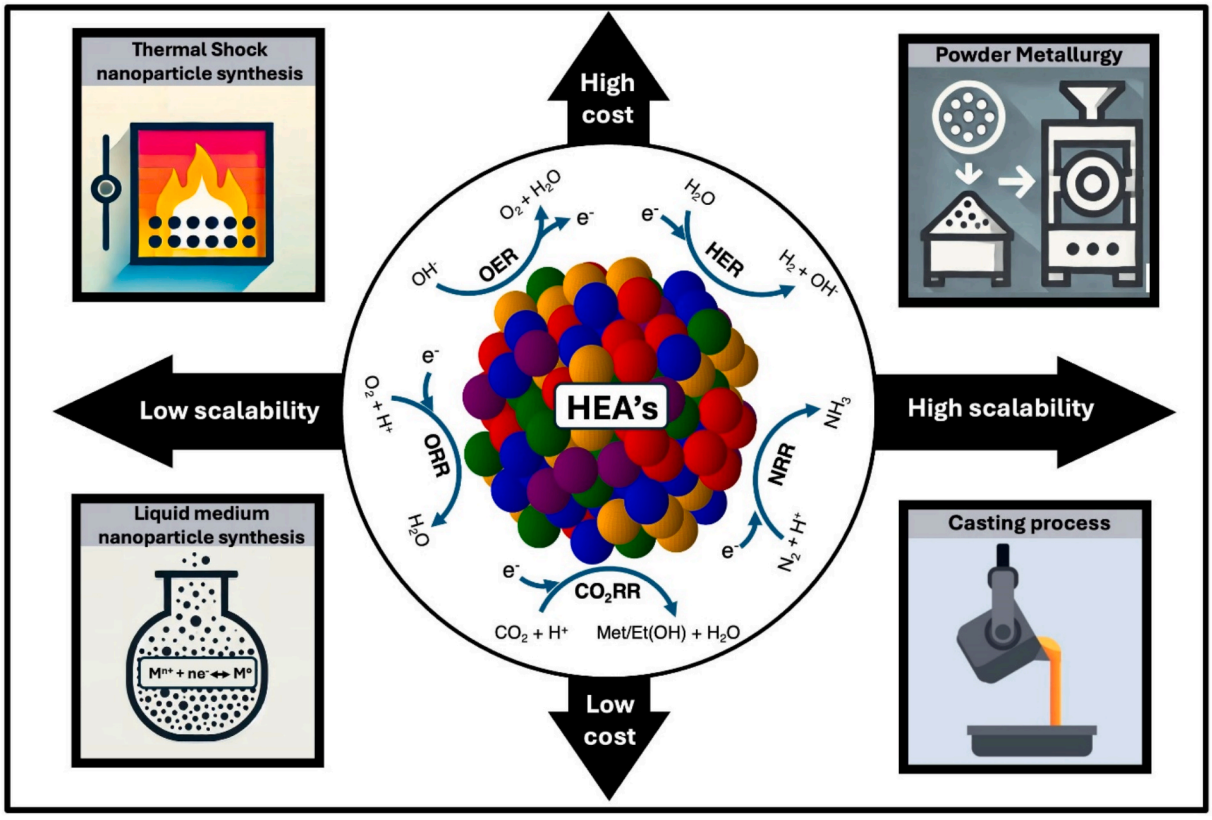

Fig. 8. Schematic comparison of HEAs synthesis methods based on cost and scalability, and their application in key electrochemical reactions studied in this review.

with tailored catalytic behavior (Fig. 8). The structural complexity enables the formation of solid solutions stabilized by configurational entropy, allowing for enhanced thermal and electrochemical stability, tunable electronic structures, and synergistic interactions among elements [97,98] These characteristics translate into improved catalytic activity, enhanced selectivity, and extended durability in reactions such as HER, OER, ORR, and CO_2RR.

Some of the most interesting properties they have are exhibiting pronounced lattice distortion due to the incorporation of multiple principal elements with differing atomic radii. This structural irregularity induces local strain fields that profoundly alter the electronic structure at the surface, enabling fine-tuning of adsorption energies for key intermediates such as H* during HER and O* during OER. Wang et al. [99] demonstrated that lattice distortion leads to modifications in atomic coordination environments, which reduce the activation energy barriers for electrochemical steps and thereby enhance overall reaction kinetics. In parallel, Lee et al. [100] highlighted that such distortion facilitates the breaking of conventional linear scaling relationships between adsorbed intermediates, allowing the simultaneous optimization of multiple elementary steps in complex multi-electron processes like OER. These synergistic effects not only contribute to superior intrinsic catalytic activity but also support enhanced structural stability under prolonged electrochemical operation.

Another critical feature that enhances the electrocatalytic performance of HEAs is their inherently defect-rich surface architecture, which arises from compositional complexity and tailored nanostructuring strategies. These surface defects serve as catalytically active centers by providing heterogeneous binding environments that facilitate the adsorption, dissociation, and transport of reactive species. Cai et al. reported that engineering surface defects in nanostructured HEAs leads to an increase in the number and diversity of active sites, thus significantly improving reaction kinetics [101]. In a more recent study, Liu et al. [102] developed a defect-rich FeCoNiMnRu HEA via rapid Joule heating, and revealed that these defects reorganize the structure of interfacial water by transforming strongly hydrogen-bonded molecules into free water species, thereby accelerating water dissociation and the mobility of H_2O*/OH* intermediates in alkaline and seawater electrolytes. This behavior was corroborated through in-situ FTIR spectroscopy and ab initio molecular dynamics simulations, establishing a direct link between surface defect engineering and enhanced HER kinetics in HEA-based systems.

Designing HEAs for electrocatalysis, however, presents both challenges and opportunities. Phase formation is governed by a delicate balance of mixing entropy, enthalpy, atomic radii differences, and electronic interactions. Computational methods, particularly density functional theory (DFT) and machine learning (ML), have become essential tools for predicting phase stability and guiding the rational design of HEAs with application-specific performance [16,39]. Remarkably, despite their inherent compositional complexity, many HEAs have been shown to form stable single-phase structures, further supporting their potential as next generation electrocatalysts.

The versatility of HEA synthesis methods, ranging from traditional approaches like arc melting [103] and powder metallurgy [80] to advanced techniques such as liquid-phase synthesis and carbothermal shock methods, has significantly expanded the scope of their applications [104]. These methods not only allow precise control over composition and microstructure but also facilitate the production of HEA nanoparticles [105], thin films [106], and porous structures [106]. Each of these forms offers unique advantages for electrocatalysis, such as increased surface area, improved charge transfer, and enhanced exposure of active sites.

The integration of HEAs into electrocatalysis represents more than a technological advancement: it is a shift in the scientific approach to catalyst design [107]. Unlike conventional materials, HEAs challenge researchers to think beyond binary or ternary systems, embracing a multicomponent strategy that leverages configurational entropy to stabilize novel phases. This new paradigm encourages the exploration of uncharted compositional landscapes, opening the door to innovative discoveries and transformative applications [108].

The irregularity of HEA surfaces, combined with their compositional diversity, delivers an abundance of active sites, facilitating complex electrocatalytic processes [7]. Furthermore, the ability to incorporate non-precious metals into HEAs without compromising performance addresses the economic and sustainability challenges associated with traditional noble metal catalysts [85,109,110]. As a result, HEAs are poised to redefine the limits of what is possible in electrocatalysis, offering a platform for breakthroughs in hydrogen production, carbon capture, and renewable energy storage.

In recent years, the incorporation of interstitial elements has emerged as a powerful strategy to further modulate catalytic activity, selectivity, and stability. These interstitials not only distort the lattice and increase local strain, but also modify the charge distribution, orbital hybridization, and bonding environment at catalytically active sites, as well as the microstructure and the elemental distribution among the equilibrium phases. For example, Liu et al. [111] demonstrated that oxygen interstitials in TiZrNb-based HEAs can be stabilized up to 12.4 at.% without forming brittle oxide phases, leading to both mechanical robustness and increased defect density, features highly beneficial for electrocatalytic performance. Similarly, nitrogen-doped refractory HEAs have shown suppressed phase ordering and enhanced electronic conductivity, key traits for sustained activity under harsh electrochemical conditions [112]. The local distortion introduced by interstitials creates unsaturated coordination sites. Furthermore, emerging computational studies combining DFT and machine learning have begun to quantify the thermodynamic and electronic impacts of interstitials in catalytically active HEAs [113].

Another relevant aspect is related to ordering phenomena in HEAs lattices. It has been found that some medium- and high-entropy alloys exhibit chemical short-range ordering (SRO) – exhibiting local atomic arrangements over a few nanometers facilitated by preferential thermodynamical bonding between certain pairs of elements [114]. In electrocatalysis, SRO phases, often described as amorphous or low-crystallinity structures, may enhance performance due to the abundant undercoordinated sites, grain boundaries, and oxygen vacancies, which can significantly enhance catalytic activity compared to their highly crystalline and totally random counterparts, highlighting particular strategies such as surface chemistry tuning, electronic interactions, and reaction kinetics in high-entropy alloy electrocatalysts. Some efforts have been done modelling or detecting [114] SRO in HEAs, but its potential for electrocatalytic applications has not been exploited yet.

Next, the most relevant works for the electrocatalytic reactions mentioned above will be shown, and the synthesis, characterization and electrocatalytic performance will be discussed.

4.1. *Electrocatalytic alcohol oxidation*

Direct alcohol fuel cells (DAFCs), including direct ethanol (DEFC) and direct methanol fuel cells (DMFC), have been investigated since the mid-20th century as compact power sources due to the high energy density of alcohols. However, early implementations were hindered by safety concerns and the complexity of fuel storage and handling. In recent years, DMFCs have gained renewed attention as a viable alternative to lithium-ion batteries in portable and off-grid applications [115]. A critical limitation in these systems is the sluggish kinetics of the methanol oxidation reaction (MOR), which is further exacerbated by CO poisoning of Pt-based catalysts, currently the state-of-the-art in commercial electrocatalysis. The formation of strongly adsorbed CO intermediates on Pt surfaces blocks active sites, leading to severe performance losses. One mitigation strategy has been the development of bimetallic systems that incorporate oxophilic elements such as Ru or Sn to promote OH radical formation, enhancing CO oxidation and

improving catalyst resilience[116].

One of the earliest studies to explore high-entropy-like multimetallic nanoparticles for electrocatalytic methanol oxidation was reported by Tsai et al [117]. The authors synthesized nanoparticles with the general composition PtxFe(100 − x)/5Co(100 − x)/5Ni(100 − x)/5Cu(100 − x)/5Ag(100 − x)/5 (x = 22, 29, 52, 56) using radiofrequency sputtering onto carbon cloth substrates. All compositions crystallized in face-centered cubic (FCC) phases Fig. 9, with lattice parameters increasing alongside Pt content, consistent with its larger atomic radius. SEM revealed an increase in particle size with longer deposition times, and energy-dispersive EDX confirmed homogeneous elemental distribution. Among the tested compositions, $Pt_{52}Fe_{11}Co_{10}Ni_{11}Cu_{10}Ag_8$ exhibited the highest mass activity (462–504 mA/mg), likely due to an optimal balance between Pt content, particle size, and electronic synergy. However, increasing the Pt content further (Pt_{56}) resulted in reduced performance, attributed to particle coarsening and diminished electrochemically active surface area.

Despite the promising performance of the Pt_{52}-based alloy, it was ultimately outperformed by a binary $Pt_{43}Ru_{57}$ catalyst synthesized under identical conditions. The $Pt_{43}Ru_{57}$ sample exhibited significantly higher mass activity and an if/ib ratio of 1.57,indicative of enhanced CO tolerance, while the HEA systems displayed nearly constant if/ib values (~1.09), suggesting limited ability to oxidize CO intermediates Fig. 9b. The authors proposed that the electrochemical instability of less noble elements (Fe, Co, Ni, Cu, Ag) may have led to partial anodic dissolution during cycling, resulting in Pt-enriched surfaces and a loss of multimetallic synergy. This highlights a critical challenge in the design of HEA-based electrocatalysts: ensuring surface stability under operating conditions to preserve the intended compositional effects. Nevertheless, the study underscores the potential of sputter-deposited multicomponent systems to achieve competitive performance with reduced noble metal usage, provided that structural and compositional integrity can be maintained during electrochemical operation.

Yusenko et al. [118] synthesized a series of noble-metal-based high-entropy alloys (HEAs) composed of iridium (Ir), osmium (Os), rhenium (Re), rhodium (Rh), ruthenium (Ru), and platinum (Pt) through thermal decomposition of single-source precursors, resulting in well-defined crystalline structures with electrocatalytic potential for methanol oxidation. Specifically, the alloy with composition $Ir_{0.19}Os_{0.22}Re_{0.21}Rh_{0.20}Ru_{0.19}$ crystallized in a hexagonal close-packed (HCP) phase, while the $Ir_{0.18}Os_{0.18}Pt_{0.16}Re_{0.17}Rh_{0.16}Ru_{0.15}$ alloy exhibited a mixed structure combining both face-centered cubic (FCC) and HCP phases (Table 3). Both materials showed considerable

Table 3
Elemental and phase compositions for synthetized PGM-based HEAs [118].

Elemental composition according to SEM/EDX	Elemental composition according to SEM/EDX	hcp/fcc	hcp/fcc
$Ir_{0.24(1)}$ $OS_{0.21(1)}Re_{0.16(1)}Rh_{0.18(1)}$ $Ru_{0.20(1)}$	$Ir_{0.19(1)}OS_{0.22(1)}$ $Re_{0.21(1)}Rh_{0.20(1)}Ru_{0.19(1)}$	$hcp_{0.61}fCC_{0.93}$	hcp
$Ir_{0.18(1)}$ $OS_{0.25(1)}$ $Pt_{0.14(1)}$ $Re_{0.15(1)}$ $Rh_{0.14(1)}$ $Ru_{0.14}$	$Ir_{0.18(1)}$ $OS_{0.18(1)}$ $Pt_{0.16(1)}$ $Re_{0.17(1)}$ $Rh_{0.16(1)}$ $Ru_{0.15}$	$hcp_{0.50}fcc_{0.50}$	hcp/fcc
$Ir_{0.19(1)}$ $OS_{0.16(1)}$ $Pt_{0.22(1)}Rh_{0.17(1)}$ $Ru_{0.26(1)}$	No data	$hcp_{0.42}fcc_{0.58}$	hcp/fcc
$Ir_{0.23(1)}OS_{0.10(1)}Pt_{0.25(1)}Rh_{0.22(1)}$ $Ru_{0.19(3)}$	No data	$hcp_{0.29}fCC_{0.71}$	hcp/fcc
$Ir_{0.26(1)}$ $OS_{0.05(1)}$ $Pt_{0.31}Rh_{0.23(1)}$ $Ru_{0.15(1)}$	No data	$hcp_{0.20}fcc_{0.80}$	hcp/fcc

electrocatalytic activity toward the MOR in acidic solution, with onset potentials around 0.503 V vs. SHE, surpassing the performance of the individual constituent metals. The enhanced activity was attributed to synergistic interactions among the multiple metallic elements, which are believed to modulate the electronic structure, particularly the position of the d-band center, thereby optimizing the adsorption energies of reaction intermediates and lowering the energy barriers for oxidation. Additionally, the observed structural stability under acidic electrochemical conditions suggests good resistance to phase degradation, positioning these HEAs as strong candidates for long-lasting and efficient MOR catalysts.

On the other hand, Zhao et al. [119] developed a platinum-based HEA supported on graphene oxide for methanol oxidation, utilizing a novel synthesis strategy that combines spray-drying with thermal decomposition in a reductive atmosphere. The precursors, consisting of water-soluble salts of Co, Cu, Fe, Ir, Ni, Pd, Pt, Rh, Ru, and W, were mixed with graphene oxide and spray-dried at 165 °C to form a homogenous dispersion. Subsequent reduction in H_2 at temperatures above 300 °C yielded HEA nanoparticles containing ten typically immiscible elements. XRD confirmed the formation of single-phase FCC without elemental segregation, indicating successful entropy stabilization at the nanoscale. Among the alloy compositions tested, a six-element formulation, PtCoCuRuNiFe, was selected for electrocatalytic evaluation. Cyclic voltammetry in 0.5 M H_2SO_4 and 0.5 M CH_3OH revealed exceptional methanol oxidation activity, with a specific current density of 1511 mA/mg_{pt} and a mass activity five to eight times higher than that of commercial Pt/C (20 wt%, Johnson Matthey). These results underscore the synergistic effects of multimetallic interactions and the potential of

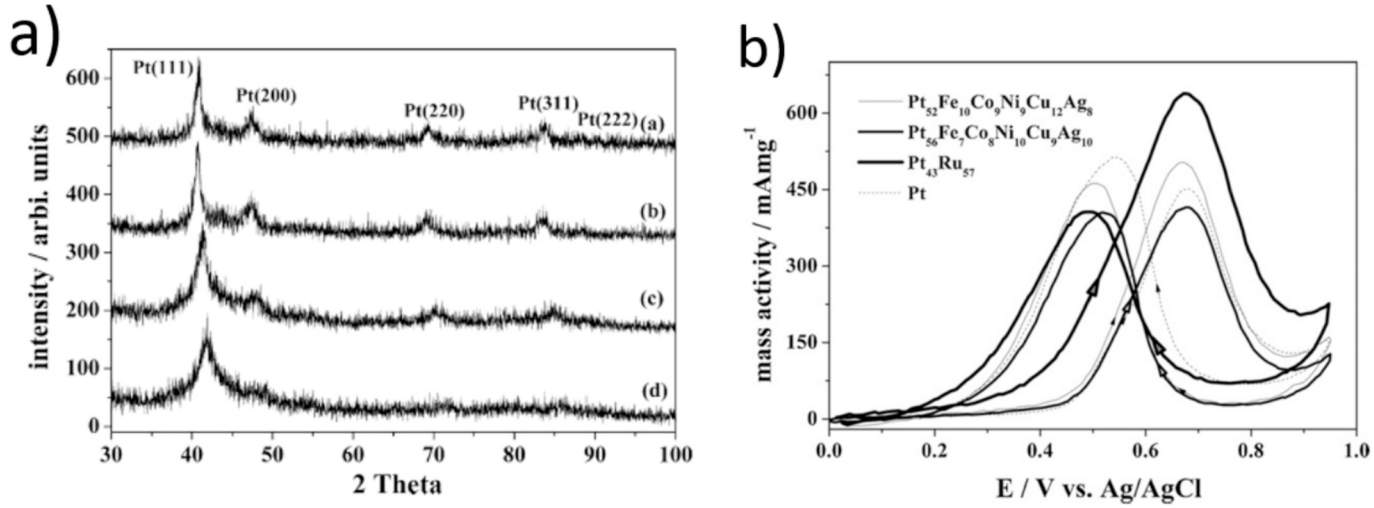

Fig. 9. A) a comparison of x-ray diffraction patterns is presented for carbon clothes coated with multi-element alloy films deposited for120 min. The compositions of the films are as follows: (a) $Pt_{56}Fe_7Co_8Ni_{10}Cu_9Ag_{10}$, (b) $Pt_{52}Fe_{11}Co_{10}Ni_{11}Cu_{10}Ag_8$, (c) $Pt_{29}Fe_{14}Co_{15}Ni_{15}Cu_{13}Ag_{14}$, and (d) $Pt_{22}Fe_{14}Co_{15}Ni_{14}Cu_{18}Ag_{17}$. Additionally, cyclic voltammetry curves for the mass activities of $Pt_{56}Fe_7Co_8Ni_{10}Cu_9Ag_{10}$, $Pt_{52}Fe_{10}Co_9Ni_9Cu_{12}Ag_8$, Pt, and $Pt_{43}Ru_{57}$ are presented for the 100th cycle [117].

entropy-driven stabilization to reduce noble metal loading while enhancing catalytic performance. The study not only demonstrates the viability of producing compositionally complex HEA catalysts with low Pt content but also highlights the role of advanced synthesis routes in controlling structure, dispersion, and activity in next generation electrocatalysts.

Nanomaterials are highly beneficial when applied to various systems due to their significant influence on the electrocatalytic activity of materials [120]. However, the challenge of maintaining reproducible morphology under harsh conditions is crucial. In this context, Hu et al. [121] developed a solvothermal strategy to synthesize PdPtPbSnNi HEA nanowires, aiming to overcome phase segregation and morphological instability typically encountered in multicomponent nanostructures. TEM revealed that the resulting nanowires possessed uniform stacking and an average diameter of 12.5 nm. To investigate the role of individual elements in morphological control, a comparative series (PdPtPbNi, PdPtSnNi, and PdPtNi) was synthesized. While most compositions retained the nanowire structure, PdPtSnNi exhibited irregular morphologies, suggesting that lead plays a critical role in stabilizing one-dimensional growth. Elemental distribution determined via energy-dispersive X-ray spectroscopy (EDS) revealed that metal incorporation follows the sequence Pd > Pb > Sn > Pt > Ni, closely aligned with the standard reduction potentials, except for Pt, which undergoes kinetically limited reduction. XRD confirmed the formation of a single-phase FCC across the HEA composition. Electrocatalytic evaluation of PdPtPbSnNi nanowires EOR and methanol demonstrated superior performance over commercial benchmarks (Pd/C, Pt/C, and PdPt), with peak current densities of 4.36 and 4.34 A $mg_{p(pd^{-}_{+pt})}1$, respectively. These values correspond to 5.6-fold and 9.0-fold improvements over Pt/C and Pd/C in MOR, and the specific activity reached 10.81 mA $cm^{-}2$,exceeding all tested references. Chronopotentiometry stability tests over 4000 cycles revealed excellent durability and minimal deactivation, highlighting the alloy's resistance to CO* poisoning. The authors attribute this exceptional activity and stability to the ligand effect within a high-entropy coordination environment, which promotes favorable electronic modulation and robust surface dynamics. This study demonstrates that controlling kinetics and composition-driven morphology in HEA nanowires can yield highly active and durable electrocatalysts for alcohol oxidation.

In this context, Ling et. al [20] developed a surfactant-assisted strategy for synthesizing ultrathin PdPtCuAgAuPbCo HEA nanowires, highlighting the importance of molecular self-assembly in controlling one-dimensional morphology. By varying surfactant types and counterions, the authors demonstrated that long hydrophobic chains and specific anions (e.g., Br^{-} over Cl^{-}) promote micelle formation and directional growth, while hydrazine serves as a rapid, non-selective reductant. The resulting nanowires, characterized by XPS, SEM/TEM, and ED), exhibited near-equimolar composition and formation of a solid solution, supported by oxidation state variations and core-level shifts in XPS. Among various compositions tested, PdPtCuAgAuPbCo nanowires showed the highest mass (9.9 A $mg_{p}d^{-1}_{+pt}$) and specific activity (30.60 mA cm^{-2}) for the ethanol oxidation reaction (EOR), along with superior electrochemical surface area and CO poisoning resistance (If/Ib = 2.7), outperforming both simpler HEAs and commercial Pd catalysts. The enhanced performance was attributed to a synergistic combination of ultrathin morphology, which improves mass and charge transport, and electronic modulation from multimetallic coordination, which facilitates OH* generation and weakens CH_3CO* adsorption, the rate-determining step in EOR. This study underscores the crucial role of surfactant chemistry, structural design, and compositional tuning in developing highly efficient and stable HEA-based electrocatalysts.

The comparative data presented in Table 4 highlights the substantial variability in electrocatalytic performance among HEAs used for methanol and ethanol oxidation. For instance, the PtFeCoNiCuAg HEA synthesized by sputtering reached a respectable mass activity of 462–504 mA/mg_{pt} [117], but its limited CO tolerance and moderate If/Ib ratio suggest incomplete removal of poisoning intermediates, likely due to the absence of strongly oxophilic species. In contrast, the PdPtPbSnNi nanowires achieved significantly higher mass activities for both EOR and MOR (4.36 and 4.34 A/$mg_{p}d_{+pt}$, respectively), with remarkable stability after 4000 cycles and superior specific activity (10.81 mA/cm^2), largely attributed to the structural benefits of one-dimensional nanowires and the inclusion of Sn and Pb, which aid in OH* generation and CO* oxidation [121]. The HEA developed by Zhao et al. [119], containing PtCoCuRuNiFe, further pushed the performance boundary with a specific current density of 1511 mA/mg_{pt},five to eight times higher than commercial Pt/C, demonstrating the importance of combining noble and non-noble metals with complementary electronic properties.

A clear compositional trend emerges when considering the role of specific elements. Alloys incorporating Ru, Sn, Pb, and Co, elements known to promote the formation of OH* species and facilitate the oxidative removal of adsorbed intermediates like CH_3CO*,consistently outperform those lacking such functionalities. The findings showed above suggest that the synergy between structural design and electronic modulation through multimetallic coordination is key to optimizing both activity and durability. The inclusion of late transition and post-transition metals in near-equimolar ratios enables fine-tuning of adsorption energies, while high configurational entropy stabilizes single-phase solid solutions, ensuring uniform active site distribution and long-term catalyst integrity. Overall, the table underscores that rational design of HEAs, balancing morphology, phase, and targeted elemental effects, is essential for maximizing electrocatalytic performance in alcohol oxidation reactions. HEAs offer a highly tunable and

Table 4
Summary of HEAs for alcohol oxidation.

HEA Composition	Synthesis Method	Crystal Phase	Electrode Fabrication	Electrolyte	Peak Current Density (CV)	DOI
PtFeCoNiCuAg	Sputter deposition	fcc	Carbon cloth-supported	Acidic	462–504 mA/mg Pt (mass activity)	[117]
PdNiCoCuFe	Template-assisted electrodeposition	fcc	Self-supported nanotube arrays	Alkaline (0.5 M KOH + 1.0 M CH_3OH)	~37.4 mA/cm^2	[122]
PtFeNiCoCu	Solvothermal synthesis	fcc	CdS-supported photocatalyst	Water-based for photocatalysis	Not CV-based; photocatalytic H_2: 7.15 mmol $g^{-1}h^{-1}$	[123]
CuAgAuPtPd	Casting + Cryomilling	fcc + amorphous	Ink based	Acidic	152 nm $g^{-1}h^{-1}$	[123]
PdPtCuAgAu	One-pot surfactant	fcc	catalyst-coated substrate	Alkaline	7.7 A/mg Pd + Pt	[124]
PtFeCoNiCu	Annealing at 700 °C and 400 °C	fcc	ink-based	Acidic	Higher for HEA-700 vs HEA-400,	[125]
PdPtSnPbNi	Solvothermal synthesis	fcc	likely catalyst film	Acidic	4.34 A/mg Pd + Pt (MOR), 4.36 A/mg Pd + Pt (EOR)	[126]
PdPtCuAgAuPbCo	One-pot rapid reduction with surfactant	fcc	Ink-based	Alkaline	9.9 A/mg Pd + Pt	[20]

synergistic catalytic platform for the electrooxidation of alcohols, addressing key limitations in conventional noble-metal-based catalysts. Their intrinsic multi-elemental configuration promotes a wide distribution of d-band centers, which can be strategically engineered to modulate the adsorption energies of reaction intermediates such as CO_{ads} and CH_3OH_{ads}. This enables tailored Sabatier behavior across active sites, improving both catalytic activity and tolerance to poisoning species. For instance, the incorporation of oxophilic metals (e.g., Ru, Pb, Sn, Co) within the HEA matrix facilitates the generation of surface-bound hydroxyl groups (OH_{ads}), which assist in the oxidative removal of adsorbed CO mitigating one of the principal causes of deactivation in Pt-based systems.

Therefore, from a design perspective, performance can be further optimized by: (i) fine-tuning elemental ratios to balance the electronic effects (e.g., increasing Co or Pb to modulate charge transfer and improve OH_{ads} availability), (ii) reducing particle size via colloidal or solvothermal methods to increase electrochemical surface area (ECSA), and (iii) engineering 1D or porous morphologies (e.g., nanowires, dealloyed frameworks) to enhance mass transport and active site accessibility. Moreover, defect engineering and strain modulation, introduced during synthesis (for example, via rapid thermal shocks or cryomilling), can further manipulate local coordination environments and promote desirable electronic configurations.

Collectively, these features make HEAs not only durable and compositionally flexible but also highly efficient under realistic fuel cell operating conditions, paving the way for the development of low-Pt or Pt-free electrocatalysts with superior long-term performance and cost-effectiveness.

4.2. Electrocatalytic HER

HER is a fundamental half-reaction in water electrolysis and has garnered growing interest as a cornerstone of sustainable hydrogen production. With a specific energy density of 143 MJ kg^{-1}, nearly three times higher than that of natural gas or gasoline, hydrogen is considered a high-efficiency energy vector, particularly when utilized in fuel cells where energy conversion is not limited by the Carnot cycle [127]. In addition to its energy performance, hydrogen oxidation yields only water as a byproduct, offering a zero-emission pathway for chemical-to-electrical energy conversion [128].

The HER mechanism proceeds through multiple electrochemical steps that are strongly influenced by the pH and nature of the electrolyte. In acidic media, the process typically begins with the Volmer step, in which protons are adsorbed onto the surface of the electrocatalyst via electron transfer, forming intermediate adsorbed hydrogen species (H*). Subsequent steps include either electrochemical desorption (Heyrovsky step) or recombination of two H* atoms (Tafel step) to form molecular hydrogen. The rate-determining step is often governed by the balance between hydrogen adsorption and desorption, making the interaction between the catalyst surface and H* species a critical factor in determining catalytic efficiency [129].

For optimal HER performance, the adsorption free energy of hydrogen ΔG (H*) should be close to thermoneutral (~0 eV), ensuring both strong enough binding for activation and sufficiently weak binding for desorption. This requirement places stringent demands on the electronic structure and surface properties of the catalyst. Traditional noble metal-based catalysts such as Pt meet this criterion nearly ideally but suffer from high cost and limited availability. This challenge has sparked intense research into alternative materials including HEAs that offer tunable surface energetics and compositional flexibility to optimize ΔG (H*) while enhancing durability and reducing precious metal content [130].

In an effort to reduce the cost of HEA electrocatalysts, Zhang et al. [77] synthesized a non-noble metal HEA composed of first-row transition metals, $Ni_{20}Fe_{20}Mo_{10}Co_{35}Cr_{15}$, via vacuum arc melting, followed by thermal treatment at 1150 °C to achieve a FCC structure (shown in Fig. 10a). he FCC phase exhibited superior HER activity compared to commercial platinum in 0.5 M H_2SO_4, with a low onset potential of ~ 44 mV, a Tafel slope of 41 mV dec^{-1}, and an overpotential of 281 mV at 100 mA cm^{-2}, remarkable values for a noble-metal-free catalyst Fig. 10c. In alkaline media (1 M KOH), the same alloy showed excellent activity, delivering 10 mA cm^{-2} at an overpotential of 172 mV (Fig. 10b. The enhanced performance was attributed to the highly disordered atomic surface inherent to the FCC structure, which increases the coordination number of surface atoms and promotes favorable hydrogen adsorption and rapid charge transfer. Moreover, the compositional synergy among Ni, Fe, and Mo, elements known for their HER activity in alkaline and acidic environments, amplifies the electronic

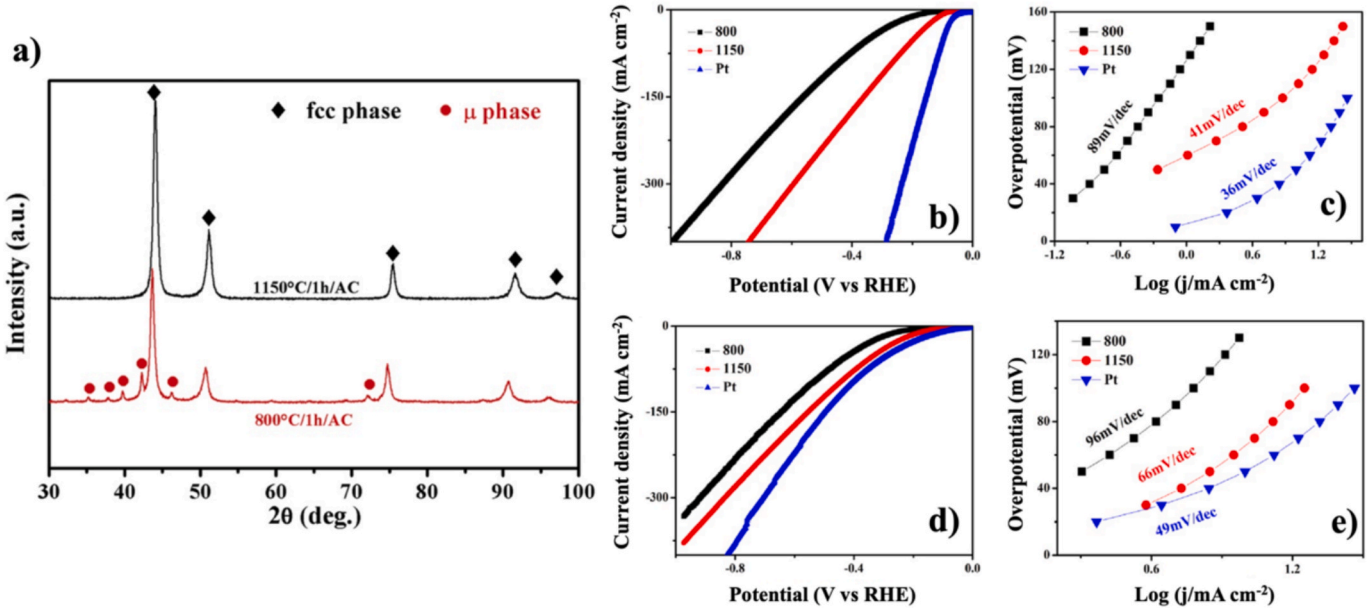

Fig. 10. A) xrd patterns of nifemococr heas annealed at 800 °C and 1150 °C.- b) Polarization curves of dual-phase alloy, high-entropy alloy and commercial Pt catalysts in a 0.5 M H_2SO_4 solution. c) Tafel plots of polarization curves in b). d) Polarization curves were also recorded for the samples in a 1.0 M KOH solution. e) Tafel plots were derived from the polarization curves in (c) [77].

coupling and facilitates water dissociation and H* formation. This study exemplifies how tuning phase stability and incorporating earth-abundant elements in HEAs can yield cost-effective and efficient electrocatalysts for hydrogen evolution.

On the other hand, HEAs containing precious metals alloyed with cheaper metals have been studied to test cost reduction strategies and effectiveness for the HER hydrogen evolution reaction. Jin et al. [78] explored a cost-effective design strategy for HER catalysts by synthesizing HEAs composed of both noble and earth-abundant metals. The authors initially formed precursor alloys of the type NiCoIrX (X = Mo, Nb, V) through arc melting, followed by remelting with a high concentration of aluminum to obtain $Al_{96}Ni_1Co_1Ir_1X_1$ compositions. These precursors were subsequently chemically dealloyed in alkaline solution, selectively removing aluminum and producing nanoporous HEA structures (np-HEAs) with enhanced surface area and compositional uniformity. Among the tested compositions, AlNiCoIrMo exhibited the most promising performance, achieving a Tafel slope of 33 mV dec^{-1},comparable to that of commercial Pt/C (30 mV dec^{-1}), and requiring an overpotential of only 250 mV to reach 10 mA cm^{-2}, outperforming Pt/C under the same conditions (320 mV). The improved catalytic activity was attributed to the bicontinuous nanoporous morphology, which exposes many accessible active sites, and to the synergistic electronic effects introduced by alloying Ir with transition metals such as Mo and Co. This work underscores the potential of combining dealloying strategies with HEA design to optimize surface structure and reduce reliance on platinum group metals without compromising HER efficiency.

Yao et al. [131] reported the synthesis of a CuAlNiMoFe-based HEA monolith with a BCC crystal structure and exceptional catalytic performance toward HER. The synthesis followed a dealloying route similar to that described by Li et al [78], where precursor metals were alloyed in an aluminum matrix and subsequently subjected to chemical dealloying in potassium hydroxide to remove intermetallics and dissolve secondary phases. The resulting material featured a homogeneous, nanoporous lamellar architecture, which was confirmed by high-angle annular dark-field scanning transmission electron microscopy (HAADF-STEM) and energy-dispersive spectroscopy (EDS), revealing uniform elemental distribution at the nanoscale and well-defined BCC lattice planes. Electrochemical evaluation demonstrated outstanding HER activity in both alkaline and neutral media: in 1 M KOH, the electrode reached a current density of 1840 mA cm^{-2} at an overpotential of ~ 240 mV, while in 1 M phosphate-buffered saline (PBS), it achieved 100 mA cm^{-2} at ~ 183 mV. Notably, long-term durability testing showed stable current output over 200 h at an overpotential of only 50 mV, indicating excellent electrochemical stability and corrosion resistance. The superior performance is attributed to the high surface area and interconnected porosity, which facilitate electrolyte accessibility and gas diffusion, as well as the electronic synergy among the constituent transition metals, which optimize hydrogen adsorption and accelerate charge transfer. This work exemplifies how controlled microstructural engineering combined with multi-elemental design can yield HEAs with industrially relevant HER performance and long-term operational robustness.

As previously explained, the most interesting transition metals for electrocatalytic reactions are noble metals, due to their unique properties in electrocatalytic mechanisms studied so far. This has led to the development of intriguing theories, such as the Sabatier principle [132–134]. Jeong et al. [9] addressed the challenge of reducing noble metal content in electrocatalysts by synthesizing AuPdFeNiCo HEA nanoparticles with tailored surface and electronic properties suitable for hydrogen evolution across a wide pH range. The HEAs were prepared via a wet-chemical route involving the co-reduction of five metal chlorides in the presence of poly(N-vinyl-2-pyrrolidone) (PVP), which served as a stabilizing and capping agent. XRD and HR-TEM confirmed the formation of uniformly distributed nanoparticles (~13.5 nm) with an FCC crystal structure. X-ray photoelectron spectroscopy revealed significant core-level shifts across all constituent metals, indicating electronic redistribution and strong inter-element charge transfer. These modifications are consistent with the ensemble effect and electronic synergy typically observed in HEAs, which can optimize the hydrogen binding energy during HER. Electrochemical testing in acidic (0.5 M H_2SO_4), neutral (1 M PBS), and alkaline (1 M KOH) media showed that the AuPdFeNiCo nanoparticles outperformed both bulk metal foils and commercial 10 % Pt/C, delivering overpotentials of just 45, 279, and 43 mV at 10 mA cm^{-2}, respectively. Tafel slopes were also notably low,32, 132, and 55 mV dec^{-1},indicating fast reaction kinetics, particularly in acidic and alkaline conditions where the Volmer–Heyrovsky mechanism dominates. These results suggest that, despite the reduced Pd content, the combination of noble and base metals in an entropy-stabilized FCC matrix enables favorable H* adsorption–desorption dynamics across diverse electrolyte conditions. The findings support the potential of compositionally tuned HEAs to serve as cost-efficient and highly active HER catalysts under both acidic and non-acidic environments.

The study by Chen et al. [107] represents a fundamental shift in electrocatalyst design by reframing the long-standing Sabatier principle within the context of HEA surfaces, Traditionally, HER catalyst development has been guided by the principle that an optimal adsorption free energy for hydrogen (ΔG H*),ideally close to zero, maximizes activity. However, this approach assumes a uniform catalytic surface, which is inherently unrealistic for HEAs composed of dissimilar atomic species and complex coordination environments. Chen et al. [107] challenge this paradigm by demonstrating that the catalytic surface of HEAs follows a Gaussian distribution of ΔGH^* values, arising from the local heterogeneity intrinsic to multimetallic systems. This distribution generates a spectrum of active sites, where strongly binding sites activate H^+, while weakly binding sites promote rapid desorption of H*, thus collectively enabling the full HER pathway to proceed efficiently across the entire ensemble of sites.

To validate this theory, the authors engineered a PtFeCoNiCu HEA catalyst with dual compositional and electronic gradients, leveraging controlled atomic dispersion and lattice distortions to maximize the diversity of surface environments. The result is a nanostructured catalyst that transcends the classical volcano plot limitations, achieving an exceptionally low overpotential of 10.8 mV at − 10 mA cm^{-2} and intrinsic activity 4.6 times higher than commercial Pt/C. More significantly, they introduced a quantitative statistical descriptor for HER activity, using the mean (μ) and standard deviation (σ) of the ΔGH^* distribution to predict and tune catalytic behavior, an unprecedented move toward data-driven, probabilistic catalyst design. This approach not only captures the complex surface energetics of HEAs but also provides a rational framework for optimizing future multicomponent systems beyond trial-and-error or DFT-guided single-site analysis. In essence, this work bridges statistical thermodynamics with catalysis, opening a pathway toward predictive, multiscale control of activity through atomic-level compositional tuning. It sets a new benchmark in the field by demonstrating that maximizing the diversity of catalytic environments, rather than their uniformity, is key to breaking long-standing performance ceilings in HER catalysis.

HEAs represent a highly versatile platform for electrocatalytic hydrogen evolution reaction HER, owing to their compositional complexity, surface heterogeneity, and tunable electronic structures. The incorporation of five or more principal elements within a single or multiphase matrix allows the formation of statistically distributed adsorption sites with varying local coordination environments and diverse hydrogen binding energies. This enables the circumvention of the traditional Sabatier optimum, as HEAs can simultaneously host sites optimized for both hydrogen adsorption and desorption, leading to enhanced intrinsic activity.

To further improve HER performance, HEA catalysts could benefit from: (i) machine-learning-guided compositional tuning to identify synergistic combinations in underexplored compositional spaces (for example, 3d–4d–5d transitions or s-block integration); (ii) surface reconstruction engineering via in situ activation or electrochemical cycling to expose metastable high-index facets; and (iii) dual-phase

architectures, in which conductive matrices (for example, FCC-Ni-rich) are embedded with catalytically active intermetallic or amorphous domains to balance conductivity and reactivity. Additionally, leveraging support effects from conductive scaffolds such as nitrogen-doped graphene or MXenes could further improve charge transport and H* spillover dynamics.

Combined, these approaches position HEAs not merely as passive multielement systems, but as active, designable catalytic frameworks capable of meeting the demands of next-generation hydrogen production, with enhanced activity, long-term durability, and reduced reliance on noble metals.

HEAs presented in Table 5 exemplify the growing sophistication in catalyst design for HER, emphasizing the strategic use of both noble and earth-abundant elements. Transition metals such as Ni, Co, Fe, and Mo provide essential electronic and coordination environments that promote water dissociation and hydrogen adsorption, especially in alkaline conditions. Noble metals like Pt, Pd, and Ir, while present in lower concentrations, enhance intrinsic activity and electron conductivity. Elements such as Cu and Al, though catalytically less active, play important structural roles by modifying lattice strain and facilitating nanoporous architectures upon dealloying. The broad variety of combinations highlights a fundamental shift from targeting individual active sites to engineering catalytic surfaces as statistical ensembles, where local heterogeneity, rather than atomic uniformity, becomes the key driver of reactivity. This design logic is well-supported by recent work that leverages distributions of adsorption energies instead of fixed optimal values [107].

From an application standpoint, the most promising HEA systems demonstrate catalytic activities that rival or exceed commercial Pt/C in terms of overpotential, Tafel slope, and long-term stability, often under

Table 5
Summary of HEAs applied to HER.

High-Entropy Alloy Composition	Synthesis Method	Crystalline Phase	Electrode Configuration	Electrolyte	η (Overpotential)	Tafel Slope (mV/dec)	Stability	Reference
PdFeCoNiCu	Oil-phase synthesis	FCC	Catalyst ink on glassy carbon (5 mg catalyst + Nafion + ethanol)	0.1 M KOH (alkaline)	η = 18 mV @10 mA/cm^2	39 mV/dec	Chronopotentiometry at 10 mA/cm^2 for 15 days (no decay)	[135]
Ni20Fe20Mo10Co35Cr15	Arc melting + homogenization (implied from HEA context)	FCC	Self-supported rolled sheet (2.4 mm, no binder)	0.5 M H_2SO_4 (acidic) and 1 M KOH (alkaline)	η = 107 mV (acid), 172 mV (alkaline) @10 mA/cm^2	88 mV/dec	Stable HER performance after long-term testing in acid and base	[77]
CoCrFeNiAl	Mechanical alloying + Spark Plasma Sintering (SPS)	FCC (after SPS + activation)	Self-supported HEA disk after HF treatment and CV activation	0.5 M H_2SO_4	η = 73 mV @10 mA/cm^2	39.7 mV/dec	4000 CV cycles in 0.5 M H_2SO_4 (stable current retention)	[85]
PtNiCuMnMo (dual-phase)	High-temperature synthesis (not explicitly detailed)	Dual-phase FCC–BCC	Catalyst ink on glassy carbon (5 μL drop-casting, Nafion)	1 M KOH	η = 44 mV @10 mA/cm^2	39 mV/dec	Chronopotentiometry at 200 mA/cm^2 for 72 h (no performance loss)	[23]
FeCoNiMnZn	Fast-moving bed heating (FH)	FCC	Catalyst on N-doped CNTs deposited on glassy carbon	1 M KOH	η = 184 mV @10 mA/cm^2	112 mV/dec	Chronopotentiometry at 10 mA/cm^2 for 10 h (stable)	[22]
AlNiCoIrMo	Dealloying	FCC	Self-supported dealloyed nanoporous monolith	0.5 M H_2SO_4	η ≈ 20 mV @10 mA/cm^2 (reported as record-low)	24 mV/dec	Chronoamperometry: stable current at 10 mA/cm^2 for 12 h	[78]
CuAlNiMoFe	Dealloying	Surface FCC HEA on porous Cu	Nanoporous monolith used directly as working electrode	1 M KOH and pH 7 buffer	η = 240 mV (KOH), 183 mV (pH 7) @ ~100 mA/cm^2	85 mV/dec (KOH)	Chronopotentiometry at 50 mV overpotential for 200 h (no decay)	[131]
RuRhPdIrPt	One-pot polyol process	Amorphous-like (broad XRD)	Catalyst ink drop-cast on glassy carbon (20 μg metal/cm^2)	0.05 M H_2SO_4 and 1.0 M KOH	η = 25 mV (acid), 25 mV (alkaline) @ unspecified current	25 mV/dec	Stable after HER cycling test vs Pt/C (0.05 M H2SO4 & 1.0 M KOH)	[136]
PdMoGaInNi	Solution-phase synthesis (nanosheets)	Amorphous nanosheets	Self-supporting nanosheet film on electrode	0.5 M H_2SO_4	η = 13 mV @10 mA/cm^2	28 mV/dec	200 h stability in PEM electrolyzer (acid, constant voltage)	[137]
PtRuFeCoNi	Electrochemical reconstruction	FCC (with Co_2RuO4 surface layer)	Catalyst on glassy carbon; ink with Nafion binder	1 M KOH	η = 11.8 mV @10 mA/cm^2	27.8 mV/dec	Chronopotentiometry at 10 mA/cm^2 and 50 mV: stable over 100 h	[24]
AuPdFeNiCo	Wet impregnation	FCC)	Catalyst ink (AuPdFeNiCo + Nafion) drop-cast on GCE (0.07 cm^2)	Acidic, alkaline, and neutral pH	100 mA/cm^2 @ 540 mV (neutral)	60 mV/dec	Chronoamperometry: stable current @ 100 mA/cm^2 in neutral pH	[9]
NiCoFePtRh	Chemical co-reduction	FCC	Catalyst ink (ultrasmall HEA + Nafion) on GCE	0.5 M H_2SO_4	27 mV @ 10 mA/cm^2	47 mV/dec	10,000 CV cycles in 0.5 M H_2SO_4: stable performance	[138]

both acidic and alkaline conditions. These results suggest real potential for HEAs to serve as drop-in replacements or durable alternatives in proton exchange membrane and anion exchange membrane electrolyzers. Additionally, the versatility of synthesis methods, from wet chemical reduction to alloying–dealloying routes, offers scalability and adaptability to different substrate integration strategies. The success of these HEAs in producing stable, high-surface-area nanostructures, such as nanoporous networks or ultrathin nanowires, opens pathways for hybrid device integration, including membrane–electrode assemblies and porous transport layers. Future challenges lie in optimizing compositional space using data-driven tools, reducing noble metal content further, and improving activity in neutral media where current performances still lag. However, the underlying materials science framework is now well established: HEAs are no longer conceptual materials, but viable candidates for next-generation hydrogen production systems.

4.3. Electrocatalytic OER

The oxygen evolution reaction (OER) is a key bottleneck in several energy conversion technologies, including metal–air batteries, electrochemical water splitting, and regenerative fuel cells [29,139]. Its sluggish kinetics stem from a complex four-electron transfer mechanism and the formation of multiple high-energy intermediates, resulting in substantial kinetic overpotentials that limit overall efficiency [140,141]. Although precious-metal-based catalysts, such as IrO_2 and RuO_2, have shown excellent intrinsic activity and durability under harsh electrochemical conditions, their scarcity and high cost remain significant obstacles for large-scale deployment. As such, the development of cost-effective and earth-abundant alternatives with comparable or superior OER performance has become a central focus in electrocatalysis research.

As in the case of the HER, the incorporation of first-row transition metals into offers a promising route to cost-effective OER catalysts. Cui et al [76] investigated two such HEAs, FeCoNiCrAl and FeNiMnCrCu, synthesized via powder metallurgy followed by repeated arc melting to ensure homogeneity The FeCoNiCrAl alloy crystallized into a single FCC phase, while the FeNiMnCrCu alloy exhibited a mixed structure consisting of two FCC phases and one BCC phase (Fig. 11). When tested in alkaline media, both alloys outperformed Pt in terms of overpotential for OER: FeCoNiCrAl required 342 mV, and FeNiMnCrCu just 317 mV to reach 10 mA cm^{-2}, compared to 471 mV for Pt. Tafel slopes of 75, 58, and 66 mV dec^{-1} for FeCoNiCrAl, FeNiMnCrCu, and Pt respectively, further confirmed the superior reaction kinetics of the HEAs. Durability tests also revealed stable performance over 10 h at an overpotential of 438 mV. Notably, FeNiMnCrCu demonstrated the best catalytic performance, which the authors attributed to the substitution of Al and Co with Cu and Mn. This substitution increased the number of d-orbital vacancies and expanded the lattice parameters, both of which can enhance electronic conductivity and facilitate oxygen intermediate adsorption and desorption. These results highlight the critical role of electronic structure engineering and lattice distortion in optimizing the OER activity of multicomponent alloys.

On the other hand, Tang et al. [84]. explored the impact of induced porosity on the electrocatalytic performance of HEAs by modifying a well-known Cantor-type alloy, CoCrFeNiMo, through microwave sintering with magnesium as a sacrificial spacer (Fig. 12 and Fig. 13). During the ball milling process, Mg was introduced in 0 %, 10 %, and 20 % proportions to modulate porosity in the final sintered structure. X-ray diffraction confirmed that all samples retained a single FCC phase, with no structural disruption from Mg, which evaporated completely during sintering. Electrochemical testing in alkaline media revealed that the porous CoCrFeNiMo-20 Mg alloy achieved significantly lower overpotentials,ranging from 220 mV to 310 mV to reach current densities of 10–100 mA cm^{-2},compared to its non-porous counterpart, which required 270–330 mV under the same conditions. Despite the improved

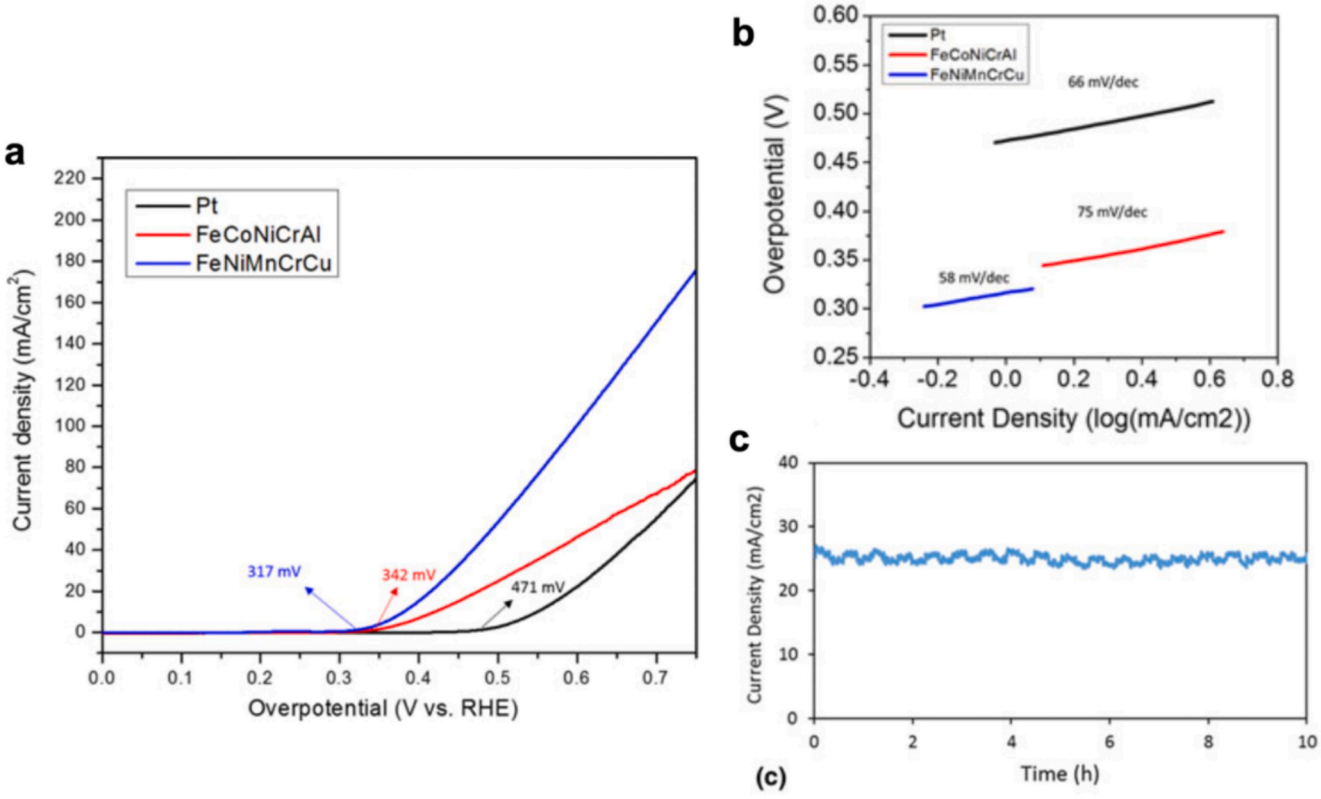

Fig. 11. A) polarization curves for the oxygen evolution reaction were obtained for the feconicral and fenimncrcu electrodes.b) Tafel slopes respetively c) The potential response over a 10-hour chronoamperometric water-splitting reaction was monitored at a constant DC potential of 438 mV overpotential. [76].

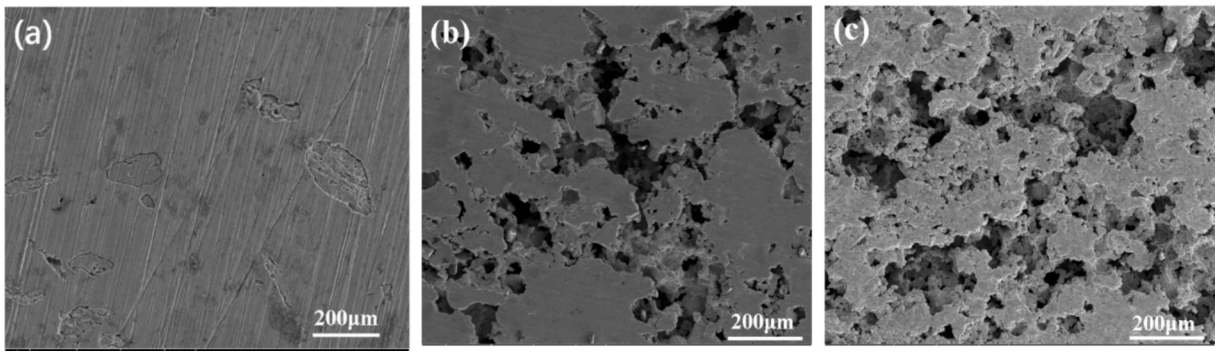

Fig. 12. SEM images. (a) CoCrFeNiMo HEA; (b) CoCrFeNiMo-20 Mg HEA before testing; (c) CoCrFeNiMo-20 Mg HEA after testing [84].

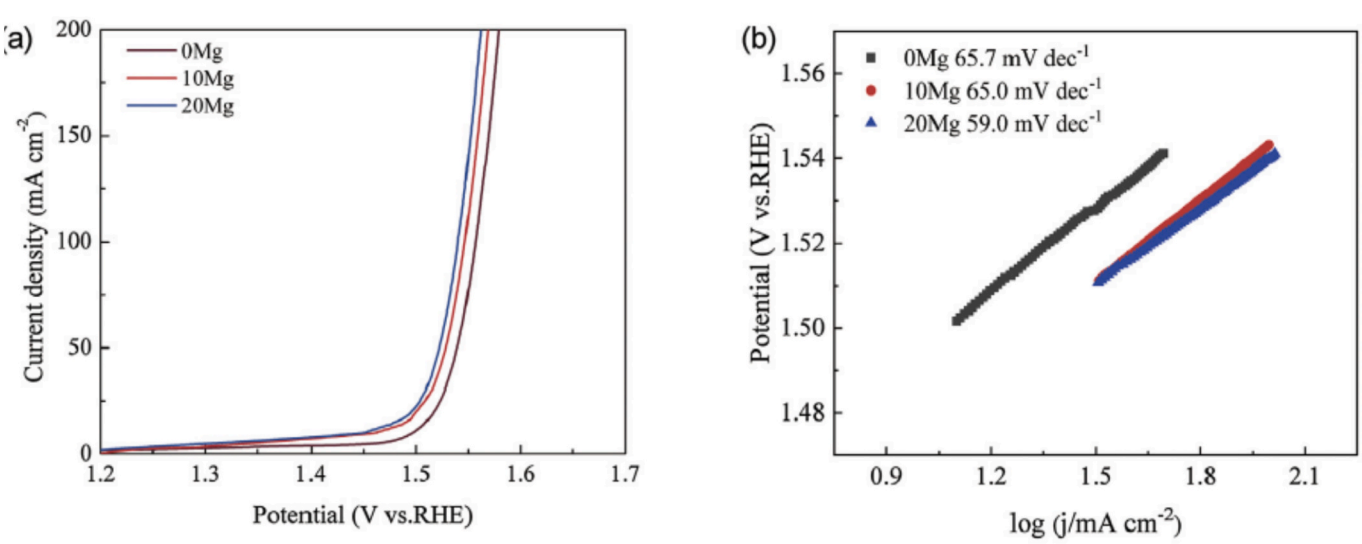

Fig. 13. (a) Polarization curves and (b) corresponding Tafel plots in 1.0 M KOH solution. [84].

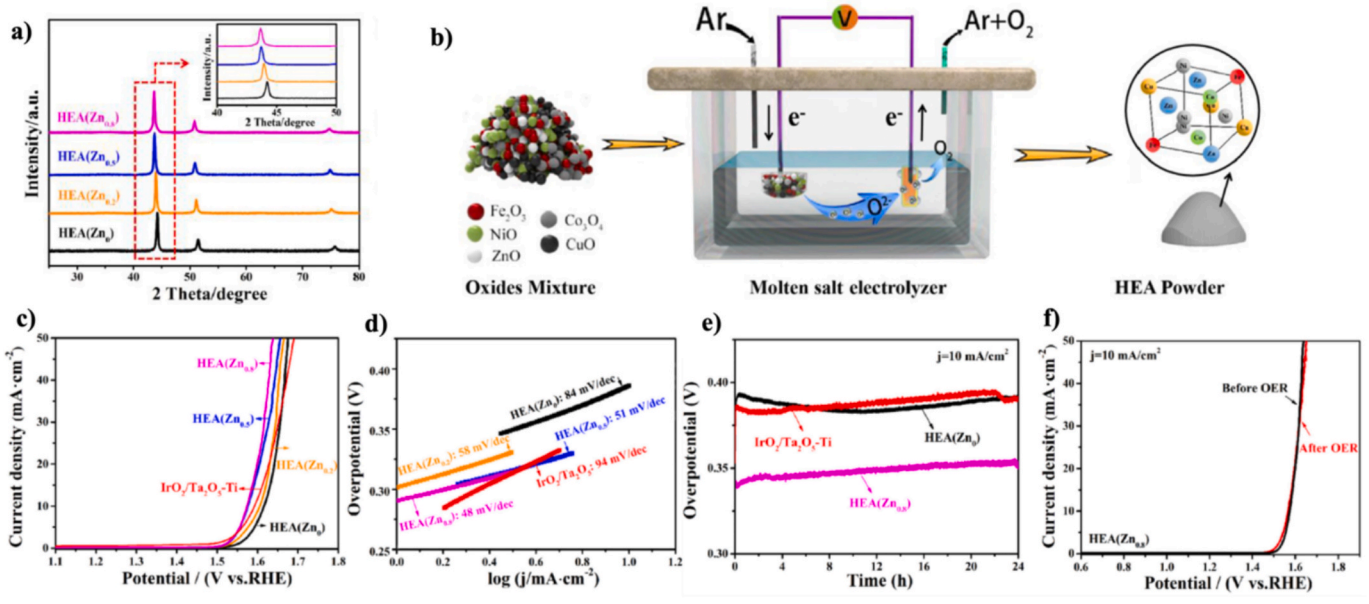

Fig. 14. A) xrd patterns of the electrolytic products with different zn contents at 1123 K and 2 V for 4 h [142]. b) Schematic illustration of the molten-salt electrolytic preparation of $Fe_{0.5}$ CoNiCuZn$_x$ HEAs. c) Polarization curves of $Fe_{.5}$CoNiCuZn$_x$ electrodes in a 1 M KOH solution. (d) The corresponding Tafel slopes of (c). (e) Chronopotentiometry for various electrodes operated at 10 mA cm^{-2} for 24 h. (f) Polarization curves before and after a 24-hour chronopotentiometry test at 10 mA cm^{-2} [142].

activity, the Tafel slopes showed minimal variation, indicating that the fundamental anodic reaction mechanism remained unchanged. The enhanced performance is therefore attributed to the increased electrochemically active surface area and improved mass transport enabled by the porous microstructure, rather than alterations in intrinsic catalytic pathways. This study highlights the importance of microstructural engineering,particularly porosity modulation,as a complementary strategy to compositional tuning in optimizing HEA-based OER electrocatalysts.

Among the various methods of synthesis of HEAs to be used as electrodes, Huang et al. [142] explored an unconventional synthesis route for high-entropy alloys (HEAs) based on high-temperature electrodeoxidation of mixed metal oxides in molten carbonate salts, offering a sustainable alternative to arc melting that utilizes pure metals Fig. 14. In their process, equimolar mixtures of Fe_2O_3, Co_3O_4, NiO, CuO, and varying amounts of ZnO were compacted and sintered, then reduced electrochemically in molten Na_2CO_3–K_2CO_3 at 1123 K using a nickel box cathode. The resulting solid solutions crystallized in a face-centered cubic (FCC) structure, with Zn content modulating both phase formation and electrocatalytic performance. Electrochemical characterization in 1 M KOH revealed a clear enhancement in OER activity with increasing Zn content: the $Fe_{0.5}CoNiCuZn_{0.8}$ alloy exhibited the best performance, with a low overpotential of 340 mV at 10 mA cm^{-2} and a Tafel slope of 48 mV dec^{-1}, outperforming commercial IrO_2 catalysts under similar conditions. The superior activity was attributed to the electronic effect of Zn, which increases lattice distortion and modulates the d-band structure, facilitating intermediate adsorption and improving charge transfer. This study demonstrates that molten salt electrodeoxidation not only enables low-cost HEA production but also allows compositional tuning via oxide precursors, potentially expanding the library of catalytically active HEAs for energy applications.

Wei et al. developed FeNiCoCrMn HEA nanosheets through a salt-assisted synthesis, aiming to enhance OER performance via nanostructure engineering [143]. Equimolar metal salts were combined with NaCl, which served as a growth-directing medium, then annealed under an Ar/H_2 atmosphere at varying temperatures (700–850 °C). The FeCoNiCrMn750 sample exhibited optimal crystallinity and morphology, with large lateral nanosheets and uniform elemental dispersion confirmed via SEM, EDS, and elemental mapping. XRD analysis verified the formation of a single-phase FCC structure, and the presence of NaCl was found to be critical in suppressing elemental segregation. Electrochemical evaluation in 1 M KOH showed that FeCoNiCrMn750 nanosheets delivered superior catalytic activity, requiring only 294 mV and 358 mV to reach 10 and 100 mA cm^{-2}, respectively, and 434 mV at 300 mA cm^{-2}. These values outperform both commercial IrO_2 and simpler HEA systems such as FeCoNi and FeCoNiMn. The enhanced performance is attributed to the synergistic combination of a high-entropy-stabilized FCC structure, increased surface area from the nanosheet morphology, and optimized intermediate binding through tailored d-band modulation. Interestingly, the OER activity followed a volcano-shaped trend with respect to annealing temperature, with 750 °C representing the optimal balance between crystallinity and active site exposure.

Li et al. [144] systematically investigated the influence of molybdenum incorporation on the oxygen evolution reaction (OER) performance of FeNiCoMn-based high-entropy alloys (HEAs), demonstrating a clear compositional–activity correlation. The HEAs were synthesized via molten salt electro-deoxidation of equimolar oxide precursors, followed by sintering to yield single-phase FCC alloys. XRD analysis revealed increasing lattice distortion with Mo content, indicating successful integration into the alloy matrix. Electrochemical characterization in 1 M KOH showed a dramatic decrease in overpotential at 10 mA cm^{-2}, from 460 mV (Mo_0) to 279 mV (Mo_1), accompanied by a reduction in Tafel slope from 99.1 to 56.1 mV dec^{-1},reflecting accelerated OER kinetics with higher Mo loading. Additionally, Nyquist plots confirmed improved charge transfer dynamics for the Mo_1 composition, with the lowest measured Rct (2.30 Ω) and Rs (0.52 Ω). The Mo-rich alloy also demonstrated remarkable long-term durability, maintaining stable operation for over 1000 h at 10 mA cm^{-2} and withstanding harsh industrial conditions (6 M KOH, 60 °C, 400 mA cm^{-2} for 300 h) without degradation. These results underline the dual role of Mo in enhancing electronic conductivity and surface reactivity, positioning FeNiCoMnMo as a highly efficient and industrially relevant OER electrocatalyst.

Table 6 highlights the strategic advantages of HEAs in catalyzing the oxygen evolution reaction under alkaline conditions. A clear trend emerges: HEAs that incorporate Mo, Mn, or Cu alongside Ni, Fe, and Co consistently outperform commercial IrO_2 benchmarks in terms of overpotential and Tafel slope, underscoring the importance of electronic modulation and synergistic redox interactions among multivalent centers. Most high-performing systems exhibit FCC structures, which offer favorable surface atom coordination and defect accommodation, enhancing both catalytic turnover and stability. Synthesis routes such as molten salt electro-deoxidation and template-assisted annealing stand out for enabling high surface area morphologies and controlled phase formation, both of which are critical for maximizing electrochemical activity. Additionally, durability metrics, particularly operational lifetimes exceeding 1000 h at industrially relevant current densities, suggest that HEAs are not only promising from a performance standpoint, but also from a scalability and cost-effectiveness perspective. Overall, the table captures how rational compositional tuning, guided by structural and electrochemical descriptors, is central to overcoming the kinetic and thermodynamic barriers inherent to OER, positioning HEAs as front-runners in next-generation water-splitting technologies.

The rapid expansion of HEAs in OER research stems from their exceptional compositional flexibility and structural tunability, which enable the rational design of multifunctional and stable electrocatalysts. Across the reviewed studies, diverse synthesis approaches, such as mechanical alloying, molten salt electro-deoxidation, electrodeposition, and template-assisted thermal treatments, have been employed to generate nanostructured HEAs. These techniques yield both self-supported electrodes (e.g., dealloyed monoliths, pressed powders) and nanocomposites deposited on conductive supports. Mechanical alloying offers precise control over phase formation and element distribution, while electrochemical and template-assisted routes facilitate high surface area and porosity, key factors in maximizing active site exposure and improving mass transport during OER. The resulting catalysts have demonstrated not only low overpotentials and favorable Tafel slopes but also long-term operational durability under alkaline and even industrial conditions.

Looking forward, several strategies may further advance HEA-based OER catalysts. Selective doping with rare-earth or alkaline-earth elements (e.g., La, Sr) can enhance electronic conductivity and accelerate surface redox cycling. Surface amorphization and defect engineering, achieved via electrochemical activation or rapid thermal quenching, can introduce highly reactive, non-crystalline domains. In parallel, nanostructuring via dealloying or hydrothermal methods may boost electroactive surface area while facilitating ion transport. Importantly, operando spectroscopy and density functional theory (DFT) simulations will be essential to reveal the dynamic evolution of active species and guide electronic structure tuning. HEAs offer a robust platform to overcome conventional OER limitations by enabling a distribution of surface adsorption energies across multivalent metal centers, thus breaking traditional scaling constraints. These characteristics position HEAs as a versatile and cost-effective alternative for alkaline electrolyzers and metal–air batteries, delivering a favorable balance between performance, durability, and material sustainability.

4.4. Electrocatalytic ORR

The growing global energy demand, coupled with increased urbanization and technological development, has led to a heavy dependence on fossil fuels, significantly accelerating atmospheric CO_2 emissions and contributing to climate change. According to the International Energy

Table 6
Summary of HEAs for OER.

HEA Composition	Synthesis Method	Crystal Phase (XRD)	Electrode Configuration	Electrolyte	η @10 mA cm^{-2} (mV)	Tafel Slope (mV dec^{-1})	Stability	DOI
FeCoNiCuMn	Solvothermal synthesis of MOF precursor + thermal reduction under Ar/H_2	FCC	Self-supported (porous HEA nanoparticles)	1.0 M KOH	196	55	Chronopotentiometry, 75 h at 10 mA cm^{-2}, stable	[145]
FeNiCoCuMo	Mechanical alloying + hot-press sintering	FCC + BCC	Self-supported	1.0 M KOH	370	77	Chronopotentiometry, 100 h at 10 mA cm^{-2}, stable	[80]
FeMnCuCo	One-step electrodeposition	FCC	Self-supported ¿	1.0 M KOH	226	58	Chronoamperometry, 100 h at 50 mA cm^{-2},	[145]
CoNiRuIrMn	One-pot co-reduction method	FCC	Supported (details not specified)	1.0 M KOH	169	58	Chronoamperometry, 40 h at 10 mA cm^{-2}, stable; 20 h at 100 mA cm^{-2}, stable	[146]
CoCrFeNiMo	Microwave sintering using	FCC	Self-supported	1.0 M KOH	220	59	Chronopotentiometry, 24 h at 10 mA cm^{-2}	[84]
FeCoNiCrMo	Electrochemical dealloying	FCC + σ	Self-supported (nanoporous dealloyed film)	1.0 M KOH	280	69	Chronopotentiometry, 50 h at 10 mA cm^{-2}	[147]
CoFeGaNiZn (CFGNZ)	Inert gas condensation and cyclic voltammetry activation	FCC	Supported	1.0 M KOH	370	71	Chronoamperometry, 10 h, stable	[148]
$Fe_{0.5}CoNiCuZn_x$ (optimal at $Zn_{0.8}$)	Molten salt electrolysis	FCC	Self-supported (sintered monolith)	1.0 M KOH	340	79	Chronopotentiometry, 24 h, stable	[142]
FeCoNiCrMn	Salt-templated approach with NaCl + annealing at 750 °C	FCC	Self-supported	1.0 M KOH	294	55	Chronopotentiometry, 100 h at 100 mA cm^{-2},	[142]
FeCoNiIrRu (Ir@HEA/CNF)	Electrospinning + thermal treatment	FCC	Supported (in carbon nanofibers)	0.5 M H_2SO_4	241	154	Chronopotentiometry, 20 h at 50 mA cm^{-2}	[149]
CoCuFeNiMnMo	Mechanical alloying and ink deposition	FCC + BCC	Supported	1.0 M KOH	272	55.7	Chronopotentiometry, 72 h at 10 mA cm^{-2},	[150]
FeCoNiMnM	Molten salt electrolysis of solid oxides	FCC	Self-Supported	1.0 M KOH	279	56	Chronopotentiometry, 1000 h at 10 mA cm^{-2},	[144]

Agency, global energy consumption is projected to increase by the equivalent of 18 billion tons of oil by 2035, resulting in 43 gigatons of CO_2 emissions. Among emerging energy technologies, fuel cells represent a promising pathway to decarbonization due to their high energy efficiency and zero carbon emissions. Proton Exchange Membrane Fuel Cells (PEMFCs) and Alkaline Fuel Cells (AFCs) have gained traction for both stationary and transportation applications, offering energy efficiencies of up to 60 %, significantly higher than those of conventional internal combustion engines (~15 %).[127,151].

One of the bottle necks in fuel cell performance lies in the oxygen ORR at the cathode. Unlike hydrogen oxidation at the anode, which proceeds with relatively low overpotential and minimal catalyst loading, ORR is inherently sluggish due to its multi-step mechanism involving O_2 adsorption, O–O bond cleavage, formation of O–H intermediates, binding of intermediates to the active sites and desorption of oxygen containing species. These processes require high overpotentials and impose strict demands on the catalytic surface, especially on electrolytes commonly used in fuels like acidic and alkaline electrolytes. Traditionally, platinum-based catalysts have dominated this area, but their high cost and scarcity motivate the exploration of less-costly alternatives. HEAs emerge as promising candidates, offering tunable surface chemistry and complex adsorption landscapes by varying their multicomponent compositions. The combination of a distorted but ordered crystal lattice and a statistically rich distribution of local atomic environments allows HEAs to modulate oxygen binding energy and increase the density of active sites. However, identifying optimal HEA compositions for ORR remains challenging due to the vast compositional space and the limited availability of predictive computational models [152].

Batchelor et al. [153], developed a statistical modeling framework to predict catalytic activity on high-entropy alloy (HEA) surfaces by quantifying adsorption energies of key oxygen intermediates, *OH and *O, through DFT. Focusing on an equimolar IrPdPtRhRu alloy, selected for its low enthalpy of mixing, similar atomic radii, and high oxidation resistance, they simulated adsorption behavior on an FCC (111) surface (Fig. 15). The model partitions the local atomic environment surrounding adsorption sites into multiple coordination zones: surface and subsurface neighbors contributing single or dual coordination interactions. For *OH adsorption, DFT calculations across 871 unique 2 × 2 surface configurations revealed significant variation in binding energies, depending on the atomic ensemble at the on-top sites. Similarly, for *O adsorption at FCC hollow sites, 998 configurations were evaluated, involving 35 possible three-metal site combinations. This distribution of binding energies reflects the intrinsic heterogeneity of HEAs and provides a statistical descriptor space rather than a single binding energy value. By applying a simple machine learning regression, the authors established a direct and predictive correlation between local surface geometry and adsorption energy. The resulting model enables efficient screening of HEA compositions for ORR, where intermediate adsorption energy serves as a key activity descriptor, thereby offering a computational roadmap to bypass the limitations of trial-and-error alloy discovery [154].

Electrocatalysts based on HEA data have also been obtained experimentally for ORR. Chen et al [155] synthesized PdCuPtNiCo HEA nanoparticles using a core–shell strategy that leverages intermetallic templating for precise structural control. Initially, PdCu B2-type intermetallics served as seeds onto which Pt, Ni, and Co were deposited, forming core@shell PdCu@PtNiCo nanoparticles (Fig. 16). Subsequent annealing facilitated interdiffusion and phase homogenization, resulting in uniform FCC-phase PdCuPtNiCo HEA nanoparticles with diameters ranging from 10 to 50 nm. Energy-dispersive X-ray spectroscopy (EDS) and elemental mapping confirmed the homogeneous elemental distribution across the particles. When supported on carbon, these HEAs exhibited superior electrocatalytic performance for the oxygen reduction reaction (ORR), showing a more positive onset potential and higher half-wave potential (0.83 V) compared to both the core@shell precursor and commercial Pt/C (0.81 V). Furthermore, the HEA/C catalyst demonstrated outstanding durability, retaining activity after 10,000

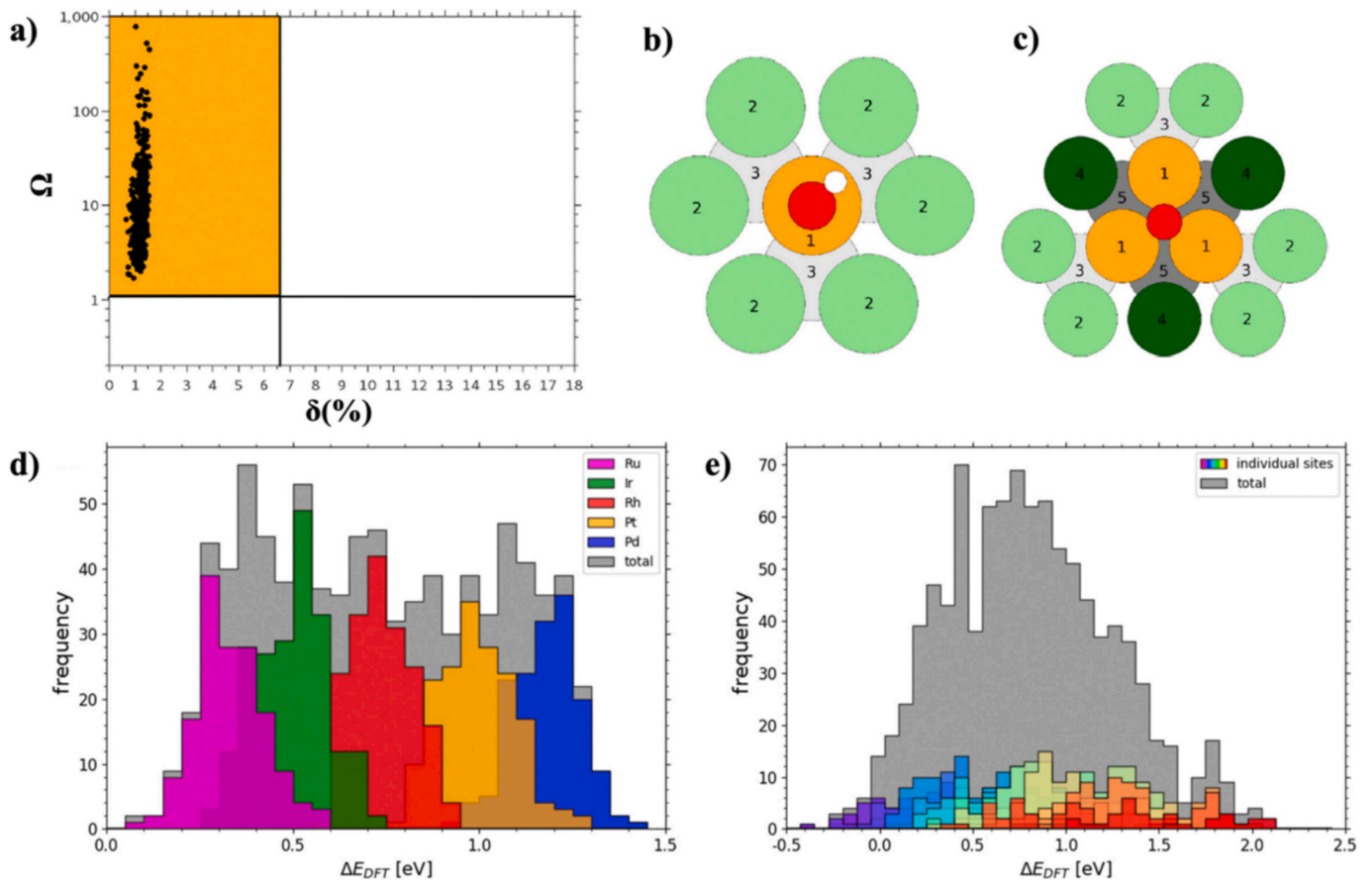

Fig. 15. A) the solid solution phase of the hea is illustrated in a graph where the values of omega (ω) are plotted against the values of delta (δ) for each 8-atom bulk hea unit cell. b) OH and *O adsorbates on-top and fcc hollow binding sites, calculated with DFT and its expanded model in c). d) Distribution of DFT Adsorption Energies of binding between *OH and *O to 871 and 998 different 2 × 2 unit cells and its individual sites in e) [153],.

accelerated cycles. The enhanced ORR performance is attributed to the synergistic electronic interactions among the multimetallic constituents and the high dispersion and uniformity of the nanoparticles, which ensure abundant active sites and facilitate optimal adsorption–desorption dynamics for oxygen intermediates.

Li et al. [79] developed a series of nanoporous np-HEA) electrocatalysts with reduced Pt loadings, aiming to overcome the cost limitations of conventional ORR catalysts that typically rely on 60–70 wt% Pt. Using a melt-spinning technique followed by chemical dealloying in NaOH, they fabricated AlCuNiPtX alloys (X = Mn, Ir, Pd, Ti, etc.) with open porous architectures and FCC crystal structures. Among the synthesized quinary alloys, AlCuNiPtMn showed the highest ORR performance, achieving a half-wave potential of 0.945 V in acidic medium and a mass activity ~ 16 times higher than commercial Pt/C. Superior activity is attributed to both the optimized electronic structure and the high surface area of the np-HEA. XPS revealed shifts in the Pt 4f binding energy to lower values compared to Pt/C, indicating electron transfer from surrounding alloying elements to Pt, which modifies the d-band center and enhances $*O_2$ adsorption–desorption kinetics. Furthermore, post-cycling XPS analysis showed a reduction of surface oxides and enrichment of metallic states, particularly in Cu and Ni, contributing to increased ECSA and long-term catalytic stability. These findings demonstrate that compositional tuning through Mn incorporation and structural control via dealloying can synergistically enhance both the intrinsic and extrinsic properties of Pt-based HEAs, offering a viable pathway toward low-Pt, high-performance ORR electrocatalysts.

Xueru et al [156] designed a nitrogen-doped HEA catalyst featuring a Pt-rich shell surrounding a PtCoFeNiCu core supported on carbon (N–Pt/HEA/C), aiming to enhance ORR performance through dual surface engineering strategies. The synthesis involved annealing metal precursors in a H_2/He atmosphere to form the HEA core, followed by nitrogen doping via NH_3 treatment and acid leaching to remove surface oxides. XRD and STEM-EDS confirmed the formation of a uniform core–shell structure with homogeneously distributed metals and nitrogen. The catalyst delivered a high mass activity of 1.34 A $mgPt^{-1}$ at 0.9 V, surpassing that of commercial Pt/C, and retained over 80 % of its activity after 30,000 cycles. This enhancement was attributed to the combined effects of the HEA core, which modulates the electronic structure and optimizes O_2 and OH adsorption energies, and nitrogen doping, which facilitates charge transfer and stabilizes the Pt shell. XPS analysis confirmed the incorporation of nitrogen species, notably pyridinic and graphitic N, which contribute to improved electron conductivity and metal–N coordination, reinforcing structural stability and catalytic longevity. This study highlights the synergistic potential of heteroatom doping and entropy-driven design in developing durable and high-performance ORR catalysts for fuel cell technologies.

Zhang et al. [157] reported the fabrication of ultrasmall PtAuPdFeCoNiCu HEA nanoparticles using a carbon thermal shock (CTS) strategy, where rapid Joule heating enables the in situ alloying of metal precursors directly onto carbon cloth substrates. The resulting nanocatalyst exhibited a uniform FCC crystal structure with a narrow size distribution centered at ~ 2 nm, as confirmed by HRTEM and XRD. Elemental mapping revealed homogeneous distribution of all seven metals, indicating successful entropy-driven alloy formation without phase segregation. The hierarchical architecture, consisting of HEA nanoparticles tightly anchored onto a flexible, conductive support, contributed to exceptional electrochemical durability, retaining structural integrity after 20,000 CV cycles. Electrochemical evaluation in acidic electrolyte

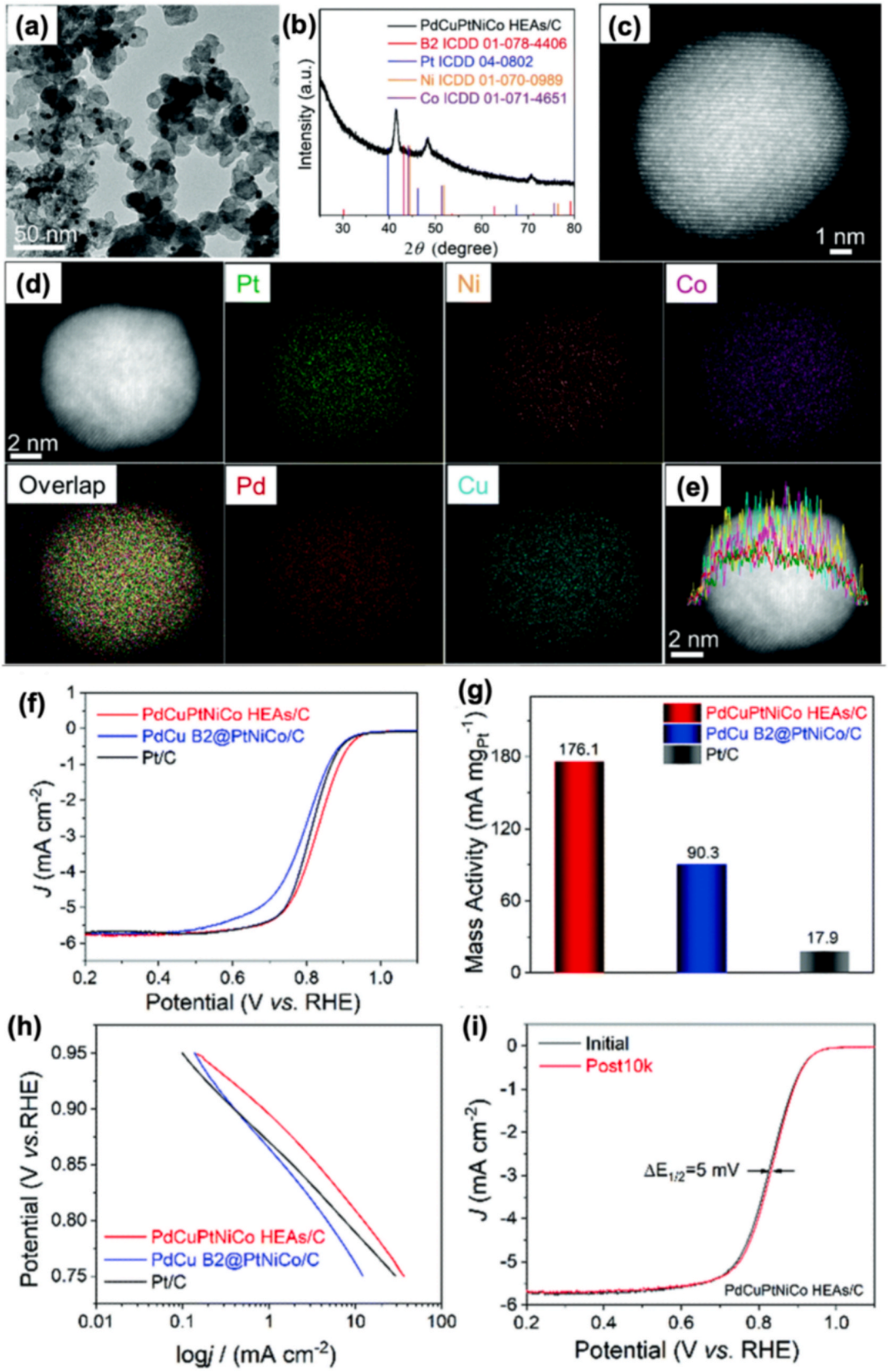

Fig. 16. Morphological and compositional analysis of PdCuPtNiCo high-entropy alloys supported on carbon (HEAs/C) is presented through various techniques: (a) TEM bright-field image, (b) XRD pattern, (c) STEM-HAADF image, (d) STEM-EDS elemental mapping images, and (e) line scan profile (f) Polarization curves recorded in O_2-saturated 0.1 M KOH solution at a rotation rate of 1600 rpm, (g) Mass activity measured at 0.9 V, and (h) Tafel plots. (i) ORR polarization curves of the PdCuPtNiCo HEAs/C before and after 10,000 cycles are compared. (e) line scan profile. [155].

($0.1\ M\ HClO_4$) revealed promising oxygen reduction reaction (ORR) activity, with an onset potential of 0.88 V, a half-wave potential ($E_1/_2$) of 0.78 V vs. RHE, and a kinetic current density of 1.5 $mA{\cdot}cm^{-2}$ at 0.9 V. The catalyst also demonstrated fast kinetics, reflected in a Tafel slope of 57.7 $mV{\cdot}dec^{-1}$, and a near-ideal four-electron transfer mechanism with low H_2O_2 yield (~4.95 %), pointing to efficient and selective O_2 reduction.

The outstanding ORR performance is attributed to synergistic interactions between noble metals (Pt, Au, Pd) and first-row transition metals (Fe, Co, Ni, Cu), which modulate the electronic structure of the active sites, particularly through d-band tuning of Pt, optimizing adsorption energies for O_2 and reaction intermediates. The multimetallic matrix suppresses phase separation and promotes long-term stability under acidic operating conditions. Notably, when integrated into a direct borohydride fuel cell (DBFC) as a cathode, the HEA catalyst outperformed commercial Pt/C by achieving a peak power density of 477 $mW{\cdot}cm^{-2}$ and sustaining continuous operation for over 41 h at 50 $mA{\cdot}cm^{-2}$. These results highlight the efficacy of the CTS synthesis approach not only for producing uniformly dispersed, multicomponent HEA nanoparticles, but also for enabling scalable and robust electrode integration. Collectively, this study underscores the potential of entropy-stabilized nanocatalysts as next-generation ORR electrocatalysts with competitive activity, durability, and reduced noble metal content for practical fuel cell applications.

The recent study by Bib Khan et al. [25] presents a compelling case for the development of platinum-free HEA catalysts for ORR and OER, using a low-temperature pulse microwave (PM) synthesis strategy. Two novel HEAs, $Cr_{18.2}Zr_{13.5}Ti_{5.3}Co_{17.8}Ni_{8.4}Cu_{8.5}Fe_{28.3}$ and $Al_{15.3}Mn_{18.2}Ti_{3.7}Co_{23.2}Ni_{5.9}Cu_{5.9}Fe_{27.8}$,were uniformly anchored on reduced graphene oxide (rGO) sheets. Advanced characterization (TEM, EDS, and XRD) confirmed the formation of uniformly dispersed nanocrystals with lattice fringes and good crystallinity. The CrZr-HEA-rGO sample in particular exhibited exceptional performance: for OER, an overpotential of just 500 mV at 8 mA cm^{-2} and a low Tafel slope of 75.33 mV dec^{-1} were achieved, far surpassing commercial Pt/rGO benchmarks. Additionally, it demonstrated the highest electrochemical surface area (737 $cm^2\ g^{-1}$) and the lowest charge-transfer resistance.

For the ORR, the CrZr-HEA-rGO catalyst again outperformed its counterparts, achieving a half-wave potential of ~ 700 mV and a limiting current density of 27.1 mA cm^{-2},both higher than Pt/rGO and the AlMn-HEA-rGO variant. A Tafel slope of 85.32 mV dec^{-1} underscores the superior kinetics. Stability was also thoroughly evaluated: chronoamperometry and long-term i–t curves revealed remarkable anti-CO poisoning behavior and electrodurability over extended cycles. These findings highlight not only the efficiency of the PM method in fabricating HEA catalysts but also position CrZr-based HEAs as a leading alternative to Pt-based materials for sustainable and high-performance energy applications. The integration of transition metals with complementary properties in a configurationally complex matrix, anchored on a conductive rGO support, provides a synergistic platform to overcome traditional ORR/OER catalytic limitations.

Table 7 shown the comparative analysis of HEA-based catalysts summarized in the ORR performance table underscores the strategic impact of compositional complexity and nanostructuring on electrocatalytic activity in fuel cell cathodes. Alloys such as PtCoFeNiCu, synthesized via wet impregnation and acid leaching, deliver exceptional mass activity (1.34 A $mgPt^{-1}$) and a half-wave potential ($E_1/_2$) of 0.924 V vs. RHE [156], outperforming commercial Pt/C. Similarly, $Al_{96}Cu_{1.}$ $Ni_1Pt_1Mn_1$ prepared by top-down dealloying exhibits a remarkably high mass activity of 3.5 A $mgPt^{-1}$ and $E_1/_2$ of 0.954 V, despite its dilute Pt content [79]. These results highlight the critical role of transition metals such as Mn, Co, and Ni in modulating the electronic environment of Pt and promoting optimal oxygen intermediate adsorption energies. Notably, the outstanding performance of the AlCuNiPtMn system confirms that atomic-scale dispersion of Pt within a high-entropy matrix can drastically increase its utilization efficiency.

Table 7
Summary of HEAs for ORR.

HEA Composition	Synthesis Method	XRD Phase	Electrode Type	Electrolyte	E_{onset} (V)	$E_{1/2}$ (V)	Tafel Slope (mV/dec)	Mass Activity (A mg_Pt or cat^-1)	Specific Activity (mA cm^-2)	Electrons	Stability	Reference
AlCuNiPtMn	Top-down dealloying	FCC	Supported (GC/CP)	0.1 M $HClO_4$, 0.1 M KOH	1.00	0.945 / 0.954	66	3.5	5.5	4.0	30,000 CV + chronoamperometry	[79]
FeNiCrCoMn	NaBH4 reduction + annealing	FCC	Supported (CNTs)	0.1 M KOH	0.87	0.84	69.2	0.79	1.38	4.0	24 h chronoamperometry	[144]
CrMnFeCoNi	Solution-phase synthesis	FCC	Supported (GCE)	0.1 M KOH	0.88	0.78	37.9	0.43	0.78	3.95	30 h chronoamperometry	[158]
PtRhNiFeCu	Solution-phase synthesis + annealing	FCC	Supported (Carbon)	0.1 M $HClO_4$	0.92	0.90	45	1.23	2.67	~4.0	10,000 CV	[159]
FeCoNiMnV	One-step pyrolysis	FCC	Supported (N-CNT)	0.1 M KOH	0.951	0.851	41	0.82	6.22	3.91–3.95	10,000 CV,	[160]
PtCoFeNiCu1	Wet impregnation + acid leaching	FCC	Supported (C)	0.1 M $HClO_4$	0.96	0.924	55.6	1.34	1.93	4.0	30,000 CV	[156]

Furthermore, Pt-free systems like FeCoNiMnV demonstrate respectable ORR activity (0.82 A mg_{cat}^{-1}) and a specific activity of 6.22 mA cm^{-2} [160], confirming that entropy-driven alloying of base metals can yield stable and catalytically competent surfaces. Structurally, most of the top-performing alloys exhibit FCC phases, which are known to offer favorable surface energetics and active site symmetry for O_2 activation. These HEAs are especially promising for application in PEMFC and DBFC systems, where long-term stability and Pt reduction are critical. Collectively, the table highlights that tailored elemental design, combining noble and non-noble metals within a high-entropy lattice, can effectively decouple catalytic performance from noble metal content, offering a viable path toward next-generation, cost-effective ORR electrocatalysts.

The studies reviewed in this section highlight the remarkable potential of HEAs as next-generation catalysts for the ORR, particularly in the context of fuel cell technologies. Through strategic elemental engineering and advanced synthesis techniques, including thermal shock methods, chemical dealloying, and wet-chemical assembly, HEAs demonstrate the ability to modulate surface electronic structures, optimize oxygen intermediate binding energies, and enhance catalytic turnover frequency. Notably, both Pt-rich systems (e.g., PtCoFeNiCu and AlCuNiPtMn) and Pt-free compositions (e.g., FeCoNiMnV and CrZrTiCoNiCuFe) have achieved high mass activities, favorable onset and half-wave potentials, and long-term operational durability, thereby challenging the traditional reliance on monometallic Pt-based catalysts.

The presence of transition metals such as Mn, Co, Fe, and Ni enhances charge transfer and adsorption site diversity, while the introduction of noble metals like Pd, Au, or Pt in low concentrations maximizes utilization efficiency. Moreover, the consistent use of FCC phases and hierarchical nano-architecture contributes to improved reaction kinetics and corrosion resistance in acidic environments. Collectively, the integration of HEA catalysts into PEMFCs and direct DBFCs offers a promising path toward scalable, cost-effective, and high-performance energy conversion devices, reinforcing the importance of multimetallic design in the future of electrocatalysis.

4.5. *Electrocatalytic CO_2RR*

The global release of carbon dioxide has reached approximately 4.4 metric tons per capita, primarily due to the combustion of fossil fuels for energy generation [161]. As a long-lived greenhouse gas, CO_2 has been a major contributor to climate change for over four decades. One promising strategy to mitigate anthropogenic CO_2 emissions involves its electrochemical conversion into value-added fuels and chemicals, mimicking natural photosynthesis [162]. However, the inherent thermodynamic stability and linear geometry of the CO_2 molecule result in high activation barriers and sluggish reaction kinetics, limiting the selectivity and efficiency of conventional catalytic processes [163].The adsorption and subsequent activation of CO_2 on catalyst surfaces remain key challenges that must be addressed to enable practical and scalable electrochemical CO_2RR.

Electrocatalytic CO_2RR has gained considerable attention due to several inherent advantages [164]: (i) it can be carried out under mild temperatures and pressures; (ii) the selectivity and product distribution can be tuned by controlling reaction parameters such as electrode potential, electrolyte composition, and catalyst morphology; (iii) when powered by renewable electricity, the process can operate carbon-neutrally; and (iv) it offers the potential to selectively produce high-value multicarbon products, including methane (CH_4), methanol (CH_3OH), and ethylene (C_2H_4), thereby enhancing economic viability [80–84]. Nevertheless, a persistent challenge in aqueous media is the competitive HER, which diminishes faradaic efficiency by diverting electrons away from CO_2 conversion pathways. Overcoming this competition is essential for improving the selectivity toward deeply reduced carbonaceous species and advancing CO_2RR toward commercial relevance [165–168].

Pedersen et al. [26] developed a probabilistic framework to identify promising HEA compositions for selective CO_2 electroreduction by integrating DFT with supervised machine learning. Specifically, they modeled the adsorption energies of key intermediates, CO* and H* on two multicomponent surfaces: CoCuGaNiZn and AgAuCuPdPt (Fig. 17). By focusing on the (111) facets of FCC structures, which closely resemble experimentally exposed surfaces, the authors generated a Gaussian process regression model to predict adsorption energy distributions across compositional space with high fidelity to DFT benchmarks. Their results showed that the distribution of adsorption energies can be modulated by adjusting the elemental ratios, thereby enabling control over catalytic behavior. Using a dual-descriptor approach, weak *H adsorption (to suppress H_2 evolution) and strong *CO binding (to favor CO_2RR pathways),they identified compositionally disordered alloys with optimal local environments for selective CO_2 reduction. This study provides a fundamental basis for rational HEA design by highlighting how compositional tuning impacts the energy landscape of intermediate binding, offering a predictive route to accelerate discovery beyond trial-and-error approaches.

Building upon the theoretical framework proposed by Pedersen[26], Nellaiappan et al. [169] experimentally synthesized a nanostructured high-entropy alloy (HEA) composed of AuAgPtPdCu for electrocatalytic CO_2 reduction. The HEA was prepared via arc melting followed by cryomilling, yielding nanoparticles with a uniform FCC structure as confirmed by X-ray diffraction, and an average size of 16 ± 10 nm. When coated onto a glassy carbon electrode, the HEA displayed remarkable electrocatalytic activity under low overpotentials. CV and XPS revealed that the redox-active Cu centers, especially the Cu^{2+}/Cu^0 redox pair, played a dominant role in facilitating CO_2 reduction, while the noble metals (Au, Ag, Pt, Pd) provided electronic stabilization and structural integrity, promoting a synergistic enhancement in catalytic performance. Notably, the system achieved nearly 100 % faradaic efficiency toward gaseous CO_2 reduction products at a low applied potential of –0.3 V vs. RHE, significantly outperforming monometallic Cu catalysts under identical conditions. These findings not only validate the predictive utility of machine-learning-guided DFT models but also demonstrate the viability of HEAs as tunable, multi-site electrocatalysts for efficient and selective CO_2RR at low energetic cost.

With the aim of exploiting the capacity of HEAs to generate electrocatalytic processes, Cavin et al [170] explored the integration of HEA chemistry with two-dimensional (2D) transition metal dichalcogenides (TMDs) to design highly active electrocatalysts for CO_2 reduction. Using density functional theory (DFT), they evaluated the thermodynamic stability of several quinary and quaternary sulfide-based HEAs, namely $(MoWNbV)S_2$, $(MoWNbTa)S_2$, $(MoVNbTa)S_2$, and $(MoWVNbTa)S_2$, by calculating their formation enthalpies and configurational entropy as a function of temperature. Among these, $(MoWVNbTa)S_2$ was identified as the most promising composition due to its favorable adsorption energy profile for CO desorption. These materials were synthesized via single-zone chemical vapor transport (CVT) followed by liquid-phase exfoliation to produce nanoflakes. Atomic force microscopy (AFM) and STEM-HAADF imaging confirmed the successful fabrication of ultrathin, layered structures comprising 8–16 atomic layers. When employed as a cathode, $(MoWVNbTa)S_2$ exhibited outstanding CO_2RR performance, achieving a current density of 0.51 A cm^{-2} and a turnover frequency (TOF) of 58.3 s^{-1} at low overpotentials. The high activity and selectivity toward CO production were attributed to the low binding energy of CO on the multimetallic active sites, which facilitated rapid intermediate desorption and suppressed competing reactions. This work opens a new design paradigm by combining entropy stabilization with 2D catalytic architectures, positioning HEA-TMD hybrids as a versatile platform for efficient and scalable CO_2 electroreduction.

Yan Zhu et. al [156] reported the synthesis of a high-entropy perovskite catalyst, $Sr_2Fe_{0.4}V_{0.4}Mo_{0.4}Ni_{0.4}Ti_{0.6}O_6{-}\delta$ (SFVMNT), via a citrate–nitrate sol–gel method, followed by self-combustion and laser processing to produce a well-oxidized perovskite phase. To enhance

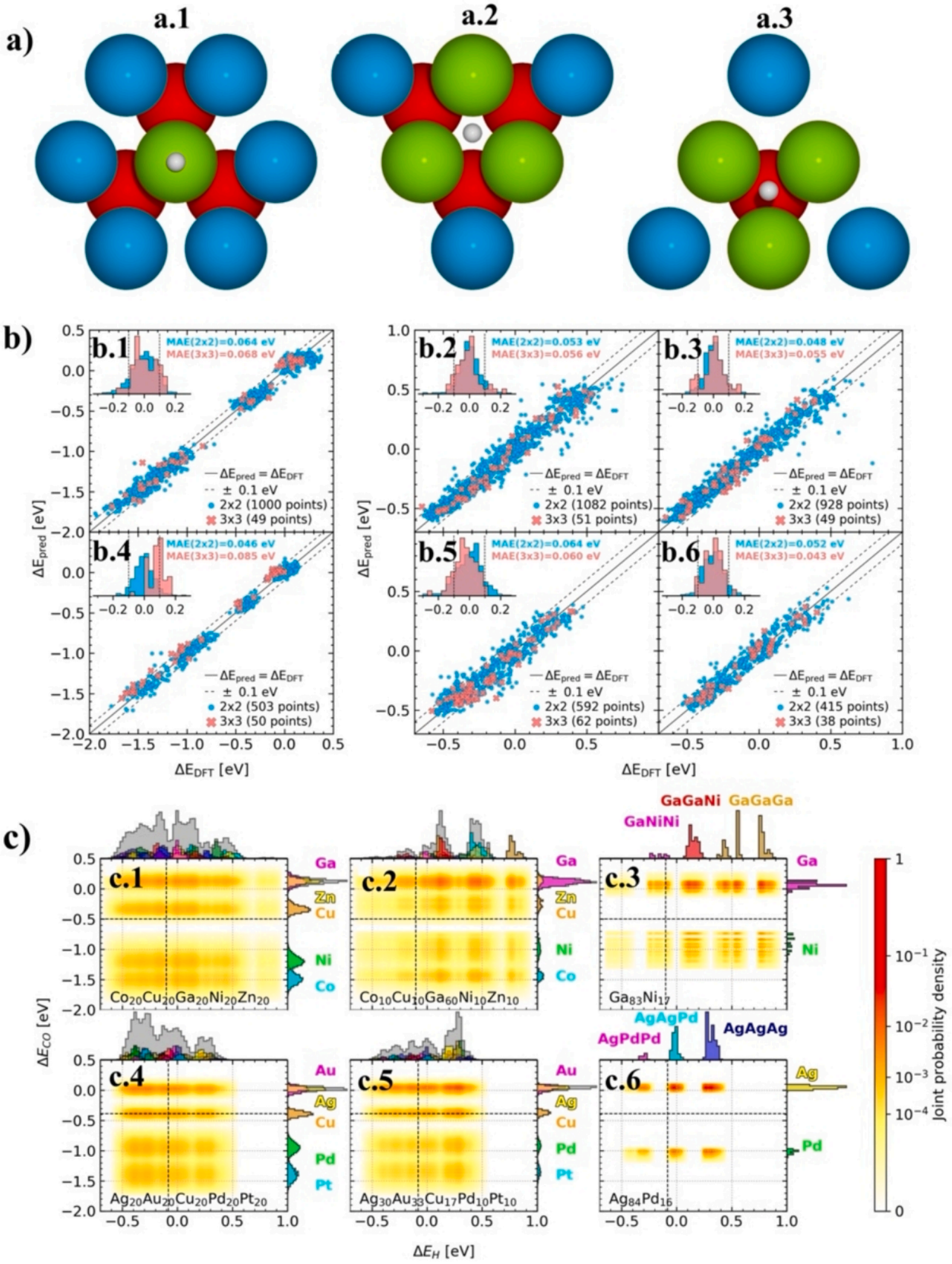

(caption on next page)

Fig. 17. Surface microstructure configurations are depicted, showcasing the arrangement of neighboring atoms used to simulate the chemical surroundings around an adsorption site on a (111) surface for three different types of adsorptions: (a) on-top, (b) FCC-hollow, and (c) HCP-hollow. The illustration uses white circles to represent the adsorbing intermediate, green circles for the adsorbing atoms on the surface, blue circles for the closest surface neighbors, and red circles for the closest subsurface neighbors. [26]. (b) Plots illustrate the GPR-predicted (ΔE_{pred}) versus DFT-calculated (Δ_{EDFT}) adsorption energies for two sets of alloys: CoCuGaNiZn and AgAuCuPdPt. Specifically, the adsorption energies for on-top CO, FCC-hollow H, and HCP-hollow H are shown. The insets display the distribution of the prediction errors in eV, defined as $\Delta E_{pred} - \Delta_{EDFT}$ [26]. (c) The plot displays the distributions of H and CO adsorption energies for six disordered (111) alloys. Two sets of alloys are used as starting points: (a-c) CoCuGaNiZn and (d-f) AgAuCuPdPt. Three scenarios are shown for each set: (a, d) equimolar compositions, (b, e) optimal compositions with at least 10 % of each element, and (c, f) locally optimal compositions without constraints. The histograms along the axes represent the distributions of H and CO adsorption energies, with colors indicating the corresponding adsorption sites. [26]. (For interpretation of the references to colour in this figure legend, the reader is referred to the web version of this article.)

catalytic functionality, an in situ exsolution strategy was employed, resulting in the formation of NiFe alloy nanoparticles embedded on the surface of the cubic-phase high-entropy perovskite. This dual-phase architecture, comprising electronically active alloy nanoparticles and a compositionally disordered oxide matrix, enabled strong interfacial coupling and enhanced electron transport across the catalyst surface. Structurally, the high-entropy perovskite provides a stable and tunable host lattice, while the exsolved NiFe alloy introduces catalytically active sites with optimized binding energies for CO_2 intermediates.

Electrochemical evaluation of the NiFe@SFVMNT catalyst revealed outstanding performance in high-temperature CO_2 reduction reaction (CO_2RR). At 800 °C and 1.5 V, the system achieved a current density of 1.66 A cm^{-2}, maintaining continuous operation for over 200 h without significant degradation, outperforming several benchmark cathode materials. The observed durability and activity are attributed to the synergistic effects between the multivalent cations in the high-entropy oxide and the metallic NiFe phase, which together enhance charge transfer kinetics, stabilize active sites, and facilitate CO_2 activation. This work highlights the emerging role of entropy-stabilized perovskites as robust, thermochemically resilient platforms for advanced CO_2 electroreduction, especially under solid oxide electrolysis conditions.

The high-entropy alloy (HEA) catalysts summarized in Table 8 for CO_2RR illustrate the immense potential of these materials in transforming electrochemical CO_2 conversion into a scalable, efficient, and selective process. Alloys such as equimolar AuAgPtPdCu synthesized via cryomilling and annealing demonstrate nearly 100 % Faradaic efficiency for CH_4 and C_2H_4 production at − 0.3 V vs. RHE, with an onset potential between − 0.1 and − 0.2 V, and current density of 4.5 mA cm^{-2},clearly outperforming monometallic Cu under identical conditions [169]. Another compelling system, the CuCoAlFeNi HEA, produced ethanol (C_2H_5OH) with 36.56 % Faradaic efficiency at − 1.2 V, achieving a current density of 102.4 mA cm^{-2}, indicative of its ability to stabilize C–C coupling intermediates [171]. These results suggest that HEAs, by virtue of their multimetallic synergy, facilitate selective reduction pathways beyond simple CO formation, traditionally dominant in Ag- and Au-based systems.

From a compositional standpoint, the inclusion of both noble (e.g., Pt, Au, Ag) and earth-abundant metals (e.g., Cu, Fe, Ni, Co, Al) in HEAs introduces a complex electronic landscape that supports diverse intermediate binding strengths. Theoretical models, such as those based on DFT and machine learning, predict favorable *CO and *H adsorption energy distributions in systems like CoCuGaNiZn and CuMnNiZn, offering design rules for future catalysts targeting specific CO_2RR products such as CH_3OH or CH_4 [172]. Importantly, the ability to modulate selectivity through composition, rather than solely morphology or support effects, marks a significant advancement in CO_2 electroreduction. Future HEA development should focus on integrating DFT-guided tuning with advanced nanostructuring and operando characterization to elucidate structure–activity relationships, ultimately enabling the rational design of CO_2RR catalysts with tailored efficiency, product distribution, and stability profiles suitable for industrial applications.

To further enhance CO_2RR performance, HEAs can be engineered via: (i) controlled doping of p-block or rare-earth elements to modulate the local charge density and electronic conductivity; (ii) surface reconstruction strategies that expose high-index or defect-rich planes to maximize the density of active sites; and (iii) nanostructuring combined with porous or hybrid supports (e.g., carbon aerogels, N-doped graphene) to boost mass transport and reduce concentration gradients. Furthermore, the integration of operando characterization with DFT modeling is essential for understanding structure–function relationships and guiding rational design based on key descriptors such as ΔG_{CO2}, ΔG_{COOH}, or ΔG_{HCOO}.

In summary, HEAs offer a highly tunable and durable platform for CO_2 electroreduction, capable of addressing longstanding trade-offs between selectivity, activity, and stability, thus paving the way for scalable and sustainable CO_2 valorization technologies.

4.6. Electrocatalytic NRR

Ammonia (NH_3) is a cornerstone of the global chemical economy, ranking as the second most produced industrial compound worldwide. Beyond its critical role in fertilizer production, it is gaining attention as a potential carbon-free fuel and hydrogen carrier, owing to its high energy density (4.3 kWh kg^{-1}), ease of liquefaction at mild conditions (−33 °C), and high hydrogen content (17.6 wt%) [173–175]. At present, over 80 % of global NH_3 production is realized via the Haber–Bosch (HB) process ($N_2 + 3H_2 \rightarrow 2NH_3$), which operates at elevated temperatures (400–550 °C) and pressures (15–25 MPa), typically over Fe- or Ru-based catalysts. While thermodynamically favorable ($\Delta H^\circ = -45.9$ kJ mol^{-1}), the HB process is energy-intensive and heavily reliant on fossil-derived H_2, contributing significantly to global CO_2 emissions [176].

Driven by the urgent need for greener ammonia synthesis routes,

Table 8
HEAs applied to CO_2RR.

HEA Composition	Synthesis Method	Crystal Phase	Electrode Fabrication	Electrolyte	Faradaic Efficiency (%)	Products	Onset Potential (V vs. RHE)	Current Density (mA/cm²)	Stability Test	DOI
AuAgPtPdCu (equimolar)	Cryomilling followed by annealing at 800 °C	FCC	drop-cast on glassy carbon)	0.5 M $KHCO_3$	Approximately 100 % at − 0.3 V	CH_4, C_2H_4, CO, H_2	Between − 0.1 and − 0.2 V	4.5 at − 0.3 V	Chronoamperometry (10 h)	[169]
CuCoAlFeNi (non-equimolar)	Solvothermal synthesis	FCC	Supported (carbon paper, 0.4 mg)	1 M $KHCO_3$	36.56 % (C_2H_5OH) at − 1.2 V	C_2H_5OH, minor H_2	Around − 0.2 V	102.4 at − 1.2 V	Chronoamperometry, CV, EIS, Tafel (10 h)	[171]

electrocatalytic nitrogen reduction reaction (NRR) under ambient conditions has emerged as a compelling alternative. Inspired by biological nitrogenase enzymes, NRR offers the potential to directly convert N_2 and H_2O into NH_3 at room temperature and atmospheric pressure, with no greenhouse gas emissions [18,177]. Thermodynamically, the process is up to 20 % more efficient than HB, but its practical implementation is hindered by low faradaic efficiencies and the competing hydrogen evolution reaction (HER). Noble metals have shown promise as NRR catalysts; however, due to cost and scalability concerns, research has shifted toward transition metal-based systems. These materials offer tunable electronic configurations, high Earth abundance, and catalytic surfaces capable of activating the inert N≡N bond via their partially filled d orbitals and available vacant states [177,178]. The development of robust, selective, and energy-efficient NRR electrocatalysts thus remains a major challenge and opportunity in the pursuit of sustainable ammonia production[179].

High entropy alloys are expected to provide highly reactive surfaces for these reactions. Yu et al [180] conducted a comprehensive DFT investigation of FeCoNiCuPd-based HEAs to evaluate their catalytic potential for ambient nitrogen reduction. Using Special Quasirandom Structures (SQS) generated via Monte Carlo simulated annealing within the Alloy Theoretic Automated Toolkit (ATAT), six alloy compositions with varying elemental concentrations were analyzed, including FeCoNiCuPd, and Ni-enriched variants such as $Ni_{0.3}(FeCoCuPd)_{0.75}$. Adsorption of N_2 on the (111) facets were evaluated as the initial step, with an optimal range of adsorption energies defined by Sabatier's principle (−1.5 to − 0.5 eV). Among the tested compositions, $Ni_{0.3}(FeCoCuPd)_{0.75}$ exhibited the most promising characteristics: N_2 adsorbed vertically at Ce–Fe bridge sites with an energy of − 0.92 eV, elongating the N≡N bond to 1.14 Å and facilitating activation. This catalyst followed the associative distal mechanism with a low theoretical overpotential of 0.34 eV and a kinetic barrier of 0.50 eV for the rate-determining step ($*N_2 \rightarrow *NNH$), outperforming the parent equimolar alloy and Pd- or Cu-enriched variants. In contrast, alloys such as FeCoNiCuPd and $Pd_{0.3}$(FeCoNiCu) favored horizontal adsorption on Fe–Co or Fe–Fe–Co sites with comparable binding energies but less favorable reaction kinetics. These findings underscore the critical role of local atomic environment and compositional tuning, particularly Ni enrichment, in stabilizing key intermediates and reducing both thermodynamic and kinetic barriers for NRR on HEA surfaces.

Zhang et al. [181] developed a low-temperature synthesis strategy (<250 °C) to fabricate RuFeCoNiCu high-entropy alloy nanoparticles (HEA-nps) for nitrogen electroreduction (Fig. 18). The synthesis involved the co-reduction of metal precursors followed by annealing at 220 °C, yielding homogeneously alloyed nanoparticles with an average size of ~ 15 nm and a hexagonal close-packed (HCP) crystalline structure, as confirmed by X-ray diffraction (Fig. 16.c and d). When evaluated in 0.1 M KOH, the catalyst achieved exceptional electrocatalytic NRR performance at a remarkably low overpotential of 0.05 V vs. RHE, attaining a Faradaic efficiency (FE) of 38.5 % and an ammonia yield of 57.1 $\mu g\, h^{-1}\, mg_cat^{-1}$,significantly surpassing values reported for state-of-the-art catalysts under similar conditions (Fig. 24a–d). UV–Vis spectroscopy confirmed the selective formation of NH_3 with minimal side reactions. To understand the origin of this high performance, Monte Carlo and DFT simulations were performed. These revealed that Fe atoms in the HEA serve as the most thermodynamically favorable sites for N_2 adsorption and activation, while Co–Cu and Ni–Ru pairs promote efficient surface hydrogenation through *H intermediates, facilitating NH_3 formation. This cooperative mechanism, driven by the spatial and electronic distribution of multiple metal centers, demonstrates the unique catalytic advantages of entropy-stabilized nanoparticles and highlights the feasibility of HEA catalysts synthesized under mild conditions for ambient NRR applications.

Chen et al. [182] reported the synthesis of high-entropy boride (HEB) electrocatalysts based on $(TiVCrMo)B_2$, employing an ultrafast high-temperature sintering (UHS) technique (Fig. 19). This method

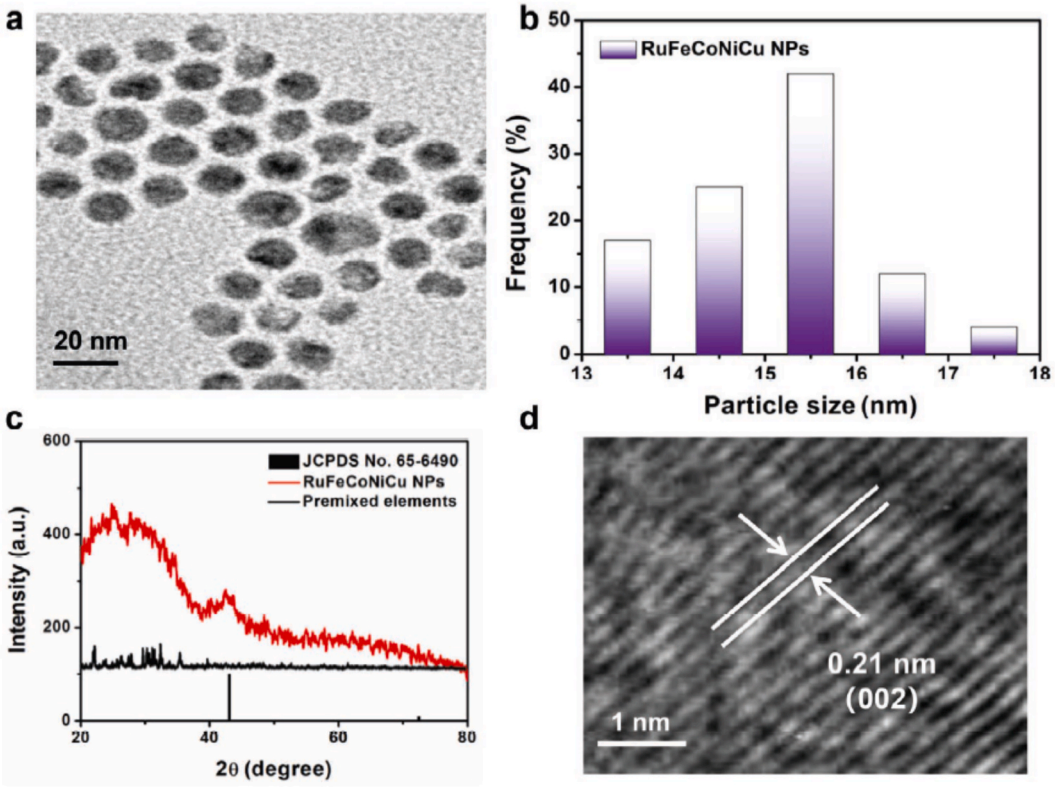

Fig. 18. A) tem image showing rufeconicu nanoparticles (nps). b) distribution of particle sizes for the rufeconicu nanoparticles (nps). c) xrd pattern of the premixed elements and the rufeconicu nanoparticles (nps). d) hrtem images of the rufeconicu nanoparticles (nps).[181].

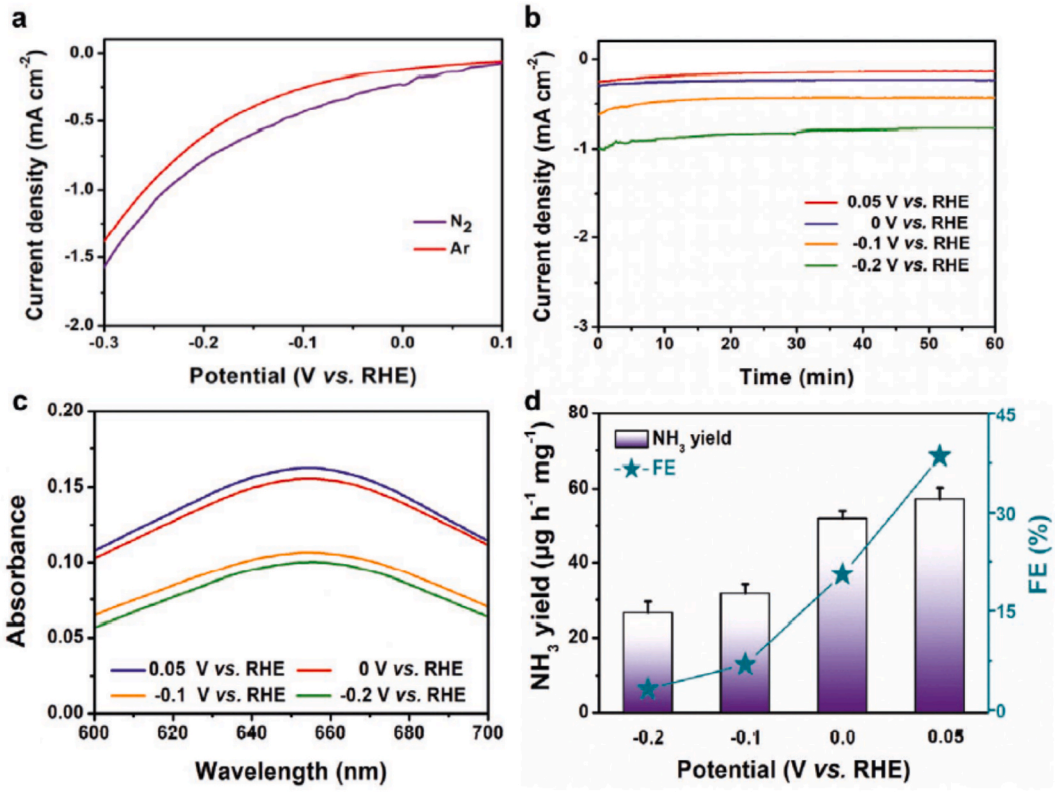

Fig. 19. A) polarization curves of rufeconicu/cp in 0.1 M KOH using a scan rate of 5 mVs^{-1}. b) Time-dependent current density curves at various potentials in N_2-saturated 0.1 M KOH. c) UV–visible absorption spectra of the 0.1 M KOH electrolytes stained with indophenol indicator after 1 h of electrolysis under N_2 at each specified potential. d) Ammonia (NH_3) yields and Faradaic Efficiencies at each specified potential in 0.1 M KOH. [181].

involved pressing stoichiometric mixtures of metal oxides and boron carbide, followed by rapid thermal treatment under argon atmosphere to achieve dense, crystalline diboride structures. To tailor electrocatalytic performance, transition metals Co, Ni, and Fe were introduced into the lattice, generating a series of compositionally complex borides. Structural and morphological characterizations via XRD, SEM, EDS, and XPS confirmed homogeneous elemental distribution and the preservation of the HEB diboride phase. Among the variants, the Co-doped HEB catalyst exhibited superior electrochemical performance for nitrate reduction to ammonia, achieving a Faradaic efficiency of 97.9 % and an NH_3 yield of 0.12 mmol·mg_cat^{-1}·h^{-1},one of the highest reported to date. EIS revealed a significantly reduced charge transfer resistance in the Co-HEB, indicating enhanced surface kinetics.

Mechanistic insights obtained from in situ FT-IR and electron paramagnetic resonance (EPR) spectroscopy highlighted the role of Co dopants in promoting *NO_3^- hydrogenation intermediates and facilitating electron transfer during the reaction pathway. Compared to Fe- and Ni-doped analogues, Co substitution resulted in faster reaction kinetics and more efficient electron delivery to nitrate species, ultimately accelerating NH_3 production. The catalyst also displayed exceptional stability under extended operating conditions, maintaining its activity and structural integrity, an essential criterion for industrial-scale nitrate valorization. These findings position Co-doped high-entropy borides as a highly promising class of electrocatalysts for sustainable ammonia synthesis, expanding the functional landscape of HEAs and high-entropy ceramics beyond N_2 activation into NO_3^- conversion pathways.

The data summarized in the NRR section's Table 9 clearly demonstrate the promise of high-entropy alloys (HEAs) as next-generation electrocatalysts for ammonia synthesis under ambient conditions. Notably, systems such as RuFeCoNiCu HEAs [181] exhibit exceptional activity, achieving a Faradaic efficiency of 38.5 % and NH_3 yields as high as 57.1 μg h^{-1} mg^{-1} at an overpotential of just 0.05 V vs. RHE. This level of performance at low overpotential underscores the superior kinetic and thermodynamic characteristics enabled by multimetallic synergy, especially when leveraging iron-centered active sites and Cu–Co/Ru–Ni configurations for *H formation and N_2 activation. Similarly, B-doped FeCoNiCuPd HEAs [184] exhibit excellent NO_3^--to-NH_3 conversion with Faradaic efficiencies near 40 % and significant current densities, driven by their uniform active surface and carbon nanofiber supports that enhance electron transfer.

Moreover, structural diversity plays a critical role in performance tuning. HE-MOF-derived systems such as FeNiCoVZn [185] offer a layered crystalline framework that not only stabilizes key reaction intermediates (*NNH, *NH_2) but also promotes multielectron transfer processes. These systems, by combining electrochemical robustness and favorable energetics for N_2 adsorption, represent scalable platforms for green ammonia synthesis. Particularly, the FeCoNiCuMn/NCNS catalyst [183] stands out with a Faradaic efficiency of 79.77 % and area-specific NH_4^+ yields exceeding 1100 μmol h^{-1} cm^{-2},some of the highest reported to date. These advances collectively position HEAs as chemically and structurally versatile catalysts with the potential to bypass the limitations of the Haber–Bosch process, paving the way toward decentralized, low-energy ammonia production.

HEAs represent a highly promising design platform for electrochemical nitrogen reduction due to their ability to host compositionally diverse, structurally disordered active sites capable of selectively adsorbing and activating N_2 molecules while suppressing the competing HER. Incorporation of early transition metals such as Mo, Ti, V, and Zr, well known for their π-backdonation capabilities and moderate N_2 binding strengths, enables the stabilization of *N_{2ads} through both end-on and side-on configurations, favoring associative reduction pathways. Furthermore, the intrinsic lattice distortion and electronic heterogeneity in HEAs lead to a broad distribution of adsorption energies for both *N_2 and *H, allowing for thermodynamic decoupling between NRR and

Table 9
Summary of HEAs applied to NRR.

HEA Composition	Synthesis Method	Crystal Phase	Electrode Configuration	Electrolyte	Faradaic Efficiency (FE)	Products Formed	Current Density / Yield	Overpotential	Stability	reference
FeCoNiCuMn	Calcination of HEA and Pulse Laser	Spinel	Supported on carbon cloth (CC)	0.2 M $NaHCO_3$ + 100 ppm $NaNO_2$	79.77 %	NH_4^+	1101.48 μmol h^{-1} cm^{-2}	−0.8 V vs. Ag/AgCl	5 h chronoamperometry at −1.6 V	[183]
RuFeCoNiCu	Oil-phase synthesis (≤250 °C)	hcp	Ketjen Black on carbon paper	0.1 M KOH, HCl, Na_2SO_4, Li_2SO_4	38.5 %	NH_3	11.4 μg h^{-1} cm^{-2}	0.05 V vs. RHE	100 h continuous test	[181]
B-doped FeCoNiCuPd	Electrospinning + carbonization of PVP	Dual fcc	Supported on CNFs	0.1 M Na_2SO_4	39.2 %	NH_3	24.8 μmol h^{-1} cm^{-2}	−0.6 V vs RHE	20 h cronopotenciometry	[184]
HE-MOF (FeNiCoVZn)	Pyrolysis of multimetallic MOF	Layered crystalline (MO_6 octahedra)	Glassy carbon	0.1 M Na_2SO_4 (acid) / 1 M KOH (alkaline)	~33.2 % (acid)	NH_3	11.6 μg h^{-1} cm^{-2} @ −0.2 V (acid)	−0.2 V vs. RHE	100 h in alkaline medium	[185]

HER. Surface-active elements such as Cr and Fe modulate the d-band center to weaken *H binding, thereby minimizing HER activity, while Nb and W introduce localized high-charge-density regions that promote protonation of $*N_{2ads}$, often the rate-determining step in the overall reaction mechanism.

To further enhance NRR performance, several rational design strategies have emerged: (i) DFT-guided compositional screening to achieve optimal ΔGN_2 *and* ΔGH values across distinct local atomic environments; (ii) defect or vacancy engineering to stabilize reaction intermediates such as $*N_2H$ or $*NH_2$ by inducing localized charge redistribution; and (iii) integration with hydrophobic or proton-conducting supports to spatially limit proton availability and suppress HER. Moving forward, the synergy between operando electrochemical–spectroscopic characterization and machine-learning–driven high-throughput screening will be crucial in accelerating the discovery of high-performing HEA-based NRR catalysts. Overall, the compositional tunability, thermochemical robustness, and multifunctional reactivity of HEAs position them as next-generation materials to overcome the long-standing limitations of ambient ammonia electrosynthesis.

5. Outlook

HEAs have evolved from a metallurgical curiosity to a transformative platform for electrocatalysis. Their hallmark, vast compositional freedom, allows the integration of multiple metallic elements into single-phase solid solutions, enabling exceptional structural tunability, surface complexity, and electrochemical versatility. This flexibility creates synergistic active sites that drive multi-step reactions with enhanced kinetics, selectivity, and durability. The design space further expands with non-metallic incorporation, unlocking new electronic states and catalytic pathways. Parallel advances in synthesis, from powder metallurgy and arc melting to thin film deposition, carbothermal shock, and additive manufacturing, now provide unprecedented control over atomic-scale structure–property–activity relationships. Beyond metals, high-entropy ceramics, borides, and engineered heterostructures with oxides, nitrides, or chalcogenides open new horizons for defect and interface engineering.

Translating these advances into industrial reality requires scalable, cost-effective fabrication and operational robustness. Thermal shock techniques, such as Joule heating, can be adapted to continuous or batch production, delivering defect-rich HEAs with minimal energy cost. Hybrid synthesis strategies, combining spray pyrolysis, microwave-assisted growth, or CVD with in-line compositional control, enable direct integration into industrial electrocatalyst lines, including PEM electrolyzers. Additive manufacturing emerges as a powerful enabler for architected components with hierarchical porosity, maximizing surface-to-volume ratios. Thin film synthesis offers precise stoichiometry and crystallography control, while short-range order (SRO) tuning is gaining traction as a design lever for optimizing active site distribution.

The convergence of computational modelling and data-driven design is accelerating discovery. Machine learning (ML) models, trained on curated datasets of elemental properties, phase stability, and catalytic performance, are increasingly coupled with DFT and Monte Carlo simulations to navigate the near-infinite HEA space. Autonomous high-throughput experimentation platforms enable rapid validation and closed-loop optimisation, compressing development timelines from years to weeks. Achieving the full potential of these approaches will require standardized synthesis protocols, benchmarking metrics, and testing environments to ensure comparability across studies and facilitate industrial adoption.

Looking ahead, HEAs are poised to play a defining role in next-generation electrochemical energy systems. Their performance scalability–sustainability triad positions them to reduce reliance on critical noble metals, enable cleaner energy conversion, and drive the transition towards a circular, low-carbon economy. The integration of large-scale

metallurgical infrastructure with precision nanostructuring will allow tailored catalysts for water electrolysis, CO_2 reduction, ammonia synthesis, and beyond. By bridging fundamental discovery with process integration, HEAs are not just materials for the future, they are a blueprint for sustainable energy innovation

CRediT authorship contribution statement

Víctor M. Jiménez-Arévalo: Writing – review & editing, Writing – original draft, Visualization, Validation, Supervision, Project administration, Investigation, Formal analysis, Data curation, Conceptualization. **P. Martin:** Writing – review & editing, Writing – original draft, Visualization, Validation, Investigation, Data curation. **María Fernanda Sepúlveda:** Writing – review & editing, Writing – original draft. **Manuel I. Azocar:** Software, Resources. **Xiaorong Zhou:** Supervision, Resources, Methodology, Funding acquisition, Formal analysis, Data curation. **Felipe M. Galleguillos Madrid:** Writing – review & editing, Validation, Methodology, Investigation, Formal analysis. **C.G. Ramirez:** Writing – original draft, Visualization, Software. **José H. Zagal:** Validation, Supervision, Methodology, Formal analysis, Data curation. **Maritza Páez:** Validation, Supervision, Resources, Funding acquisition, Formal analysis, Data curation.

Declaration of competing interest

The authors declare that they have no known competing financial interests or personal relationships that could have appeared to influence the work reported in this paper.

Acknowledgements

V. Jimenez-Arevalo appreciate the financial assistance provided by the Vicerrectoria de Postgrado from the Universidad de Santiago de Chile and postdoctorate project DICYT N° 022442PC, Vicerrectoría de Investigación, Innovación y Creacion. The work is supported by the UK Engineering and Physical Sciences Research Council for support of LiME (EP/N007638/1). Additionally, P. Martin acknowledges the Fondecyt Postdoctorado 3250677 project. The authors would like to thank the Programa de Doctorado en Energía Solar of the Universidad de Antofagasta, Chile; the support of ANID-Chile through the research project FONDECYT Iniciación 11230550; and ANID/FONDAP 1523A0006 Solar Energy Research Center SERC-Chile, 2nd extension.

Data availability

No data was used for the research described in the article.

References

[1] H.V. Mcgregor, J. Gergis, S.J. Phipps, The Industrial Revolution kick-started global warming much earlier than we realised, Published Online (2016).
[2] S.R. Bull, Renewable energy today and tomorrow, Proc. IEEE 89 (8) (2001) 1216–1226, https://doi.org/10.1109/5.940290.
[3] F. Martins, C. Felgueiras, M. Smitková, Fossil fuel energy consumption in European countries, Energy Procedia 153 (2018) 107–111, https://doi.org/10.1016/j.egypro.2018.10.050.
[4] J. Masa, C. Andronescu, W. Schuhmann, Electrocatalysis as the Nexus for Sustainable Renewable Energy : the Gordian Knot of activity , Stability , and Selectivity Angewandte Minirevie, Published Online (2020) 15298–15312, https://doi.org/10.1002/anie.202007672.
[5] M. Du, X. Li, H. Pang, Q. Xu, Alloy Electrocatalysts. Energychem. 5 (2) (2023) 100083, https://doi.org/10.1016/j.enchem.2022.100083.
[6] A. Govind Rajan, J.M.P. Martirez, E.A. Carter, Why do we use the Materials and Operating Conditions we use for Heterogeneous (Photo)Electrochemical Water Splitting? ACS Catal. 10 (19) (2020) https://doi.org/10.1021/acscatal.0c01862.
[7] S. Jiao, X. Fu, S. Wang, Y. Zhao, Perfecting electrocatalysts: Via imperfections: Towards the large-scale deployment of water electrolysis technology, Energy Environ. Sci. 14 (4) (2021) 1722–1770, https://doi.org/10.1039/d0ee03635h.
[8] K. Meyer, M. Ranocchiari, J.A. Van Bokhoven, Metal organic frameworks for photo-catalytic water splitting, Energy Environ. Sci. 8 (7) (2015) 1923–1937, https://doi.org/10.1039/c5ee00161g.
[9] S. Jeong, A.J. Branco, S.W. Bollen, C.S. Sullivan, M.B. Ross, Universal pH electrocatalytic hydrogen evolution with Au-based high entropy alloys, Nanoscale 16 (24) (2024) 11530–11537, https://doi.org/10.1039/d4nr01538j.
[10] K.L. Turner, S. He, B. Marchegiani, et al., Around the world in electrochemistry: a review of the electrochemistry curriculum in high schools, J. Solid State Electrochem. 28 (3–4) (2024) 1361–1374, https://doi.org/10.1007/s10008-023-05548-0.
[11] J.W. Yeh, S.K. Chen, S.J. Lin, et al., Nanostructured High-Entropy Alloys with Multiple principal elements: Novel Alloy Design Concepts and Outcomes, Adv. Eng. Mater. 6 (5) (2004) 299–303, https://doi.org/10.1002/ADEM.200300567.
[12] B. Cantor, I.T.H. Chang, P. Knight, A.J.B. Vincent, Microstructural development in equiatomic multicomponent alloys, Mater. Sci. Eng. A (2004).
[13] D.B. Miracle, High-Entropy Alloys: a Current Evaluation of founding ideas and Core Effects and Exploring "Nonlinear Alloys", JOM 69 (11) (2017) 2130–2136, https://doi.org/10.1007/s11837-017-2527-z.
[14] S. San, Y. Tong, H. Bei, B. Kombaiah, Y. Zhang, W.Y. Ching, First-principles calculation of lattice distortions in four single phase high entropy alloys with experimental validation, Mater. Des. 209 (2021) 110071, https://doi.org/10.1016/j.matdes.2021.110071.
[15] L. Gao, X. Cui, C.D. Sewell, J. Li, Z. Lin, Recent advances in activating surface reconstruction for the high-efficiency oxygen evolution reaction, Chem. Soc. Rev. 50 (15) (2021) 8428–8469, https://doi.org/10.1039/d0cs00962h.
[16] P.I. Odetola, B.J. Babalola, A.E. Afolabi, et al., Exploring high entropy alloys: a review on thermodynamic design and computational modeling strategies for advanced materials applications, Heliyon 10 (22) (2024) e39660, https://doi.org/10.1016/j.heliyon.2024.e39660.
[17] W. Xu, E. Diesen, T. He, K. Reuter, J.T. Margraf, Discovering High Entropy Alloy Electrocatalysts in Vast Composition Spaces with Multiobjective Optimization, J. Am. Chem. Soc. 146 (11) (2024) 7698–7707, https://doi.org/10.1021/jacs.3c14486.
[18] X. Guo, J. Gu, S. Lin, S. Zhang, Z. Chen, S. Huang, Tackling the activity and Selectivity challenges of Electrocatalysts toward the Nitrogen Reduction Reaction via Atomically Dispersed Biatom Catalysts, J. Am. Chem. Soc. 142 (12) (2020) 5709–5721, https://doi.org/10.1021/JACS.9B13349/SUPPL_FILE/JA9B13349_SI_001.PDF.
[19] X. Yan, H. Guo, W. Yang, et al., Al0.3CrxFeCoNi high-entropy alloys with high corrosion resistance and good mechanical properties, J. Alloys Compd. 860 (2021) 158436, https://doi.org/10.1016/j.jallcom.2020.158436.
[20] X. Ling, Y. Ao, J. Zheng, M. Han, D. Xu, Facile Synthesis of High-Entropy Alloy Nanowires for Electrocatalytic Alcohol Oxidation, ChemPlusChem 89 (5) (2024) 1–8, https://doi.org/10.1002/cplu.202400010.
[21] K. Schröter, Hard metal alloys and process of making them. *USA Pat US1549615A*, Published Online (1925) 3–4.
[22] H. Ye, J. Su, G. Yang, et al., Boosting HER activity of FeCoNiMnZn high-entropy alloys supported on nitrogen-doped carbon nanotubes, Mater. Today Commun. 45 (March) (2025) 112365, https://doi.org/10.1016/j.mtcomm.2025.112365.
[23] T. Gu, F. Yu, Z. Yu, et al., Efficient dual-phase PtNiCuMnMo high-entropy alloy electrocatalyst for alkaline hydrogen evolution reaction, J. Colloid Interface Sci. 688 (2025) 308–316, https://doi.org/10.1016/j.jcis.2025.02.134.
[24] Y. Jin, X. Fan, Q. Li, et al., Self-Reconstruction of High Entropy Alloys for Efficient Alkaline Hydrogen Evolution, Small 2408165 (2025) 1–9, https://doi.org/10.1002/smll.202408165.
[25] J. Bib Khan, P. Kumar Panda, P. Dash, H.C. Te, Microwave-Assisted Synthesis of Platinum-free High-Entropy Alloy Catalysts on Reduced Graphene Oxide Sheets for Enhanced Oxygen Reduction and Evolution Reactions, Chem - A Eur J. (2025) 202403863, https://doi.org/10.1002/chem.202403863.
[26] J.K. Pedersen, T.A.A. Batchelor, A. Bagger, J. Rossmeisl, High-entropy alloys as catalysts for the co2 and co reduction reactions, ACS Catal. 10 (3) (2020) 2169–2176, https://doi.org/10.1021/ACSCATAL.9B04343/SUPPL_FILE/CS9B04343_SI_001.PDF.
[27] J. Hou, Y. Wu, B. Zhang, S. Cao, Z. Li, L. Sun, Rational Design of Nanoarray Architectures for Electrocatalytic Water Splitting, Adv. Funct. Mater. 29 (20) (2019), https://doi.org/10.1002/adfm.201808367.
[28] Z. Abdin, A. Zafaranloo, A. Rafiee, W. Mérida, W. Lipiński, K.R. Khalilpour, Hydrogen as an energy vector, Renew. Sustain. Energy Rev. 120 (2020) 109620, https://doi.org/10.1016/J.RSER.2019.109620.
[29] M.I. Jamesh, P. Moni, A.S. Prakash, M. Harb, ORR/OER activity and zinc-air battery performance of various kinds of graphene-based air catalysts, Mater. Sci. Energy Technol. 4 (2021) 1–22, https://doi.org/10.1016/J.MSET.2020.12.001.
[30] Y. Yao, H. Wang, X.Z. Yuan, H. Li, M. Shao, Electrochemical Nitrogen Reduction Reaction on Ruthenium, ACS Energy Lett. 4 (6) (2019) 1336–1341, https://doi.org/10.1021/acsenergylett.9b00699.
[31] D. Liu, M. Chen, X. Du, et al., Development of Electrocatalysts for Efficient Nitrogen Reduction Reaction under Ambient Condition, Adv. Funct. Mater. 31 (11) (2021) 1–36, https://doi.org/10.1002/adfm.202008983.
[32] A. Yuda, A. Ashok, A. Kumar, A comprehensive and critical review on recent progress in anode catalyst for methanol oxidation reaction, Catal Rev - Sci Eng. Published Online (2020), https://doi.org/10.1080/01614940.2020.1802811.
[33] Aricò AS, Baglio V, Antonucci V. Direct Methanol Fuel Cells: History, Status and Perspectives. *Electrocatal Direct Methanol Fuel Cells From Fundam to Appl*. Published online 12 de octubre de 2009:1–78. doi:10.1002/9783527627707.CH1.
[34] X. Liu, J. Zhang, Z. Pei, Machine learning for high-entropy alloys: Progress, challenges and opportunities, Prog. Mater Sci. 2023 (131) (August 2022) 101018, https://doi.org/10.1016/j.pmatsci.2022.101018.

[35] Y. Zhang, Y.J. Zhou, J.P. Lin, G.L. Chen, P.K. Liaw, Solid-solution phase formation rules for multi-component alloys, Adv. Eng. Mater. 10 (6) (2008) 534–538, https://doi.org/10.1002/adem.200700240.
[36] M.G. Poletti, L. Battezzati, Electronic and thermodynamic criteria for the occurrence of high entropy alloys in metallic systems, Acta Mater. 75 (2014) 297–306, https://doi.org/10.1016/j.actamat.2014.04.033.
[37] S. Guo, C. Ng, J. Lu, C.T. Liu, Effect of valence electron concentration on stability of fcc or bcc phase in high entropy alloys, J. Appl. Phys. 109 (10) (2011), https://doi.org/10.1063/1.3587228.
[38] X. Yang, Y. Zhang, Prediction of high-entropy stabilized solid-solution in multi-component alloys, Mater. Chem. Phys. 132 (2–3) (2012) 233–238, https://doi.org/10.1016/j.matchemphys.2011.11.021.
[39] P. Martin, C.E. Madrid-Cortes, C. Cáceres, N. Araya, C. Aguilar, J.M. Cabrera, HEAPS: a user-friendly tool for the design and exploration of high-entropy alloys based on semi-empirical parameters, Comput. Phys. Commun. 278 (2022) 108398, https://doi.org/10.1016/j.cpc.2022.108398.
[40] L. Santiago-Andrades, A. Vidal-Crespo, J.S. Blázquez, J.J. Ipus, C.F. Conde, Mechanical Alloying as a way to produce Metastable Single-phase High-Entropy Alloys beyond the Stability Criteria, Nanomaterials 14 (1) (2024), https://doi.org/10.3390/nano14010027.
[41] M.H. Tsai, R.C. Tsai, T. Chang, W.F. Huang, Intermetallic phases in high-entropy alloys: Statistical analysis of their prevalence and structural inheritance, Metals (basel). 9 (2) (2019) 1–18, https://doi.org/10.3390/met9020247.
[42] H.L. Chen, H. Mao, Q. Chen, Database development and Calphad calculations for high entropy alloys: challenges, strategies, and tips, Mater. Chem. Phys. 210 (2018) 279–290, https://doi.org/10.1016/j.matchemphys.2017.07.082.
[43] L. Fenocchio, A. Saviot, S. Gambaro, et al., CALPHAD-aided synthesis and characterization of an Al–Co–Cr–Fe–Ni–W high-entropy alloy prepared by arc melting and spark plasma sintering, J. Mater. Res. Technol. 2025 (34) (December 2024) 1252–1264, https://doi.org/10.1016/j.jmrt.2024.12.140.
[44] N.Y. Yurchenko, N.D. Stepanov, A.O. Gridneva, M.V. Mishunin, G.A. Salishchev, S.V. Zherebtsov, Effect of Cr and Zr on phase stability of refractory Al-Cr-Nb-Ti-V-Zr high-entropy alloys, J. Alloys Compd. 757 (2018) 403–414, https://doi.org/10.1016/j.jallcom.2018.05.099.
[45] L. Guo, J. Gu, X. Gong, S. Ni, M. Song, CALPHAD aided design of high entropy alloy to achieve high strength via precipitate strengthening, Sci. China Mater. 63 (2) (2020) 288–299, https://doi.org/10.1007/s40843-019-1170-7.
[46] J. Kozlík, F. Lukáč, M.C. Luna, et al., Phase Composition of AlTiNbMoV, AlTiNbTaZr and AlTiNbMoCr Refractory complex Concentrated Alloys: a Correlation of predictions and Experiment, Metall. Mater. Trans. A Phys. Metall. Mater. Sci. 55 (December) (2024) 4981–4997, https://doi.org/10.1007/s11661-024-07595-2.
[47] Alex Zunger, S.-H. Wei, L. G. Ferreira and JEB. Special quasirandom structures. *Phys Rev Lett*. 1990;96(PA):312–318. doi:10.1016/j.commatsci.2014.09.021.
[48] A.V. Ruban, H.L. Skriver, Calculated surface segregation in transition metal alloys, Comput. Mater. Sci 15 (2) (1999) 119–143, https://doi.org/10.1016/s0927-0256(99)00003-8.
[49] Z. Li, F. Körmann, B. Grabowski, J. Neugebauer, D. Raabe, Ab initio assisted design of quinary dual-phase high-entropy alloys with transformation-induced plasticity, Acta Mater. 136 (2017) 262–270, https://doi.org/10.1016/j.actamat.2017.07.023.
[50] P. Martin, C. Aguilar, J.M. Cabrera, A review on mechanical alloying and spark plasma sintering of refractory high-entropy alloys: challenges, microstructures, and mechanical behavior, J. Mater. Res. Technol. 30 (March) (2024) 1900–1928, https://doi.org/10.1016/j.jmrt.2024.03.205.
[51] D. Ma, B. Grabowski, F. Körmann, J. Neugebauer, D. Raabe, Ab initio thermodynamics of the CoCrFeMnNi high entropy alloy: Importance of entropy contributions beyond the configurational one, Acta Mater. 100 (2015) 90–97, https://doi.org/10.1016/j.actamat.2015.08.050.
[52] C. Nataraj, E.J.L. Borda, A. van de Walle, A. Samanta, A systematic analysis of phase stability in refractory high entropy alloys utilizing linear and non-linear cluster expansion models, Acta Mater. 220 (2021) 117269, https://doi.org/10.1016/j.actamat.2021.117269.
[53] V. Sorkin, Z.G. Yu, S. Chen, T.L. Tan, Z. Aitken, Y.W. Zhang, First principles-based design of lightweight high entropy alloys, Sci. Rep. 13 (1) (2023) 1–20, https://doi.org/10.1038/s41598-023-49258-z.
[54] L. Tan, K. Ali, P.S. Ghosh, et al., Design principles of low-activation high entropy alloys, J. Alloys Compd. 907 (2022) 164526, https://doi.org/10.1016/j.jallcom.2022.164526.
[55] H. Li, Y. Han, H. Zhao, et al., Fast site-to-site electron transfer of high-entropy alloy nanocatalyst driving redox electrocatalysis, Nat. Commun. 11 (1) (2020) 1–9, https://doi.org/10.1038/s41467-020-19277-9.
[56] Y. Hu, H. Zhang, J. Cheng, et al., Machine learning for hot deformation flow stress prediction and dynamic recrystallization in Fe24.75Ni19.8Co9.9Cr14.85Al10.9Mn14.85Si4.95 high-entropy alloy, Intermetallics 185 (May) (2025) 108914, https://doi.org/10.1016/j.intermet.2025.108914.
[57] X. Zhang, R. Dong, Q. Guo, H. Hou, Y. Zhao, Predicting the stacking fault energy in FCC high-entropy alloys based on data-driven machine learning, J. Mater. Res. Technol. 26 (2023) 4813–4824, https://doi.org/10.1016/j.jmrt.2023.08.194.
[58] C. Madan, S.R. Jha, N.K. Katiyar, et al., Understanding the evolution of catalytically active multi-metal sites in a bifunctional high-entropy alloy electrocatalyst for zinc-air battery application, Energy Adv. 2 (12) (2023) 2055–2068, https://doi.org/10.1039/d3ya00356f.
[59] H. Hamdi, J. Charkhchian, H.R. Abedi, On the work hardening capacity of high entropy alloys during low-temperature deformation: a review, Mater. Sci. Eng. A 915 (August) (2024) 147206, https://doi.org/10.1016/j.msea.2024.147206.
[60] C.M. Clausen, M.L.S. Nielsen, J.K. Pedersen, J. Rossmeisl, Ab Initio to activity: Machine Learning-Assisted Optimization of High-Entropy Alloy Catalytic activity, High Entropy Alloy Mater. 1 (1) (2023) 120–133, https://doi.org/10.1007/s44210-022-00006-4.
[61] J. He, Z. Li, P. Zhao, et al., Machine learning-assisted design of high-entropy alloys with superior mechanical properties, J. Mater. Res. Technol. 33 (August) (2024) 260–286, https://doi.org/10.1016/j.jmrt.2024.09.014.
[62] N. Islam, W. Huang, H.L. Zhuang, Machine learning for phase selection in multi-principal element alloys, Comput. Mater. Sci 150 (April) (2018) 230–235, https://doi.org/10.1016/j.commatsci.2018.04.003.
[63] J. Wang, H. Kwon, H.S. Kim, B.J. Lee, A neural network model for high entropy alloy design, npj Comput. Mater. 9 (1) (2023) 1–13, https://doi.org/10.1038/s41524-023-01010-x.
[64] W. Huang, P. Martin, H.L. Zhuang, Machine-learning phase prediction of high-entropy alloys, Acta Mater. 169 (2019) 225–236, https://doi.org/10.1016/j.actamat.2019.03.012.
[65] R. Bobbili, B. Ramakrishna, Prediction of phases in high entropy alloys using machine learning, Mater. Today Commun. 36 (July) (2023) 106674, https://doi.org/10.1016/j.mtcomm.2023.106674.
[66] J. Qi, D.I. Hoyos, S.J. Poon, Machine Learning-based Classification, Interpretation, and Prediction of High-Entropy-Alloy Intermetallic Phases, High Entropy Alloy Mater. 1 (2) (2023) 312–326, https://doi.org/10.1007/s44210-023-00017-9.
[67] G. Kim, H. Diao, C. Lee, et al., First-principles and machine learning predictions of elasticity in severely lattice-distorted high-entropy alloys with experimental validation, Acta Mater. 181 (2019) 124–138, https://doi.org/10.1016/j.actamat.2019.09.026.
[68] C. Yang, C. Ren, Y. Jia, G. Wang, M. Li, W. Lu, A machine learning-based alloy design system to facilitate the rational design of high entropy alloys with enhanced hardness, Acta Mater. 222 (2022) 117431, https://doi.org/10.1016/j.actamat.2021.117431.
[69] Zhu LF, Koermann F, Chen Q, Selleby M, Neugebauer J, Grabowski and B. Accelerating ab initio melting property calculations with machine learning: Application to the high entropy alloy TaVCrW. *npj Comput Mater*. Published online 2024:1–11. doi:10.1038/s41524-024-01464-7.
[70] Z. Lu, Z.W. Chen, C.V. Singh, Neural Network-Assisted Development of High-Entropy Alloy Catalysts: Decoupling Ligand and Coordination Effects, Matter 3 (4) (2020) 1318–1333, https://doi.org/10.1016/j.matt.2020.07.029.
[71] Y. Zeng, M. Man, K. Bai, Y.W. Zhang, Revealing high-fidelity phase selection rules for high entropy alloys: a combined CALPHAD and machine learning study, Mater. Des. 202 (2021) 109532, https://doi.org/10.1016/j.matdes.2021.109532.
[72] Y. Zeng, M. Man, C. Koon Ng, et al., Search for eutectic high entropy alloys by integrating high-throughput CALPHAD, machine learning and experiments, Mater. Des. 241 (April) (2024) 112929, https://doi.org/10.1016/j.matdes.2024.112929.
[73] S. Arun, N. Radhika, B. Saleh, Advances in vacuum arc melting for high entropy alloys: a review, Vacuum 226 (May) (2024) 113314, https://doi.org/10.1016/j.vacuum.2024.113314.
[74] X. Shen, Z. Guo, F. Liu, et al., Microstructural evolution and mechanical behavior of novel TiZrTaxNbMo refractory high-entropy alloys, J. Alloys Compd. 990 (April) (2024) 174459, https://doi.org/10.1016/j.jallcom.2024.174459.
[75] Y.P. Wang, B.S. Li, M.X. Ren, C. Yang, H.Z. Fu, Microstructure and compressive properties of AlCrFeCoNi high entropy alloy, Mater. Sci. Eng. A 491 (1–2) (2008) 154–158, https://doi.org/10.1016/j.msea.2008.01.064.
[76] X. Cui, B. Zhang, C. Zeng, S. Guo, Electrocatalytic activity of high-entropy alloys toward oxygen evolution reaction, MRS Commun. 8 (3) (2018) 1230–1235, https://doi.org/10.1557/mrc.2018.111.
[77] G. Zhang, K. Ming, J. Kang, et al., High entropy alloy as a highly active and stable electrocatalyst for hydrogen evolution reaction, Electrochim. Acta 279 (2018) 19–23, https://doi.org/10.1016/J.ELECTACTA.2018.05.035.
[78] Z. Jin, J. Lv, H. Jia, et al., Nanoporous Al-Ni-Co-Ir-Mo High-Entropy Alloy for Record-High Water Splitting activity in Acidic Environments, Small 15 (47) (2019), https://doi.org/10.1002/smll.201904180.
[79] S. Li, X. Tang, H. Jia, et al., Nanoporous high-entropy alloys with low Pt loadings for high-performance electrochemical oxygen reduction, J. Catal. 383 (2020) 164–171, https://doi.org/10.1016/j.jcat.2020.01.024.
[80] V.M. Jimenez-Arevalo, P. Martin, E. Pio, et al., Energy transfer by Mechanical Alloying and Electrocatalytic Performance of the As-Sintered Self-Supported High-Entropy Alloy FeNiCoCuMo, Adv. Eng. Mater. 2400807 (2024) 1–12, https://doi.org/10.1002/adem.202400807.
[81] A. Fourmont, S. Le Gallet, K. Hoummada, et al., Effects of mechanical activation on chemical homogeneity and contamination level in dual-phase AlCoCrFeNi high entropy alloy, Mater. Chem. Phys. 272 (May) (2021) 125000, https://doi.org/10.1016/j.matchemphys.2021.125000.
[82] W. Dai, T. Lu, Y. Pan, Novel and promising electrocatalyst for oxygen evolution reaction based on MnFeCoNi high entropy alloy, J. Power Sources 430 (2019) 104–111, https://doi.org/10.1016/j.jpowsour.2019.05.030.
[83] L. Liu, H. Xia, Y. Tang, et al., Microstructure and Mechanical Properties of CoCrCuFeNi High-Entropy Alloys Synthesized by Powder Metallurgy and Spark Plasma Sintering, J. Mater. Eng. Perform. 33 (24) (2023) 13882–13896, https://doi.org/10.1007/s11665-023-08996-x.
[84] J. Tang, J.L. Xu, Z.G. Ye, X.B. Li, J.M. Luo, Microwave sintered porous CoCrFeNiMo high entropy alloy as an efficient electrocatalyst for alkaline oxygen

evolution reaction, J. Mater. Sci. Technol. 79 (2021) 171–177, https://doi.org/10.1016/j.jmst.2020.10.079.
[85] P. Ma, M. Zhao, L. Zhang, et al., Self- supported high-entropy alloy electrocatalyst for highly efficient H2 evolution in acid condition, J. Mater. 6 (4) (2020) 736–742, https://doi.org/10.1016/j.jmat.2020.06.001.
[86] H. Lee, H. Jeong, W. Jeong, et al., Wet Chemistry Methods for Synthesizing High-Entropy Nanoparticles: a Review of the Synthesis strategies and Various applications, Korean J. Chem. Eng. 41 (13) (2024) 3371–3393, https://doi.org/10.1007/s11814-024-00249-4.
[87] N.L.N. Broge, A.D. Bertelsen, F. Søndergaard-Pedersen, B.B. Iversen, Facile Solvothermal Synthesis of Pt-Ir-Pd-Rh-Ru-Cu-Ni-Co High-Entropy Alloy Nanoparticles, Chem. Mater. 35 (1) (2023) 144–153, https://doi.org/10.1021/acs.chemmater.2c02842.
[88] H. Qiao, M.T. Saray, X. Wang, et al., Scalable Synthesis of High Entropy Alloy Nanoparticles by Microwave heating, ACS Nano 15 (9) (2021) 14928–14937, https://doi.org/10.1021/acsnano.1c05113.
[89] J. Zhao, Z. Wang, X. Fang, et al., Fast joule heating synthesis of NiCoFeCrMo high-entropy alloy embedded in graphene for water oxidation, J. Alloys Compd. 966 (May) (2023) 171535, https://doi.org/10.1016/j.jallcom.2023.171535.
[90] Y. Yu, Q. Wang, X. Li, et al., Laser-thermal reduction synthesis of high-entropy alloys towards high-performance pH universal hydrogen evolution reaction, Nano Mater. Sci. (2024), https://doi.org/10.1016/j.nanoms.2024.05.012.
[91] S. Gao, S. Hao, Z. Huang, et al., Synthesis of high-entropy alloy nanoparticles on supports by the fast moving bed pyrolysis, Nat. Commun. 11 (1) (2020), https://doi.org/10.1038/s41467-020-15934-1.
[92] S.K. Padamata, A. Yasinskiy, V. Yanov, G. Saevarsdottir, Magnetron Sputtering High-Entropy Alloy Coatings: a Mini-Review, Metals (basel). 12 (2) (2022) 1–17, https://doi.org/10.3390/met12020319.
[93] M.D. Cropper, Thin films of AlCrFeCoNiCu high-entropy alloy by pulsed laser deposition, Appl. Surf. Sci. 455 (February) (2018) 153–159, https://doi.org/10.1016/j.apsusc.2018.05.172.
[94] V. Soare, M. Burada, I. Constantin, et al., Electrochemical deposition and microstructural characterization of AlCrFeMnNi and AlCrCuFeMnNi high entropy alloy thin films, Appl. Surf. Sci. 358 (2015) 533–539, https://doi.org/10.1016/j.apsusc.2015.07.142.
[95] S. Alvi, D.M. Jarzabek, M.G. Kohan, et al., Synthesis and Mechanical Characterization of a CuMoTaWV High-Entropy Film by Magnetron Sputtering, ACS Appl. Mater. Interfaces 12 (18) (2020) 21070–21079, https://doi.org/10.1021/acsami.0c02156.
[96] W. Li, P. Liu, P.K. Liaw, Microstructures and properties of high-entropy alloy films and coatings: a review, Mater Res Lett. 6 (4) (2018) 199–229, https://doi.org/10.1080/21663831.2018.1434248.
[97] P. Zhou, D. Liu, Y. Chen, et al., Corrosion engineering boosting bulk Fe50Mn30Co10Cr10 high-entropy alloy as high-efficient alkaline oxygen evolution reaction electrocatalyst, J. Mater. Sci. Technol. 109 (2022) 267–275, https://doi.org/10.1016/j.jmst.2021.09.003.
[98] Y. Ma, Y. Ren, D. Sun, et al., High entropy alloy nanoparticles dual-decorated with nitrogen-doped carbon and carbon nanotubes as promising electrocatalysts for lithium–sulfur batteries, J. Mater. Sci. Technol. 188 (2024) 98–104, https://doi.org/10.1016/j.jmst.2023.11.063.
[99] S. Wang, H. Yan, W. Huo, et al., Engineering multiple nano-twinned high entropy alloy electrocatalysts toward efficient water electrolysis, Appl Catal B Environ. 363(September (2025) 2024), https://doi.org/10.1016/j.apcatb.2024.124791.
[100] S.A. Lee, J. Bu, J. Lee, H.W. Jang, High-Entropy Nanomaterials for Advanced Electrocatalysis, Small Sci. 3 (5) (2023), https://doi.org/10.1002/smsc.202200109.
[101] J. Cai, H. Zhu, Surface-engineered nanostructured high-entropy alloys for advanced electrocatalysis, Commun Mater. 6 (1) (2025), https://doi.org/10.1038/s43246-025-00838-8.
[102] G. Liu, C. Song, X. Li, et al., Defect-rich FeCoNiMnRu high-entropy alloys with activated interfacial water for boosting alkaline water/seawater hydrogen evolution. *Chem*, Eng J. 509(December (2025) 2024), https://doi.org/10.1016/j.cej.2025.161070.
[103] X. Huo, Y. Zhang, H. Yu, et al., Bulk CoCrFeNiAlMo high entropy alloy as high-efficient electrocatalyst in alkaline environment, Int. J. Hydrogen Energy 87 (September) (2024) 505–514, https://doi.org/10.1016/j.ijhydene.2024.09.075.
[104] G.M. Tomboc, T. Kwon, J. Joo, K. Lee, High entropy alloy electrocatalysts: a critical assessment of fabrication and performance, J. Mater. Chem. A 8 (30) (2020) 14844–14862, https://doi.org/10.1039/d0ta05176d.
[105] H. Wang, R. Wei, X. Li, X. Ma, X. Hao, G. Guan, Nanostructured amorphous Fe29Co27Ni23Si9B12 high-entropy-alloy: an efficient electrocatalyst for oxygen evolution reaction, J. Mater. Sci. Technol. 68 (2021) 191–198, https://doi.org/10.1016/j.jmst.2020.06.045.
[106] S. Wang, B. Xu, W. Huo, et al., Efficient FeCoNiCuPd thin-film electrocatalyst for alkaline oxygen and hydrogen evolution reactions, Appl Catal B Environ. 313 (February) (2022) 121472, https://doi.org/10.1016/j.apcatb.2022.121472.
[107] Z.W. Chen, J. Li, P. Ou, et al., Unusual Sabatier principle on high entropy alloy catalysts for hydrogen evolution reactions, Nat. Commun. 15 (1) (2024), https://doi.org/10.1038/s41467-023-44261-4.
[108] T. Löffler, A. Savan, H. Meyer, et al., Design of Complex Solid-Solution Electrocatalysts by Correlating Configuration, Adsorption Energy distribution patterns, and activity Curves, Angew Chemie Int Ed. 59 (14) (2020) 5844–5850, https://doi.org/10.1002/ANIE.201914666.
[109] J. Deng, P. Ren, D. Deng, L. Yu, F. Yang, X. Bao, Highly active and durable non-precious-metal catalysts encapsulated in carbon nanotubes for hydrogen evolution reaction, Energy Environ. Sci. 7 (6) (2014) 1919–1923, https://doi.org/10.1039/c4ee00370e.
[110] Y. Yang, Z. Lun, G. Xia, F. Zheng, M. He, Q. Chen, Non-precious alloy encapsulated in nitrogen-doped graphene layers derived from MOFs as an active and durable hydrogen evolution reaction catalyst, Energy Environ. Sci. 8 (12) (2015) 3563–3571, https://doi.org/10.1039/c5ee02460a.
[111] Z. Lei, X. Liu, Y. Wu, et al., Enhanced strength and ductility in a high-entropy alloy via ordered oxygen complexes, Nature 563 (7732) (2018) 546–550, https://doi.org/10.1038/s41586-018-0685-y.
[112] C. Liu, W. Lu, W. Xia, et al., Massive interstitial solid solution alloys achieve near-theoretical strength, Nat. Commun. 13 (1) (2022) 1–9, https://doi.org/10.1038/s41467-022-28706-w.
[113] C. Wu, Y. Gong, C. Liu, et al., Hydrogen accommodation and its role in lattice symmetry in a TiNbZr medium-entropy alloy, Acta Mater. 288(September (2025) 2024), https://doi.org/10.1016/j.actamat.2025.120852.
[114] T.J. Ziehl, D. Morris, P. Zhang, Detection and impact of short-range order in medium/high-entropy alloys, iScience 26 (3) (2023) 106209, https://doi.org/10.1016/j.isci.2023.106209.
[115] M.S. Alias, S.K. Kamarudin, A.M. Zainoodin, M.S. Masdar, Active direct methanol fuel cell: an overview, Int. J. Hydrogen Energy 45 (38) (2020) 19620–19641, https://doi.org/10.1016/J.IJHYDENE.2020.04.202.
[116] H. Tian, D. Wu, J. Li, et al., Rational design ternary platinum based electrocatalysts for effective methanol oxidation reaction, J Energy Chem. 70 (2022) 230–235, https://doi.org/10.1016/j.jechem.2022.02.021.
[117] C.F. Tsai, K.Y. Yeh, P.W. Wu, Y.F. Hsieh, P. Lin, Effect of platinum present in multi-element nanoparticles on methanol oxidation, J. Alloys Compd. 478 (1–2) (2009) 868–871, https://doi.org/10.1016/J.JALLCOM.2008.12.055.
[118] K.V. Yusenko, S. Riva, P.A. Carvalho, et al., First hexagonal close packed high-entropy alloy with outstanding stability under extreme conditions and electrocatalytic activity for methanol oxidation, Scr. Mater. 138 (2017) 22–27, https://doi.org/10.1016/J.SCRIPTAMAT.2017.05.022.
[119] P. Zhao, Q. Cao, W. Yi, et al., Facile and General Method to Synthesize Pt-based High-Entropy-Alloy Nanoparticles, ACS Nano 16 (9) (2022) 14017–14028, https://doi.org/10.1021/acsnano.2c03818.
[120] Z. Xia, S. Guo, Strain engineering of metal-based nanomaterials for energy electrocatalysis, Chem. Soc. Rev. 48 (12) (2019) 3265–3278, https://doi.org/10.1039/c8cs00846a.
[121] M. Hu, J. Li, T. Liu, Z. Wu, Y. Du, Insights into the formation and growth of high entropy PdPtSnPbNi nanowires to obtain catalysts with high alcohol electrocatalytic oxidation activity, J. Colloid Interface Sci. 675 (2024) 481–487, https://doi.org/10.1016/j.jcis.2024.07.049.
[122] A.L. Wang, H.C. Wan, H. Xu, Y.X. Tong, G.R. Li, Quinary PdNiCoCuFe Alloy Nanotube Arrays as Efficient Electrocatalysts for Methanol Oxidation, Electrochim. Acta 127 (2014) 448–453, https://doi.org/10.1016/j.electacta.2014.02.076.
[123] X. Xiang, B. Cheng, B. Zhu, C. Jiang, G. Liang, High-entropy alloy nanocrystals boosting photocatalytic hydrogen evolution coupled with selective oxidation of cinnamyl alcohol, Chinese J Catal. 68 (2025) 326–335, https://doi.org/10.1016/S1872-2067(24)60167-1.
[124] D. Fan, K. Guo, Y. Zhang, Q. Hao, M. Han, D. Xu, Engineering high-entropy alloy nanowires network for alcohol electrooxidation, J. Colloid Interface Sci. 625 (2022) 1012–1021, https://doi.org/10.1016/j.jcis.2022.06.105.
[125] D. Wang, Z. Chen, Y.C. Huang, et al., Tailoring lattice strain in ultra-fine high-entropy alloys for active and stable methanol oxidation, Sci. China Mater. 64 (10) (2021) 2454–2466, https://doi.org/10.1007/s40843-020-1635-9.
[126] A. Amiri, V. Yurkiv, A.H. Phakatkar, T. Shokuhfar, R. Shahbazian-Yassar, Insights into Formation and growth of Colloidal Multielement Alloy Nanoparticles in solution through In Situ Liquid Cell TEM Study, Adv. Funct. Mater. 34 (19) (2024) 1–15, https://doi.org/10.1002/adfm.202304685.
[127] A.E. Lutz, R.S. Larson, J.O. Keller, Thermodynamic comparison of fuel cells to the Carnot cycle, Int. J. Hydrogen Energy 27 (10) (2002) 1103–1111, https://doi.org/10.1016/S0360-3199(02)00016-2.
[128] W. Wang, W. Wang, J. Cheng, X. Lu, Y. Lu, Biomimetic hierarchical porous high entropy alloy for significantly enhancing overall seawater splitting, Chem. Commun. 60 (63) (2024) 8276–8279, https://doi.org/10.1039/d4cc01502a.
[129] M.A. Khan, H. Zhao, W. Zou, et al., Recent Progresses in Electrocatalysts for Water Electrolysis, Electrochem. Energy Rev. 1 (4) (2018) 483–530, https://doi.org/10.1007/s41918-018-0014-z.
[130] J. Hu, B. Xu, J. Xu, et al., Electrocatalysis induced reconstruction of RuNiPO for highly efficient, J ENERGY Chem. Published Online (2023), https://doi.org/10.1016/j.jechem.2023.08.025.
[131] R.Q. Yao, Y.T. Zhou, H. Shi, et al., Nanoporous Surface High-Entropy Alloys as Highly Efficient Multisite Electrocatalysts for Nonacidic Hydrogen Evolution Reaction, Adv. Funct. Mater. 31 (10) (2021), https://doi.org/10.1002/adfm.202009613.
[132] S. Hu, W.X. Li, Sabatier principle of metal-support interaction for design of ultrastable metal nanocatalysts, Science (80-) 374 (6573) (2021) 1360–1365, https://doi.org/10.1126/science.abi9828.
[133] A.J. Medford, A. Vojvodic, J.S. Hummelshøj, et al., From the Sabatier principle to a predictive theory of transition-metal heterogeneous catalysis, J. Catal. 328 (2015) 36–42, https://doi.org/10.1016/j.jcat.2014.12.033.
[134] H. Ooka, J. Huang, K.S. Exner, The Sabatier Principle in Electrocatalysis: Basics, Limitations, and extensions, Front. Energy Res. 9 (May) (2021) 1–20, https://doi.org/10.3389/fenrg.2021.654460.
[135] D. Zhang, Y. Shi, H. Zhao, et al., The facile oil-phase synthesis of a multi-site synergistic high-entropy alloy to promote the alkaline hydrogen evolution

reaction, J. Mater. Chem. A 9 (2) (2021) 889–893, https://doi.org/10.1039/d0ta10574k.
[136] D. Wu, K. Kusada, T. Yamamoto, et al., On the electronic structure and hydrogen evolution reaction activity of platinum group metal-based high-entropy-alloy nanoparticles, Chem. Sci. 11 (47) (2020) 12731–12736, https://doi.org/10.1039/d0sc02351e.
[137] X. Fu, J. Zhang, S. Zhan, et al., High-Entropy Alloy Nanosheets for Fine-Tuning Hydrogen Evolution, ACS Catal. 12 (19) (2022) 11955–11959, https://doi.org/10.1021/acscatal.2c02778.
[138] G. Feng, F. Ning, J. Song, et al., Sub-2 nm Ultrasmall High-Entropy Alloy Nanoparticles for Extremely Superior Electrocatalytic Hydrogen Evolution, J. Am. Chem. Soc. 143 (41) (2021) 17117–17127, https://doi.org/10.1021/jacs.1c07643.
[139] D.A. Agyeman, Y. Zheng, T.H. Lee, et al., Synergistic Catalysis of the Lattice Oxygen and transition Metal Facilitating ORR and OER in Perovskite Catalysts for Li-O2Batteries, ACS Catal. 11 (1) (2021) 424–434, https://doi.org/10.1021/ACSCATAL.0C02608/SUPPL_FILE/CS0C02608_SI_001.PDF.
[140] L. Li, X. Cao, J. Huo, et al., High valence metals engineering strategies of Fe/Co/Ni-based catalysts for boosted OER electrocatalysis, J Energy Chem. 76 (2023) 195–213, https://doi.org/10.1016/j.jechem.2022.09.022.
[141] K. Zhu, F. Shi, X. Zhu, W. Yang, The roles of oxygen vacancies in electrocatalytic oxygen evolution reaction, Nano Energy 73 (2020) 104761, https://doi.org/10.1016/J.NANOEN.2020.104761.
[142] J. Huang, P. Wang, P. Li, H. Yin, D. Wang, Regulating electrolytic Fe0.5CoNiCuZnx high entropy alloy electrodes for oxygen evolution reactions in alkaline solution, J. Mater. Sci. Technol. 93 (2021) 110–118, https://doi.org/10.1016/j.jmst.2021.03.046.
[143] H. Wei, Q. Wang, Y. Zhang, et al., Engineering high-entropy alloy nanosheets toward efficient electrocatalytic water oxidation, Fuel 358 (PB) (2024) 130011, https://doi.org/10.1016/j.fuel.2023.130011.
[144] P. Li, X. Wan, J. Su, et al., A Single-phase FeCoNiMnMo High-Entropy Alloy Oxygen Evolution Anode Working in Alkaline solution for over 1000 h, ACS Catal. 12 (19) (2022) 11667–11674, https://doi.org/10.1021/acscatal.2c02946.
[145] C. Zhao, W. Cai, N. Sun, S. Chen, W. Jing, C. Zhao, Facile preparation of porous high-entropy alloy FeCoNiCuMn and its OER performance, J. Phys. Chem. Solids 2024 (184) (September 2023) 111668, https://doi.org/10.1016/j.jpcs.2023.111668.
[146] S. Yan, L. Zhang, W. Li, et al., Constructing CoNiRuIrMn high-entropy alloy network for boosting electrocatalytic activity toward alkaline water oxidation, Acta Mater. 290(December (2025) 2024), https://doi.org/10.1016/j.actamat.2025.120964.
[147] Y.C. Xu, W.J. Chen, J.F. Zhou, et al., Deep Eutectic Solvent-Assisted Corrosion Boosting Bulk FeCoNiCrMo High-Entropy Alloys as Highly Efficient Oxygen Evolution Reaction Catalyst, Langmuir 40 (28) (2024) 14291–14302, https://doi.org/10.1021/acs.langmuir.4c00769.
[148] L. Sharma, N.K. Katiyar, A. Parui, et al., Low-cost high entropy alloy (HEA) for high-efficiency oxygen evolution reaction (OER), Nano Res. 15 (6) (2022) 4799–4806, https://doi.org/10.1007/s12274-021-3802-4.
[149] H. Zhu, Z. Zhu, J. Hao, et al., High-entropy alloy stabilized active Ir for highly efficient acidic oxygen evolution, Chem. Eng. J. 431 (P3) (2022) 133251, https://doi.org/10.1016/j.cej.2021.133251.
[150] A. Asghari Alamdari, H. Jahangiri, M.B. Yagci, et al., Exploring the Role of Mo and Mn in improving the OER and HER Performance of CoCuFeNi-Based High-Entropy Alloys, ACS Appl. Energy Mater. 7 (6) (2024) 2423–2435, https://doi.org/10.1021/acsaem.3c03227.
[151] Stacy J, Regmi YN, Leonard B, Fan M. The recent progress and future of oxygen reduction reaction catalysis: A review. *Renew Sustain Energy Rev*. 2017;69([1] J. Stacy, Y.N. Regmi, B. Leonard, M. Fan, The recent progress and future of oxygen reduction reaction catalysis: A review, Renew. Sustain. Energy Rev. 69 (2017) 401–414. https://doi.org/10.1016/J.RSER.2016.09.135.):401–414. doi:10.1016/J.RSER.2016.09.135.
[152] S. Wang, H. Xin, Predicting Catalytic activity of High-Entropy Alloys for Electrocatalysis, Chem 5 (3) (2019) 502–504, https://doi.org/10.1016/j.chempr.2019.02.015.
[153] T.A.A. Batchelor, J.K. Pedersen, S.H. Winther, I.E. Castelli, K.W. Jacobsen, J. Rossmeisl, High-Entropy Alloys as a Discovery Platform for Electrocatalysis, Joule 3 (3) (2019) 834–845, https://doi.org/10.1016/j.joule.2018.12.015.
[154] A Batchelor TA, Lçffler T, Xiao B, et al. Complex-Solid-Solution Electrocatalyst Discovery by Computational Prediction and High-Throughput Experimentation**. *Angew Chemie Int Ed*. 2021;60(13):6932–6937. doi:10.1002/ANIE.202014374.
[155] Y. Chen, X. Zhan, S.L.A. Bueno, et al., Synthesis of monodisperse high entropy alloy nanocatalysts from core@shell nanoparticles, Nanoscale Horiz. 6 (3) (2021) 231–237, https://doi.org/10.1039/d0nh00656d.
[156] X. Zhao, H. Cheng, X. Chen, et al., Multiple Metal-Nitrogen Bonds Synergistically Boosting the activity and Durability of High-Entropy Alloy Electrocatalysts, J. Am. Chem. Soc. 146 (5) (2024) 3010–3022, https://doi.org/10.1021/jacs.3c08177.
[157] L. Zhang, W. Chu, L. Kuang, et al., Carbon-supported high-entropy alloys as for oxygen reduction reaction, J. Alloys Compd. 2025 (1010) (October 2024) 178194, https://doi.org/10.1016/j.jallcom.2024.178194.
[158] R. He, L. Yang, Y. Zhang, et al., A CrMnFeCoNi high entropy alloy boosting oxygen evolution/reduction reactions and zinc-air battery performance, Energy Storage Mater. 2023 (58) (October 2022) 287–298, https://doi.org/10.1016/j.ensm.2023.03.022.
[159] Z. Hu, K. Chen, Y. Zhu, B. Liu, J. Shen, Synergistic Effects of PtRhNiFeCu High Entropy Alloy Nanocatalyst for Hydrogen Evolution and Oxygen Reduction Reactions, Small 20 (26) (2024) 1–8, https://doi.org/10.1002/smll.202309819.
[160] D.H. Wu, M. Ul Haq, L. Zhang, J.J. Feng, F. Yang, A.J. Wang, Noble metal-free FeCoNiMnV high entropy alloy anchored on N-doped carbon nanotubes with prominent activity and durability for oxygen reduction and zinc–air batteries, J. Colloid Interface Sci. 662 (February) (2024) 149–159, https://doi.org/10.1016/j.jcis.2024.02.044.
[161] data world bank. CO2 emissions (metric tons per capita). https://data.worldbank.org/indicator/EN.ATM.CO2E.PC.
[162] U. Mustapha, C.C. Nnadiekwe, M. Abdulkarim Alhaboudal, et al., The role of morphology on the electrochemical CO2 reduction performance of transition metal-based catalysts, J Energy Chem. 85 (2023) 198–219, https://doi.org/10.1016/j.jechem.2023.06.010.
[163] C.D. Windle, R.N. Perutz, Advances in molecular photocatalytic and electrocatalytic CO2 reduction, Coord. Chem. Rev. 256 (21–22) (2012) 2562–2570, https://doi.org/10.1016/J.CCR.2012.03.010.
[164] C. Yang, S. Li, Z. Zhang, et al., Organic–Inorganic Hybrid Nanomaterials for Electrocatalytic CO2 Reduction, Small 16 (29) (2020) 2001847, https://doi.org/10.1002/SMLL.202001847.
[165] J. Resasco, A.T. Bell, Electrocatalytic CO2 Reduction to Fuels: Progress and Opportunities, Trends Chem. 2 (9) (2020) 825–836, https://doi.org/10.1016/J.TRECHM.2020.06.007.
[166] T. Ding, X. Liu, Z. Tao, et al., Atomically Precise Dinuclear Site active toward Electrocatalytic CO2Reduction, J. Am. Chem. Soc. 143 (30) (2021) 11317–11324, https://doi.org/10.1021/JACS.1C05754/SUPPL_FILE/JA1C05754_SI_001.PDF.
[167] X. Li, Q.L. Zhu, MOF-based materials for photo- and electrocatalytic CO2 reduction, EnergyChem 2 (3) (2020) 100033, https://doi.org/10.1016/J.ENCHEM.2020.100033.
[168] Y. Chen, Z. Fan, J. Wang, et al., Ethylene Selectivity in Electrocatalytic CO2Reduction on Cu Nanomaterials: a Crystal Phase-Dependent Study, J. Am. Chem. Soc. 142 (29) (2020) 12760–12766, https://doi.org/10.1021/JACS.0C04981/SUPPL_FILE/JA0C04981_SI_001.PDF.
[169] S. Nellaiappan, N.K. Katiyar, R. Kumar, et al., High-Entropy Alloys as Catalysts for the CO2 and CO Reduction Reactions: Experimental Realization, ACS Catal. 10 (6) (2020) 3658–3663, https://doi.org/10.1021/ACSCATAL.9B04302/SUPPL_FILE/CS9B04302_SI_001.PDF.
[170] J. Cavin, A. Ahmadiparidari, L. Majidi, et al., 2D High-Entropy transition Metal Dichalcogenides for Carbon Dioxide Electrocatalysis, Adv. Mater. 33 (31) (2021) 2100347, https://doi.org/10.1002/ADMA.202100347.
[171] R. Xing, X. Wang, G. Wang, et al., Non-precious metal high-entropy alloys for CO2 electroreduction, Nanoscale. Published Online (2025:), https://doi.org/10.1039/d5nr00260e.
[172] M. Rittiruam, P. Khamloet, A. Ektarawong, et al., Screening of Cu-Mn-Ni-Zn high-entropy alloy catalysts for CO2 reduction reaction by machine-learning-accelerated density functional theory, Appl. Surf. Sci. 652(December (2024) 2023), https://doi.org/10.1016/j.apsusc.2024.159297.
[173] R.H. Dolan, J.E. Anderson, T.J. Wallington, Outlook for ammonia as a sustainable transportation fuel, Sustain Energy Fuels. 5 (19) (2021) 4830–4841, https://doi.org/10.1039/D1SE00979F.
[174] Aziz M, TriWijayanta A, Nandiyanto ABD. Ammonia as Effective Hydrogen Storage: A Review on Production, Storage and Utilization. *Energies 2020, Vol 13, Page 3062*. 2020;13(12):3062. doi:10.3390/EN13123062.
[175] Frankl S, Gleis S, Karmann S, Prager M, Wachtmeister G. Investigation of ammonia and hydrogen as CO2-free fuels for heavy duty engines using a high pressure dual fuel combustion process: *https://doi.org/101177/1468087420967873*. 2020;22(10):3196–3208. doi:10.1177/1468087420967873.
[176] M. Wang, M.A. Khan, I. Mohsin, et al., Can sustainable ammonia synthesis pathways compete with fossil-fuel based Haber–Bosch processes? Energy Environ. Sci. 14 (5) (2021) 2535–2548, https://doi.org/10.1039/D0EE03808C.
[177] X. Chen, Y. Guo, X. Du, et al., Atomic Structure Modification for Electrochemical Nitrogen Reduction to Ammonia, Adv. Energy Mater. 10 (3) (2020) 1903172, https://doi.org/10.1002/AENM.201903172.
[178] X. Zheng, Y. Yao, Y. Wang, Y. Liu, Tuning the electronic structure of transition metals embedded in nitrogen-doped graphene for electrocatalytic nitrogen reduction: a first-principles study, Nanoscale 12 (17) (2020) 9696–9707, https://doi.org/10.1039/D0NR00072H.
[179] Y. Xiao, X. Tan, Y. Guo, J. Chen, W. He, Surface modification of CeO2−x nanorods with Sn doping for enhanced nitrogen electroreduction, J Energy Chem. Published Online (2023), https://doi.org/10.1016/j.jechem.2023.08.031.
[180] Yu Y fan, Zhang W, Sun F li, et al. High electrocatalytical performance of FeCoNiCuPd high-entropy alloy for nitrogen reduction reaction. *Mol Catal*. 2022;519(November 2021):112141. doi:10.1016/j.mcat.2022.112141.
[181] D. Zhang, H. Zhao, X. Wu, et al., Multi-Site Electrocatalysts boost pH-universal Nitrogen Reduction by High-Entropy Alloys, Adv. Funct. Mater. 31 (9) (2021) 2006939, https://doi.org/10.1002/ADFM.202006939.
[182] P. Chen, W. Zhong, Z. Gong, et al., High entropy borides as efficient catalysts for electrochemical reduction of nitrate to ammonia, Catal. Today 439 (May) (2024) 114809, https://doi.org/10.1016/j.cattod.2024.114809.
[183] T. Begildayeva, J. Theerthagiri, W. Limphirat, A. Min, S. Kheawhom, M.Y. Choi, Deciphering indirect Nitrite Reduction to Ammonia in High-Entropy

Electrocatalysts using In Situ Raman and X-ray Absorption Spectroscopies, Small 20 (29) (2024) 1–16, https://doi.org/10.1002/smll.202400538.
[184] Y. Wen, W. Zhang, X. Wang, et al., Dual-phase B-doped FeCoNiCuPd high-entropy alloys for nitrogen electroreduction to ammonia, Chem. Commun. 59 (89) (2023) 13371–13374, https://doi.org/10.1039/d3cc04581a.
[185] Y. Sun, W. Wu, L. Yu, et al., Asymmetric acidic/alkaline N2 electrofixation accelerated by high-entropy metal–organic framework derivatives, Carbon Energy 5 (3) (2023) 1–12, https://doi.org/10.1002/cey2.263.